NTNU

Norwegian University of
Science and Technology

Numerical Simulation of Ice-Rubble Mound Breakwater Interactions

David Massey

Coastal and Marine Engineering and Management
Submission date: July 2018
Supervisor: Raed Khalil Lubbad, IBM

Norwegian University of Science and Technology
Department of Civil and Environmental Engineering

ERASMUS +: ERASMUS MUNDUS MOBILITY PROGRAMME

Master of Science in

COASTAL AND MARINE ENGINEERING AND MANAGEMENT

CoMEM

NUMERICAL SIMULATION OF ICE-RUBBLE MOUND BREAKWATER INTERACTIONS

Norwegian University of Science and Technology
16 July 2018

David Randal Massey

The Erasmus+: Erasmus Mundus MSc in Coastal and Marine Engineering and Management is an integrated programme including mobility organized by five European partner institutions, coordinated by Norwegian University of Science and Technology (NTNU).

The joint study programme of 120 ECTS credits (two years full-time) has been obtained at two or three of the five CoMEM partner institutions:

- Norges Teknisk- Naturvitenskapelige Universitet (NTNU) Trondheim, Norway
- Technische Universiteit (TU) Delft, The Netherlands
- Universitat Politècnica de Catalunya (UPC). BarcelonaTech. Barcelona, Spain
- University of Southampton, Southampton, Great Britain
- City University London, London, Great Britain

During the first three semesters of the programme, students study at two or three different universities depending on their track of study. In the fourth and final semester an MSc project and thesis has to be completed. The two-year CoMEM programme leads to a multiple set of officially recognized MSc diploma certificates. These will be issued by the universities that have been attended by the student. The transcripts issued with the MSc Diploma Certificate of each university include grades/marks and credits for each subject.

Information regarding the CoMEM programme can be obtained from the programme coordinator:

Øivind A. Arntsen, Dr.ing.
Associate professor in Marine Civil Engineering
Department of Civil and Environmental Engineering
NTNU Norway
Mob.: +4792650455 Fax: + 4773597021
Email: oivind.arntsen@ntnu.no

CoMEM URL: https://www.ntnu.edu/studies/mscomem

CoMEM Thesis

This thesis was completed by:
David Randal Massey

Under supervision of:
Associate Professor
Raed Lubbad
Norges Teknisk Naturvitenskapelige Universitet (NTNU)

As a requirement to attend the degree of:
Erasmus+: Erasmus Mundus Master in Coastal and Marine Engineering and Management (CoMEM)

Taught at the following educational institutions:

Norges Teknisk- Naturvitenskapelige Universitet (NTNU)
Trondheim, Norway

Technische Universiteit (TU) Delft
Delft, The Netherlands

At which the student has studied from August 2016 to July 2018. (Pahl en Kaiser 2018)

NORWEGIAN UNIVERSITY OF SCIENCE AND TECHNOLOGY
DEPARTMENT OF CIVIL AND ENVIRONMENTAL ENGINEERING

Report Title: Numerical Simulation of Ice-Rubble Mound Breakwater Interactions	Date: 16 July 2018 Number of pages (incl. appendices): 119			
	Master Thesis	X	Project Work	
Name: David Massey				
Professor in charge/supervisor: Raed Lubbad				
Other external professional contacts/supervisors: *None*				

Abstract:

Offshore activity in energy production, fishing, shipping, and tourism is projected to increase in the Arctic and Sub-Arctic. This projected increase in offshore activity means the supporting coastal infrastructure needs to be expanded. All human activity in ice-prone regions requires a specialized knowledge and understanding of ice mechanics and how to properly design against ice forces and ice-structure interactions. Analyzing ice-structure interactions is a prerequisite for any successful venture into areas where sea ice can occur. This thesis studied numerically modeling the interaction between pre-broken, rigid ice sheets and wide, sloping structures. The thesis focused on adapting a numerical model and validating the base phenomena of the simulated ride-up and pile-up.

The numerical model used in this study is the Simulator for Arctic Marine Structures (SAMS). SAMS has previously been validated for ship-shape structures, and individual modules within SAMS has been validated for a wider range of applications. However, coastal structures with wide, upward slopes were previously unanalyzed, and SAMS required a few modifications before simulations could proceed. Due to limitations in the version of SAMS used for this study, level sheet ice was approximated with a section of pre-broken, rigid bodies being driven by a significantly larger, unbroken sheet. Ice was driven by simulated current and wind, thus a limit-force scenario could theoretically be reached. Side confinement was used to reduce the three dimensional (3D) effects introduced in the rigid-body approximation.

For ride-up, 36 test conditions were used with ice thicknesses between 0.5 and 1 m, velocities between 1.0 and 2.0 m/s, and the slopes of 1:4 to 1:6. Each test combination was repeated 40 times for a total 1440 simulations. Results from the tests show ride-up is both qualitatively and quantitatively well represented with an 18.9% difference between the simulations and Christensen's analytical model for ride-up.

For pile-up, 22 tests conditions were used with values similar to those found in the North Caspian Sea. The ice thickness was 0.15 m, the velocity was 0.5 m/s, and the slope was 1:3. Simulations were designed to test the effects of ice-ice friction, ice-structure friction, and rubble geometry on the pile-up behavior of SAMS. Qualitatively, pile-up simulations showed 5 distinct stages of simulation: 1) initial ride-up, 2) initial pile-up, 3) rubble-pile development, 4) ice-sheet failure away from the pile, and 5) the unbroken ice sheet directly influencing the pile. Stages 1-3 correspond with the expected behavior of pile-up, but stages 4 and 5 represent unrealistic behavior caused by the rigid-body approximation. Quantitatively, ice loads ranged between 3 and 9 kN/m, porosity between 0.35 and 0.65, the pile sail from 1-3 m, and the pile keel was not consistently grounded. Sensitivity tests have shown pile-up in SAMS is: 1) sensitive to changes in ice-ice friction for lower friction coefficients and relatively insensitive for higher friction coefficients, 2) small increases in ice-structure friction can exaggerate the aberrant stages, and 3) triangular rubble geometry can exaggerate the aberrant stages.

Keywords:

1. CoMEM
2. Coastal Engineering
3. Arctic Engineering
4. Ice-structure interaction
5. Numerical modelling

NTNU
Faculty of Engineering Science
Department of Civil and Environmental Engineering

MASTER THESIS

(TBA4920 Marine Civil Engineering, master thesis)

Spring 2018
for
David Massey

Numerical Simulation of Ice-Rubble Mound Breakwater Interactions

BACKGROUND (On why and how)

Rubble mound structures (bank revetments, breakwaters, and artificial islands) are needed to protect coastal infrastructure and facilities. As Arctic resource exploration increases and shipping routes through the Arctic open, more coastal structures and ports are likely to be built in ice-prone areas, thus more rubble mound structures will experience ice loads. Historically, the main environmental load considered on breakwaters is wave attack. However, in areas that experience ice, the environmental loads due to ice can exceed those due to waves and must be checked.

Typically, physical models are used if ice actions are determined to be significant with the structure in question. However, using ice tanks to help design breakwaters is performed after the breakwater has been designed and tested for waves, are time consuming and expensive, suffer from scale effects, and only a few facilities exist that can perform these experiments. By using a numerical simulation, ice interactions can more easily be integrated throughout the design cycle and reduce costly redesigns at the final stage. Currently, there are not many numerical models for ice actions on structures, and those simulating rubble mound structures tend to simplify the problem to 2D simulations and look at ride-up and pile-up or global loads and stability rather than movement of individual armor units and armor layer damage. The goal of this project is to expand an existing numerical model and verify the feasibility of using it to model ice interactions on rubble mound structures in the scale of the armor unit.

TASK DESCRIPTION (Tentative work for the thesis)

Description of task

The task is to use an existing numerical model, modify it as needed to account for rubble mound structures and the ice-failure mechanisms associated with them on the scale of an armor unit, and verify the results using the available literature and data from previous studies on the subject.

Aims and purpose

The main aim is to develop and verify the feasibility of using numerical models to test the design of a rubble mound structure on the armor unit scale. Verify in this context means that the results of the model should be on the same order as the results from previous studies –that is, from empirical formulas, physical models, or well-documented events on built structures.

Subtasks and research questions

As an introduction, the candidate must show that she/he has the advanced knowledge of the field "Arctic-coastal structures" with respect to theory and methods with in general.

This thesis should answer the following questions:

- Is the existing numerical model capable of both simulating the ice actions caused by level ice on a rubble mound structure on the prototype scale and of producing global results similar to those observed in previous studies?
- Can the numerical model produce reasonably valid results on the armor unit scale?
- Is the numerical model capable of simulating a full breakwater on the armor unit scale, or does it need to be broken up into smaller design sections?
- Can the numerical model be used to simulate large-scale breakwater failure mechanisms like bulldozing?

In order to answer these questions, the following series of tasks in increasing complexity is suggested:

1. Literature review. The start of the thesis should include a comprehensive literature review in order to better understand the current theory of the physical processes behind ice actions on rubble mound structures and armor units, provide the base of previous studies and design guidelines from which the modeling tasks can be verified, and understand the current state of research into and the development of numerical models with regards to ice actions on wide, sloping marine structures.
2. Gain an understanding of SAMS. The numerical model to be used is SAMS (Simulator for Arctic Marine Structures). Before the modeling tasks can be performed, one must know how to properly configure and use SAMS. Additionally, an advanced knowledge of the assumptions, simplifications, and numerical schemes used in SAMS is needed to determine the limitations of the simulator, the theoretical order of accuracy, how it can be modified for rubble mound structures, and if the current ice-failure mechanisms implemented are adequate for wide, sloping structures with an irregular face.
3. Modeling a smooth, rigid structure. The first modeling task investigates a smooth, rigid structure (i.e. one whose armor layer cannot deform). To simulate the nature of the rubble mound structure with a smooth surface, an appropriately high friction coefficient needs to be determined and used for a cube-type armor unit. This task will be used to validate the general concept, ice-failure mechanisms for a wide sloping structure, ice ride-up and rubble formation, and global loads on the structure.
4. Modeling a rough, rigid structure. Building upon the previous task, this task reduces the friction coefficient and transforms the slope from a smooth incline to one that approximates a cube-type armor unit. The armor layer will be rigid (i.e. one solid, non-deformable surface). This task will further verify the ice-failure mechanisms, penetration of the ice into the armor layer, ice ride-up and rubble formation, and the global loads on the structure.
5. Modeling a cube-type armor layer on a breakwater. After the previous tasks are verified, this task will achieve the goal of numerically modeling a rubble mound structure on the scale of the armor unit. In

the previous tasks, the breakwater was one rigid body. With this task, each armor unit is modeled individually and is free to move as the ice interacts with it. However, the filter layers and core will be considered one rigid body. As with the previous tasks, a cube-type armor unit will be modeled. Local and global loads will be investigated, and damage to the breakwater will be analyzed similarly to damage classifications used with wave attack. *Note: the armor-failure type of 'plucking' is most likely outside the scope of this task, as the simulations will focus on moving ice sheets without the added effect of adfreeze or tides.*

6. Modeling a cube-type armor layer on a breakwater with deformable filter and core layers. Depending on the progress and results of the previous tasks, model each individual armor unit on top of deformable filter and core layers. The previous tasks look at global or local loads on the armor units, but not all failure mechanisms act on the armor layer alone – such as bulldozing. The goal of this task is to simulate some of these large-scale breakwater failure modes in addition to modes that are localized to the armor layer.

In each of the above tasks, multiple simulations involving different ice conditions (e.g. thickness and speed) and breakwater arrangements (e.g. slope and armor unit size) will be simulated to help validate the model over a range of situations. However, ice conditions will be limited to level, first-year ice.

General about content, work and presentation
The text for the master thesis is meant as a framework for the work of the candidate. Adjustments might be done as the work progresses. Tentative changes must be done in cooperation and agreement with the professor in charge at the Department.

In the evaluation thoroughness in the work will be emphasized, as will be documentation of independence in assessments and conclusions. Furthermore the presentation (report) should be well organized and edited; providing clear, precise and orderly descriptions without being unnecessary voluminous.

The report shall include:

- Standard report front page (from DAIM, http://daim.idi.ntnu.no/)
- Title page with abstract and keywords. (MScTitlePage[IBM]).
  CoMEM students must include CoMEM as one of the keywords.
- CoMEM page (Only CoMEM students) (CoMEM MSc title Page templateNTNU).
- Preface
- Summary and acknowledgement. The summary shall include the objectives of the work, explain how the work has been conducted, present the main results achieved and give the main conclusions of the work.
- Table of content including list of figures, tables, enclosures and appendices.
- A list explaining important terms and abbreviations should be included.
- List of symbols should be included
- The main text.
- Clear and complete references to material used, both in text and figures/tables. This also applies for personal and/or oral communication and information.
- Thesis task description (these pages) signed by professor in charge as Attachment 1.
- The report musts have a complete page numbering.

The thesis can as an alternative be made as a scientific article for international publication, when this is agreed upon by the Professor in charge. Such a report will include the main points as given above, but where the main text includes both the scientific article and a process report.

Submission procedure
Procedures relating to the submission of the thesis are described in IV faculty webpage
https://www.ntnu.edu/iv/master-thesis-regulation

On submission of the thesis the candidate shall submit to the professor in charge a CD/DVD('s) or a link to a net-cloud including the report in digital form as pdf and Word (or other editable form) versions and the underlying material (such as data collection, time series etc.).

Documentation collected during the work, with support from the Department, shall be handed in to the Department together with the report.

According to the current laws and regulations at NTNU, the report is the property of NTNU. The report and associated results can only be used following approval from NTNU (and external cooperation partner if applicable). The Department has the right to make use of the results from the work as if conducted by a Department employee, as long as other arrangements are not agreed upon beforehand.

Start and submission deadlines
The work on the Master Thesis starts on (date) 12 February 2018

The thesis report as described above shall be submitted digitally in DAIM at the latest (date:) 20 August 2018 at 23:59:59.

Professor in charge: Raed Lubbad

Other supervisors: *None*

Trondheim, 28.02.2018.

_____
Professor in charge (sign)

To my family

Acknowledgements

It was a long road with many detours – both physically and temporally – to get to this point. Studying on a different continent and in multiple cities is as exciting as it is challenging. While there are many people I would like to recognize and thank who made this a successful chapter in my life, I would like to pay special attention to the following people:

- My family, thank you for always supporting me and putting up with the long periods between phone calls. I could not have done it without you or your support.
- Raed, you were always there to give me direction when I questioned how to proceed and to offer moral support when research objectives did not pan out. I am happy to have had you as a mentor and supervisor from the start of this programme to its conclusion.
- Ania, my museum partner and fellow Nederland explorer. You gave me a break from engineering and science whenever I needed a distraction – and sometimes when I did not. You're awesome!
- Everyone in Track 1 – Esther, Al, Alaqel, and Ahksanul – you have been a second family to me while I have been so far away from home.
- All of my fellow CoMEMbers, it was great getting to know and study with each and every one of you. I will always remember our Christmas in Røros. #CoMEMories
- Bailey, I never would have heard about Erasmus Mundus or CoMEM without you. You encouraged me to take the first steps and apply.
- Øivind and Sonja, thank you for all of the work you put in to making the bureaucracy of the different universities run as smoothly as it did.

Contents

List of Figures

List of Tables

List of Equations

List of Symbols

A_{dry}	Cross-sectional area of the emerged structure
A_{sfc}	Surface area exposed to [wind, current]
A_{sub}	Cross-sectional area of the submerged structure
b	Width of [ice, structure]
C_m	Added mass coefficient
$D_{n\#}$	Nominal diameter (typically of stone) for the # percentile (e.g. D_{n50})
E	Modulus of elasticity
E_k	Kinetic energy
F_c	Total force from current
F_e	Total environmental force
F_H	Total horizontal force
F_w	Total force from wind
g	Acceleration due to gravity
H_B	Load required to break the sheet in bending failure
H_P	Load required to push the advancing sheet through the ice rubble
H_R	Load required to push the blocks up the slope
H_L	Load required to lift the ice rubble on top of the advancing ice sheet
H_T	Load required to turn the ice block at the top of the slope
h_i	Thickness of the ice sheet or floe
h_k	Thickness of the keel in a rubble-pile or ridge
h_p	Height of pile, applicable when pile is on a slope above a waterline
h_{ru}	Height of ride-up
h_s	Thickness of the sail in a rubble pile or ridge
h_*	Either the ice thickness or the D_{n50} – whichever is greater
K_p	Passive resistance coefficient for rock slopes
L_{beach}	Length parallel to the slope along the slope (i.e. beach)
L_b	Breaking length
L_c	Characteristic length (typically determined by elastic plate theory)
l	Ratio between L_b and L_c
n_v	Porosity in the armor layer
u_c	Average current velocity

V_{10}	Average air velocity at 10m above the surface
v_i	Velocity of ice
R	Generic resistance available
R_{edge}	Total resistance offered by a slope against stone dislodgment
R_{slide}	Total resistance a structure has against sliding
W	Work
α	Slope of the structure (with respect to the horizontal axis)
γ_i	Specific weight of ice
γ_p	Specific weight of pile (ice and air)
Δt	Time step
θ	Angle of the seaward side of a rubble pile
μ_{ii}	Ice-ice friction coefficient
μ_{is}	Ice-structure friction coefficient
ν	Poisson's ratio of ice
ρ_a	Density of air
ρ_{bulk}	Dry bulk density
ρ_i	Average density of ice
ρ_r	Density of rock or armor stone
ρ_w	Density of water
σ_f	Flexural strength
φ_p	Coefficient of internal friction within a rubble pile
φ_s	Coefficient of internal friction of the soil or sea bed
Ω	A ratio of the potential energy to the geometry of a rubble pile on a slope

1 Introduction

1.1 Background and Motivation

Human activities in the Arctic and Sub-Arctic regions require a specialized knowledge and understanding of ice mechanics and how to properly design structures against the forces and phenomena of ice. Analyzing ice-structure interactions is a prerequisite for any successful venture into areas where sea ice can occur. Arctic engineering has been driven by hydrocarbon exploration, and, as oil and gas exploration in the Arctic is typically in deep water, research has focused on ice interactions with floating structures [1] [2]. This increased offshore activity means coastal infrastructure also needs to be considered. Additionally, this increased demand on coastal infrastructure is further heightened by changes in shipping and tourism [3]. Furthermore, recent developments in the North Caspian Sea have seen Arctic designs in shallow water where bottom-founded structures are used [1] [4] [5] [6]. All of this indicates that the industry needs ways to make better informed, more robust designs in a time- and cost-effective manner for Arctic, coastal structures. Numerical modelling has helped coastal engineering with geotechnical and hydrodynamical analysis; it stands to reason that Arctic analysis will also benefit from numerical models for ice actions and effects on structures.

1.1.1 Arctic shipping routes

A side effect of global climate change is that the Arctic ice sheet is shrinking – i.e. reducing its area of extent and average thickness – and summer conditions are becoming more favorable to ships and offshore activity in the Arctic [3]. Over the last 30 years, sea ice thickness in the Central Arctic has decreased 30% with less multi-year ice and fewer pressure ridges [7]. Some models have predicted ice-free summers in the Arctic by 2050 [7]. Because of this sea-ice retreat, three shipping routes are becoming increasingly interesting to commercial maritime stakeholders: the Northern Sea Route (NSR), the Northwest Passage (NWP), and the Transpolar Sea Route (TSR) [3], see Figure 1-1.

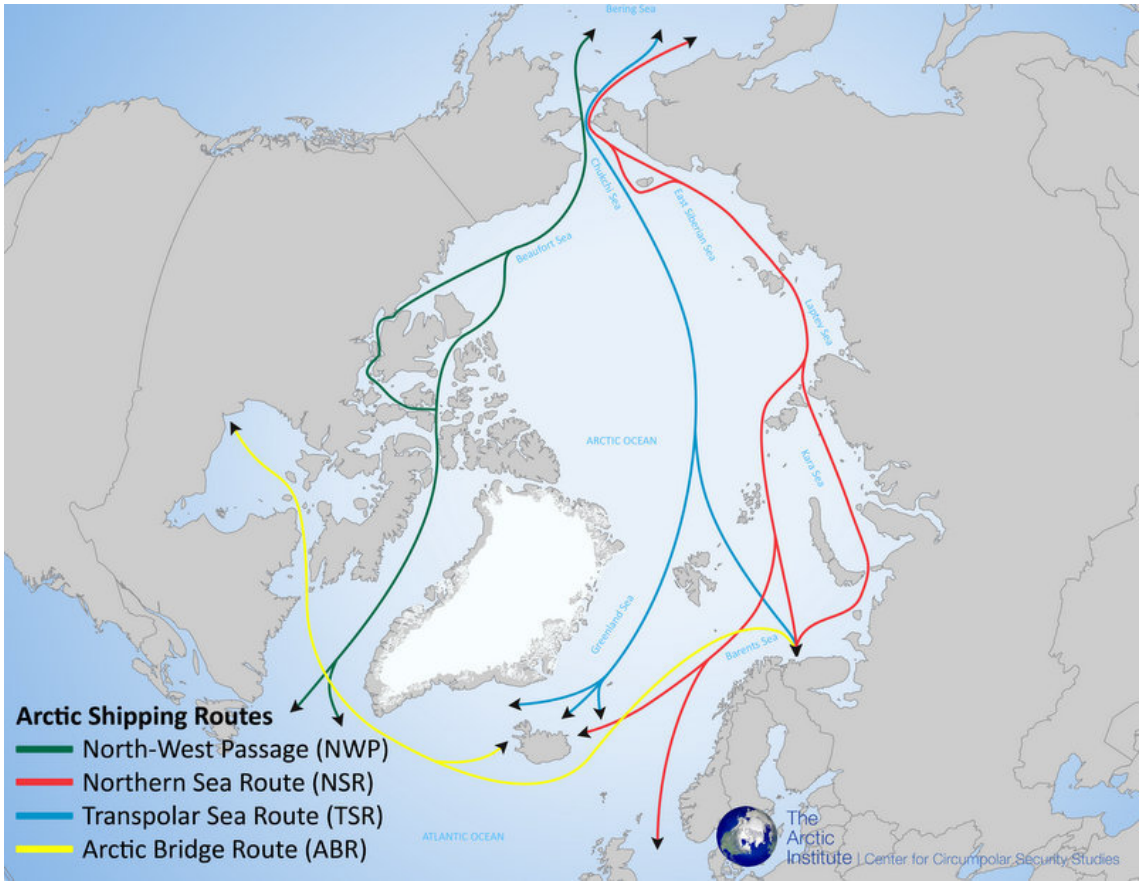

Figure 1-1 Arctic Shipping Routes [8]

The NSR, sometimes referred to as the Northeast Passage, aims to service containerized commodities between Europe and Asia. Currently, the main shipping route for the Euro-Asian market utilizes the Suez Canal. As such, the Suez Canal is seeing increasing delays due to congestion [3]. Liquid commodities (i.e. oil and gas) are less likely to utilize the NSR unless they originate in the Arctic, as pipelines are the preferred transportation method between Europe and Asia [7]. To date, the NSR has seen limited use by shipping companies despite being significantly shorter than using the Suez Canal. This is due, in part, to high fees associated with permits, the cost of hiring icebreaker escorts, and increased insurance costs due to the higher risk of Arctic sailing [9] [7]. However, if ships are able to cross the NSR without using icebreakers, the savings is estimated at 40-50% off the cost of the Suez Canal depending on the ports involved [3] with the potential for even greater savings if oil prices increase [9].

The NWP is less likely to become a major shipping route, for it is marginally longer than the NSR and has more dangerous navigation and ice conditions [3] [7]. However, unlike the NSR, the NWP currently does not have any fees directly imposed by governments [7]. While the NWP probably will not compete with the Suez Canal or the NSR, it is a likely option for tourism (e.g. cruise ships) and increased fishing activities [3]. In fact, in 2016, the first luxury

cruise ship – the Crystal Serenity – successfully sailed the NWP with 1,750 passengers and serves as a case study to the viability of the NWP for tourism [3].

The TSR is physically the shortest of the three Arctic routes and thus offers the highest savings in fuel [3]. However, since the TSR goes through the North Pole, it will continue to have ice-related hazards after the NSR and NWP have thawed to commercial use [7]. To date, it remains as a theoretical route dependent on further Arctic ice thinning. Stakeholders are still interested as it both eliminates any potential fees and permits from nations and is unhindered by navigation risks associated with shorelines [3].

As shipping activity increases along the NSR and NWP, ports and coastal infrastructure need to be able to accommodate both the number and size of ships, for ships need access to supplies and safe harbor from polar lows [3] [7]. According to 2016 reports from the World Port Index, current port capacity in the Arctic is limited. A total of 135 ports were identified as being Arctic; of those, 99 are classified as very small and 7 as medium or large. These numbers include all ports in the Arctic and not just those along the NSR or NWP (e.g. all ports in Greenland are considered Arctic). When looking at current ports along the aforementioned shipping routes, there are none classified as deep-water. This lack of Arctic port capabilities and capacity has left many to speculate that Arctic ports will see an increase in investment to transform them into what the shipping industry needs [3]. As these ports are being redesigned, ice loads and actions must be accounted for in the design, and a cost-effective way to analyze coastal infrastructure is required.

1.1.2 North Caspian Sea

Hydrocarbon prospects in the North Caspian Sea are one of the greatest in the world. The Kashagan field is one of the largest findings in recent years, and prospective drilling has started in both the Russian and Kazakh territories [1] [6]. While not technically in the Arctic, structures in the North Caspian Sea observe 3-4 months of sea ice activity each winter. Most of the North Caspian Sea has a depth less than 10 m, and a typical depth around the Kashagan field is 4 m [1] [6]. This extremely shallow depth lends designs more to shallow-water structures such as barges, detached breakwaters, and artificial islands rather than more traditional Arctic offshore structures such as ships and floating production units [1] [5] [6].

With all of these structures, vessel access during operations is required, and ice-rubble accumulation is a significant concern and design parameter [4]. Ice rubble not only restricts access for supplies to and egress from the structure, but it also increases the loads experienced

[4] [6]. These increased loads must be properly accounted for in the design. Additionally, other ice phenomena – such as rubble ride-up – affects how ice-protection structures are designed to properly minimize risk [10] [11]. Given the environmental sensitivity and potential loss of life involved with oil and gas exploration, identifying potential hazardous conditions and designing structures or operational procedures is paramount to successful projects.

1.1.3 Physical modelling

To date, Arctic engineering design has largely relied on physical models through laboratory tests. However, physical models are not without their issues. Ice tanks are relatively rare in the world, and they are expensive and time-consuming. Additionally, generating the ice is a mixture of science and art, which is dependent on the experience of the lab [12]. Physical models also suffer from scale effects. While general behavior and global loads can be to a certain extent represented in the model scale, current guidelines from the International Organization for Standardization (ISO) caution using scaled tests for local loads, for ice is a heterogeneous, anisotropic material whose properties might not be captured in small-scale tests [11]. Simulating ice through other means – such as paraffin – is normally only used for rigid-body analysis. Analogous to Computational Fluid Dynamics (CFD) models in hydrodynamics, specific types of Arctic numerical models can be used to aid in researching local loads and damages.

1.2 Objective and organization of the study

The objective of this thesis is to analyze the feasibility of using a three-dimensional (3D), physics-based numerical model on sloping, coastal structures. This model is capable of simulating both local and global ice loads and of predicting structural damage and failure on sloping, coastal structures.

While several numerical models already exist for specific types of structures or ice phenomena, a 3D physics-based model that can analyze both floating and submerged bodies is investigated. If determined feasible and the results are validated, this model can aid in the engineering design process and help answer research questions physical models might not be able to answer. Being a fully 3D, physics-based model, it has the potential to better represent what is observed in both model and prototype scales, and one can test both local and global loads without the scale effects found in physical models. Versatility of body type is important, for every project is different. Some projects will have both floating and non-floating structures

interacting with ice at the same time; being able to use one model for the entire project site increases the chance of success of a safe cost-effective design and ice-management strategy.

The types of structures investigated are wide, sloping structures in shallow water with a special consideration for rubble-mound or riprap structures. As the simulator has not previously been validated for upward-sloping structures, the ice bodies in this study are rigid – making the results more similar to using paraffin in a physical model. Therefore, in this experiment, base phenomena, behavior, and forces are focused on rather than site- or region-specific cases in order to test the broad validity of the numerical model for wide, sloping coastal structures. The results of the simulations are then compared to analytical, semi-empirical, and anecdotal data.

This thesis is organized into 8 chapters. Chapters 1 and 8 present an introduction and summary respectively. Chapter 2 presents background into Arctic engineering and the applicable ice-structure interactions for this study. Chapter 3 discusses numerical models for Arctic coastal structures; it is divided into two sections: an overview of current numerical models and detailed information concerning the model used in this thesis – methods, previous validation studies, and shortcomings for coastal structures. Chapter 4 discusses the experiment design, parameters used, and analysis techniques. Chapter 5 presents the results of the simulations while Chapter 6 compares the results to industry-accepted theory and proposes explanations for any major differences between the theory and the results. Finally, Chapter 7 presents future work in both the validation process and development suggestions for the model.

1.3 Readership

This thesis investigates ice-structure interactions for coastal structures and the application and validity of using a specific numerical model in particular. The primary readership is hence students, engineers, and scientists interested in:

- The safe design of coastal structures against ice forces from level ice;
- How different ice and structure parameters affect phenomena observed when ice interacts with coastal structures;
- Modifying and applying a general-purpose numerical model to investigate specific phenomena on the fringes of the original scope of the model;
- Validating a numerical model for previously unvalidated configurations;

Basic knowledge about physics and mechanics is required. Additionally, some knowledge of coastal engineering structures – such as breakwaters – is assumed. Knowledge about Arctic engineering and numerical modelling is desired but not required to understand and appreciate the details of this work, as all definitions required for understanding are provided. While programming was used extensively throughout the research of this thesis, programming knowledge is not required to understand the results or conclusions.

2 Literature Review

2.1 Ice as an engineering medium

2.1.1 Ice types and features

Offshore and coastal ice is typically first classified by origin and then by age. Ice can originate in fresh water (e.g. lakes and rivers), salt water (i.e. sea ice), and land (i.e. glaciers). Depending on where the ice originated, the properties of ice can vary significantly. In the case of fresh vs sea ice, this is largely due to the presence of brine pockets (concentrated, trapped sea water) inside the ice which reduces the strength. Land-originated ice is introduced into the sea when glaciers near the coast calve; this process makes icebergs and bergy bits. As they are formed by compressed snow rather than freezing still water, the crystalline structure of glacial ice is different and often contains trapped air rather than brine. Icebergs are significantly thicker than most other ice types and features [11] [13].

Sea ice is further classified by age: first-year ice and multi-year ice. First year ice is defined as ice that has not yet survived a summer melt season, and multi-year ice is ice that has survived at least one summer melt season. Ice age is inversely proportional to ice salinity (i.e. the extent of brine pockets within the ice). Thus, older ice is fresher than younger ice. This means multi-year ice is typically stronger than first-year ice of the same thickness [11] [13] [14].

Sea ice is also classified by feature type: (unfeatured) level ice, rafted ice, rubble, and ridges. Level ice has little to no deformations and has a relatively uniform thickness. Rafted ice is formed when two or more large pieces of level ice slide on top of each other. It is similar to level ice; however, the effective thickness becomes the sum of the thicknesses of the pieces. Ice rubble forms when smaller, broken pieces of ice are haphazardly moved on top of each other. Ice ridges result from rubble that has been partially to fully consolidated (underwater) and unconsolidated rubble above water. Like rafted ice, this consolidated layer increases the effective thickness, but unlike rafted ice, the layers are treated differently as they have different mechanical properties [11] [13] [14].

2.1.2 Mechanical properties of ice

Sea ice is a crystalline material that, mechanically, behaves similarly to other crystalline materials such as metal. Unlike most metals, sea ice is considered warm – that is, close to the melting point – and has relatively big crystals, substructure, and impurities. The mechanical

properties of sea ice depend on the size and orientation of the crystals – the latter making it an orthotropic material composed by a series of parallel, basal planes. The crystalline structure is weaker along the plane than perpendicular to the planes. Additionally, ice grows faster along the plane than perpendicular to the plane. When discussing level ice, the consequence of this uneven growth rate is that these planes are more or less vertically aligned (i.e. columnar ice), as the other alignments have been wedged out as the thickness increases. Because of this vertical alignment, level ice is stronger against horizontal loads (i.e. higher compressive strength) and weaker against vertical loads (i.e. lower flexural strength) [13] [14].

The mechanical properties are further influenced by defects in the crystalline structure forming basal planes (*see Figure 2-1*). As sea ice is made from sea water, there is a certain amount of trapped, concentrated sea water in small pockets within the sea ice which gives it a salinity. These brine pockets break up the molecular bonds and the planes and further decrease the strength of ice. Similarly, as ice begins to melt, melt channels start to form in the ice causing it to become "rotten". Rotten ice is significantly weaker than non-rotten ice in both compressive and flexural strength, albeit these defects affect the flexural strength more than the compressive strength [11] [14].

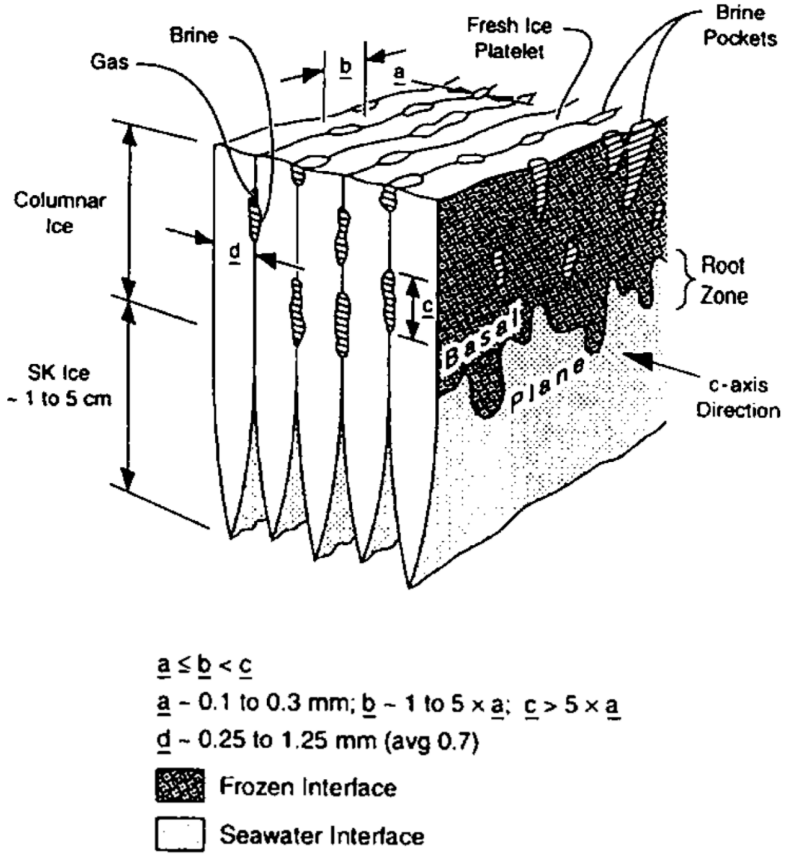

Figure 2-1 Sea-ice Crystal Structure (Kovacs, 1997, as found in Løset et al. 2006) [14].

2.1.3 Ice limiting mechanisms

Before considering the relevant ice failure modes that can occur, one must understand the limiting mechanisms present in ice-structure interactions. Estimating ice actions on a structure depends on the ice floe's mass, velocity, and intrinsic properties, the water depth, and the structure's mass or foundation type and geometry. Ice actions generally fall into one of four types of limiting mechanisms: limit energy (momentum), limit force, limit stress, and splitting [11] [13] [14]. Figure 2-2 below shows a schematic giving an overview of the different limiting scenarios.

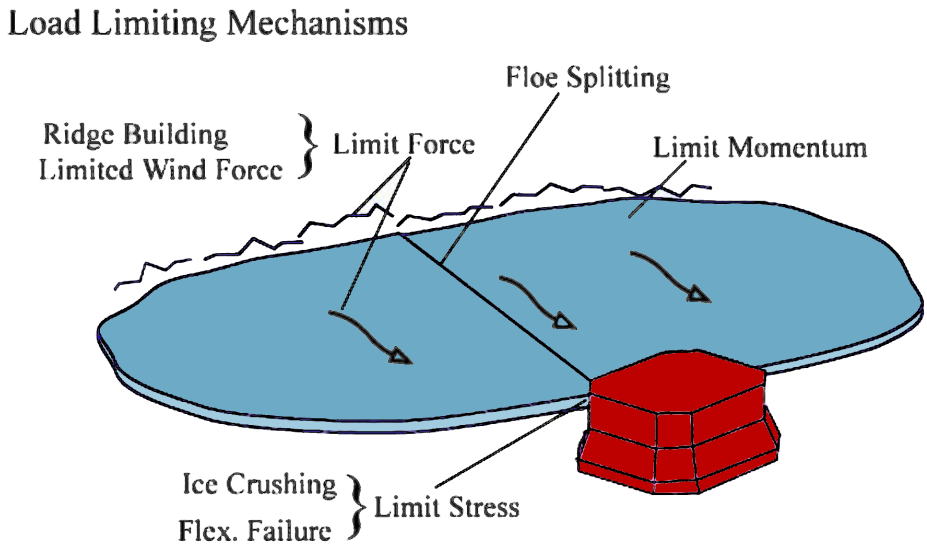

Figure 2-2 Schematic of the failure mechanisms for ice-structure interactions [12].

The *limit energy* scenario will occur when the kinetic energy of the ice is not sufficient enough to cause the ice to fail. Rather, the ice either fully stops after a certain penetration or the structure deflects the ice after some transfer of kinetic energy occurs. In either case, it is the momentum of the ice that determines the outcome. This is most relevant for ice features with small fetch such as icebergs, released stamukha, or free-floating ice ridges. As coastal structures are depth limited and icebergs and stamukha are relatively tall, limit energy is less of a concern for coastal infrastructure [13] [14].

The *limit force* scenario describes the situation where the driving forces (i.e. current, wind, and adjacent ice features) are insufficient to cause the ice to fail at the ice-structure interface. Failure could occur somewhere other than the ice-structure interface – as is the case in ridge building – or the ice floe could stop moving without failure. That is to say that the ice-structure interaction is limited by the forces driving the collision. This typically occurs when strong and thick features reach the structure; rather than the ice feature failing or deforming,

the driving forces are transferred to the structure. As neither body deforms, both bodies are considered rigid [13].

The *limit stress* scenario is when the driving forces are sufficiently strong enough to cause the ice to continuously fail at the ice-structure interface. The ice action is limited by the maximum stress an ice floe or feature can withstand before failing. The type of failure will depend on the geometry of the structure and the velocity and properties of the ice. For coastal structures, this is the limiting scenario most likely to cause the greatest loads [13].

Splitting occurs when a moderately large ice floe strikes against a structure. Sharp-edged structures are more likely to cause a splitting scenario, but splitting has been observed in smooth, circular structures as well. Some literature does not include this as a different scenario but rather incorporates it into limit stress [13] [12].

Which scenario occurs depends on the possible intensity of each, as the one that gives the lowest ice action determines which will actually occur. It should also be noted that one event can see multiple limiting scenarios occur over the entire duration. The scenario which takes place is called the limiting mechanism.

2.2 Ice on wide, sloping structures

2.2.1 Wide, sloping structure definition

Ice-structure interactions on sloping structures can be classified into two types: narrow and wide structures. Several attempts have been made to determine if a structure is wide or narrow. Some simplistic estimates just use the structure's width while others look at the aspect ratio of the structure width or the radius of curvature to the ice thickness. For the purpose of this thesis, a wide structure is one who accumulates ice rubble [13] [14]. In coastal engineering, rubble mound breakwaters are an example of a wide, sloping structure.

2.2.2 Failure modes and typical behavior

If the limiting mechanism is determined to be limit stress – as is typical when level ice is driven into a structure –, one also needs insight into the applicable failure modes of ice. The most commonly discussed failure modes are bending, crushing (i.e. brittle crushing), creep (i.e. ductile crushing), radial cracking, circumferential cracking, buckling, and spalling – with bending as the most applicable to sloping structures [13] [14] [12]. It is quite possible that one structure will experience multiple failure modes.

Bending failure occurs when ice is moved up (or down) the slope generating a bending moment in the ice sheet. When this moment exceeds the flexural strength of the ice, the ice fails and breaks. If the structure has a radius of curvature, this can result in radial or circumferential cracks; flat structures generate cracks along the structure [14] [12]. For flat structures, the most common prediction for the distance from the structure that the failure will occur uses elastic plate theory and the characteristic breaking length derived from it. Unlike circumferential and radial cracking, these estimation methods are typically independent of ice velocity, although some researchers have shown a velocity effect increasing the longitudinal compression and thus increasing the flexural strength of the ice [14]. It should be noted that the characteristic breaking length is with ideal ice, and local imperfections or minor differences in thickness can change where the break occurs [13] [14] [15]. For more information on the breaking length and block size, please refer to section 4.3.1.

The other failure types are associated more with vertical structures as opposed to sloping structures. However, it has been shown that the slope angle influences the failure type, and slopes steeper than 1:1 behave more like vertical structures [14]. As with vertical structures, velocity has been found to play a key role in the failure mechanism [14]. These failure modes are depicted in Figure 2-3 and briefly summarized below [13] [14]:

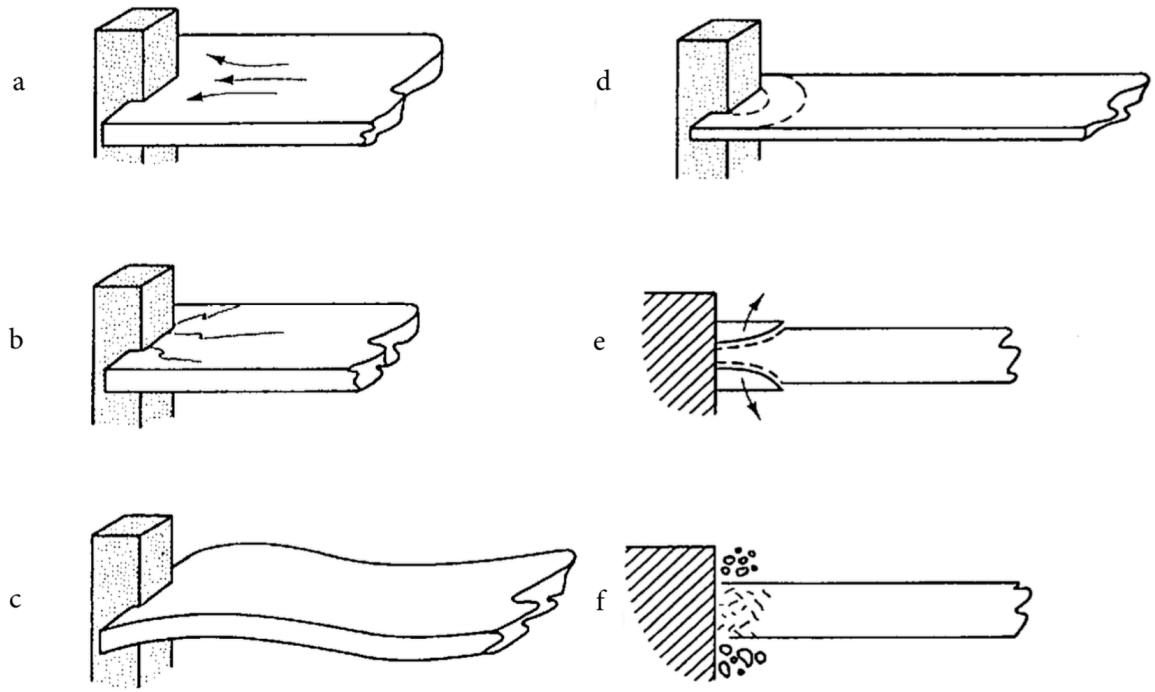

Figure 2-3 Principle failure modes for vertical structures in limit stress: (a) creep, (b) radial cracking, (c) buckling, (d) circumferential cracking, (e) spalling, (f) crushing (Sanderson, 1988 as found in [14]).

- *Crushing* will occur when the ice has a relatively high velocity causing continuous brittle failure resulting in non-uniform pressure distributions over the contact area;
- *Creep*, as opposed to crushing, occurs with relatively low velocities causing continuous failure resulting in near-uniform pressure distributions over the contact area;
- *Mixed crushing-creep* is a special case at intermediate velocities where the failure mode alternates between brittle crushing and creep causing intra-structure vibrations that can be significant;
- *Radial cracking* is associated with tensile failure with high aspect ratios resulting in cracks radiating from the structure into the ice sheet;
- *Circumferential cracking* is associated with out-of-plane bending moments caused by sheet deflection against the structure;
- *Buckling* can occur in the case of high aspect ratios and is closely associated with radial and circumferential cracking; and
- *Spalling* is when out of plane cracks propagate away from the contact area and divide the sheet into layers.

On wide, sloping structures – such as rubble mound structures –, ice loads are typically governed by the flexural strength. As previously stated, the flexural strength is less than the compressive strength, thus ice loads tend to be less for sloped coastal structures (i.e. traditional breakwaters) than for vertical structures (i.e. caisson breakwaters or piles) [16]. However, ice can fail locally in modes more associated with vertical structures or subsequent bending after the initial contact due to non-smooth surfaces caused by the structure (e.g. the armor layer of rubble mound breakwaters) or the ice rubble generated as the sheet fails [14] [12] [15]. Thus, globally the structure experiences a series of peak forces greater than those predicted purely by bending failure, and locally crushing loads can dominate the armor design. Any formulas used to predict ice loads on wide sloping structures must take this force into account [14].

The general process of interaction with a wide, sloping structure has 4 stages as detailed below and shown in Figure 2-4. First, the ice moves up the slope of the structure until it generates a sufficiently large moment causing the ice to fail in bending. Second, the broken piece of ice is pushed up the slope as the newly-formed edge of the sheet continues to advance; these two steps repeat several times causing many blocks along the surface of the structure. Third, the weight of the blocks along the structure exceeds the friction, and the blocks fall or slide down causing a rubble pile to start to form. Finally, as this process repeats itself, the weight of the pile on top of the ice sheet causes the sheet to fail – causing the pile to be partially

submerged. The new edge of the ice sheet must now push through the rubble pile, and the process repeats itself [11] [14].

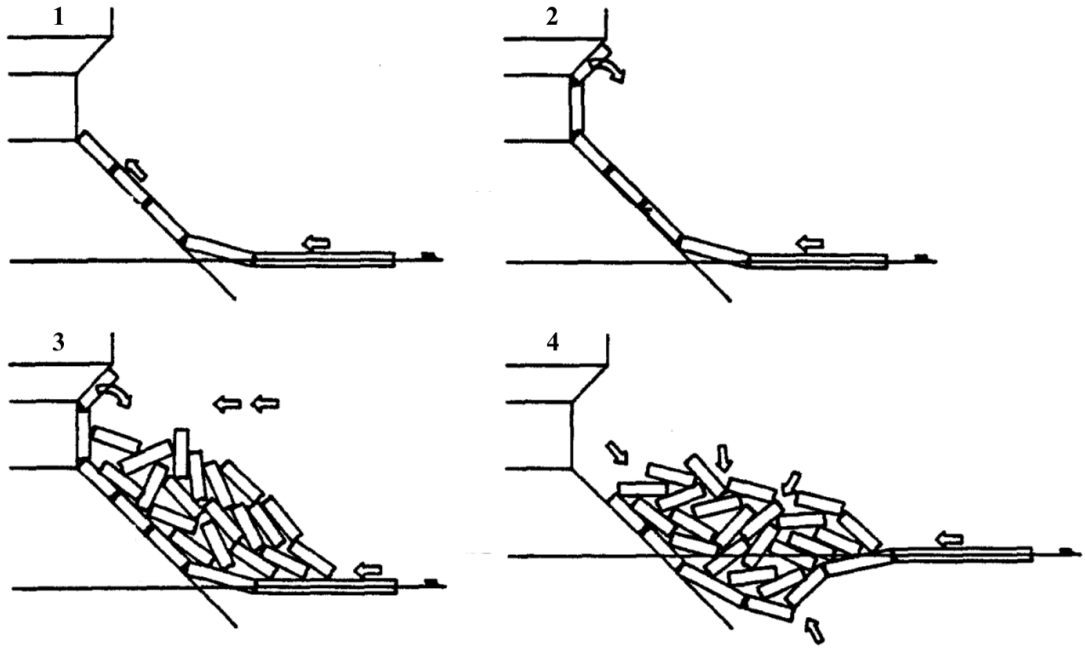

Figure 2-4 The four stages of ice acting on a wide, sloping structure [17]

2.2.3 Predicting force on wide, sloping structures – the Croasdale model

The first models to predict the force caused by level ice on wide sloping structures used just the first two stages (bending failure and moving the blocks up the slope) to predict loads, but this was shown to be insufficient as it ignores the effect of the rubble pile [14]. In work published in 1994, Croasdale and Cammaert developed a model that takes into account the ice rubble and the forces involved in moving the ice sheet through the rubble. In addition to the four steps mentioned above, they propose an additional ending step: either the rubble clears the structure, or the rubble pile grows until the ice begins to fail in a location away from the structure (i.e. changing the limiting mechanism) [17]. This method is still used and is the base for the ISO19906 guidelines for forces on wide, sloping structures [11]. Please note that this model gives a good estimate on the global loads of a sloping structure and does not account for local loads due to failure modes other than bending.

According to the model, the horizontal force on the structure is the sum of five components [11] [17]:

- H_B: the load required to break the sheet in bending failure;
- H_P: the load required to push the advancing sheet through the ice rubble;
- H_R: the load required to push the blocks up the slope;

- H_L: the load required to lift the ice rubble on top of the advancing ice sheet; and
- H_T: the load required to turn the ice block at the top of the slope.

The version in the ISO19906 remains relatively faithful to the original model, but it has been modified to account for the compressive stress in the ice resulting from the applied horizontal load. The final version becomes (*see Appendix A for the full equations including all sub-calculations*):

$$F_H = \frac{H_B+H_P+H_R+H_L+H_T}{1-\frac{H_B}{\sigma_f L_c h_i}} \quad \text{Eq1}$$

In Eq1, F_H is the total horizontal force acting on a structure, H_B to H_T are defined above, σ_f is the flexural strength of ice, L_c is the characteristic length typically defined by elastic plate theory, and h_i is the ice thickness.

2.3 Rubble-mound breakwaters in the Arctic

2.3.1 Definition and differences with non-Arctic breakwaters

Rubble-mound breakwaters are coastal structures made up of quarried rocks. Traditionally, rubble-mound breakwaters are used to protect coasts, ports, and other infrastructure from wave loads. However, in the Arctic, rubble-mound breakwaters are also used to protect infrastructure from ice loads. Similar to the more common sub-Arctic breakwaters, they typically contain a core of fine material, one or more filter layers, and an outer layer of heavy armor stone designed to withstand the environmental loads (*see Figure 2-5*).

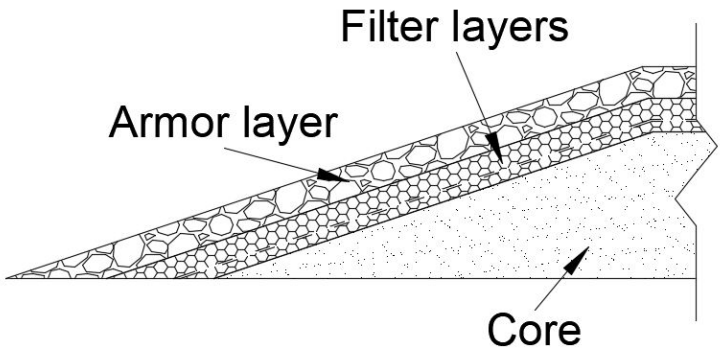

Figure 2-5 A simplified schematic showing the essential components of a breakwater.

One of the key differences between breakwaters that experience ice loads and those that do not is in armor stone placement. With ice-breakwaters, placing the armor stone to create a smoother slope reduces ice loads; with wave-breakwaters, placing the armor stone to increase

roughness helps dissipate wave energy and reduce overtopping [11] [16]. Figure 2-6 shows the same breakwater in both summer and winter conditions; please note the smooth armor placement visible during summer conditions.

Figure 2-6 Breakwater in Buffalo, NY, USA. Left) Summer conditions showing the smooth armor placement. Right) Winter conditions showing both ride-up and pile-up (Michael Mohr as found in Sodhi 2014 [19]).

2.3.2 Global Arctic-related breakwater failure

Four failure modes from ice actions are recognized for rock revetments: edge failure, global active failure, sliding failure, and decapitation [5] [18].

Global active failure is comparable to slope stability where the failure plane goes from the ice line to the downstream toe of the breakwater. This failure type is due to the global load along a nominal breakwater section. Failure along the breakwater is at least as wide as the cross-sectional width. Resistance is determined by the weight of the failing section and the interlocking along the slip circles. The Rock Manual recommends finite element analysis to determine the resistance [18].

Total sliding failure – also called bulldozing – is comparable to sliding failure due to hydrostatic pressure on dikes and levees. It occurs when ungrounded rubble distributes ice loads over the majority of the slope and the breakwater slides across the seabed – typically in weaker soils. Resistance is based on the weight of the breakwater and the shear strength of the seabed [18]. While rare, this type of failure has been observed. Figure 2-7 shows a breakwater that has experienced both total sliding failure and global active failure [19]. The Rock Manual provides a formula to estimate the total resistance of a breakwater from sliding (Eq2).

$$R_{slide} = g\left[\rho_{bulk} A_{dry} + (\rho_{bulk} + n_v(1-\rho_w) A_{sub}\right] tan\varphi_s \qquad \text{Eq2}$$

$$\rho_{bulk} = \rho_r(1-n_v) \qquad \text{Eq3}$$

R_{slide} is the resistance of a breakwater to sliding. ρ_{bulk}, ρ_r, and ρ_w are the dry bulk, rock, and water densities, respectively. n_v is the porosity in the armor layer. A_{dry} and A_{sub} are the emerged and submerged cross-sectional areas, respectively. φ_s is the internal angle of friction for the soil or seabed.

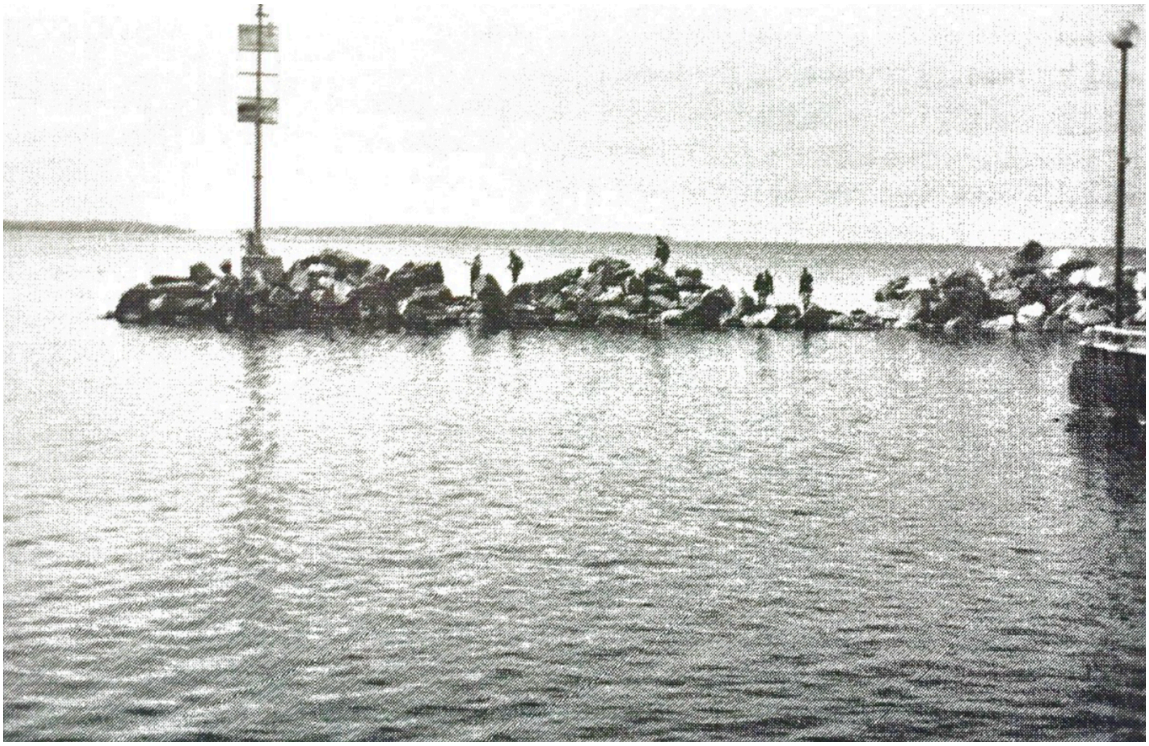

Figure 2-7 Sections of this breakwater have been 'bulldozed' during an ice event one winter [19].

Decapitation, as its name suggests, is removing the head from the body of the breakwater. It is a sliding failure where the crest (head) slides across the submerged part of the breakwater (body). It occurs when frost penetrates the entire breakwater, effectively turning all the individual elements into one solid structure, and ice then acts upon the solidified structure. According to the Rock Manual, "decapitation is only likely to occur when the crest is rigidly frozen significantly below mean water level" [18]

In addition to these 3 structural failures, there are two functional failure modes: when ice encroachment reaches and damages the structure the breakwater is trying to protect, and when rubble build up blocks access to the structure [16]. For more information, please see section 2.4 Ride-up and pile-up.

2.3.3 Local Arctic-related breakwater failure

Artificial islands and breakwaters utilizing armor stone have been successfully built in ice-prone areas. While the design of breakwater armor stone is relatively well understood for

hydrodynamic loading, the conditions and forces on armor stones due to ice loading is less understood [18]. When discussing local failure on a rubble-mound breakwater, typically one refers to the displacement of stones in the armor layer; this is true for both hydraulic and ice loads. For ice loads, local failure is normally classified as plucking or edge failure.

Plucking is when an ice sheet freezes to the armor layer and, due to tides, a rock is moved out of place. In order for plucking to occur, at low tide the ice must freeze to a rock, and the ice must be sufficiently thick enough to be able to support the rock off of buoyancy and ice strength alone. Plucking is more of a passive-type failure in the sense that it occurs from tidal actions rather than ice loads [16] [19].

Edge failure can be compared to the movement or dislodgment of individual armor units by wave forces. It caused by local ice loads. Local loads can be greater than the global loads – especially due to the irregular shape of quarry stone or concrete armor units and the uneven slope they form. Local loads are determined by stone size, slope angle, slope smoothness, and the ice acting on it. Resistance to the loads is a function of the rock diameter (D_{n50}), armor layer porosity, and the internal friction angle or interlocking of the armor layer [5] [18]. Two general guidelines exist for edge failure: the armor thickness should be at least as thick as the level ice at the structure, and the crest freeboard should be at least twice as high as the ice thickness [5]. The Rock Manual presents a formula (Eq4) for estimating the resistance [18].

$$R_{slope} = 0.5\rho_{bulk} g h_* K_p \qquad \text{Eq4}$$

R_{slope} is the resistance of the rock-armored slope. h_* is either h_i or D_{n50} – whichever is greater. K_p is the passive resistance coefficient – a function of the angle of internal friction and the steepness of the armor layer; typical values are on the order of 20 but can be larger depending on interlocking.

Guidelines for armor unit size are inconsistent and have a wide range of suggested values [16]. It is commonly believed that breakwaters properly designed for wave attack can withstand ice forces [16] [18], however several experiments in ice tanks debate this [20] [21]. Additionally, especially in the North Caspian Sea, the extremely shallow depths limit wave actions to the point where ice loads can determine the final design [5] [6]. While some guidelines claim damage to the armor layer from ice loads is acceptable due to the low hydrodynamic forces during icy conditions [18], others caution that repairs would then need to take place during summer and autumn months when storms are more likely [16]. Experts in ice

engineering suggest a D_{n50} anywhere from 0.5 to 3 times the ice thickness [5] [19] [21] [22]. Most recommend a D_{n50} at least as thick as the design ice sheet if special care is taken to stone placement, as 3 times the ice thickness can lead to an impractically large stone requirement [16] [18] [22].

2.4 Ride-up and pile-up

2.4.1 Definition

Ice ride-up occurs as ice is pushed against a sloping structure and pieces of ice slide up the slope. Unimpeded ice can ride-up large distances; this is especially true for shallower slopes such as beaches. When ice rides up past the crest of the slope, it is called ice encroachment or over-ride [11] [16].

Ice pile-up typically occurs from instabilities during the ride-up process causing the rubble to slide down the structure and onto the advancing ice sheet. That is, rather than moving up the slope, the ice rubble piles up into a mound [10] [11]. For smooth slopes, instabilities usually occur where there is a change in slope angle either causing the ice to rotate and fall or generating sufficient compression (i.e. back pressure) between the individual ice pieces (*see Figure 2-8*) [10]. For smooth slopes, it is recommended that the engineer designs the structure to induce pile-up at the waterline [10] [11]. For irregular slopes – such as rubble-mound breakwaters – irregularities in the surface cause the instabilities in a similar manner – that is, rotating the ice or generating sufficient compression.

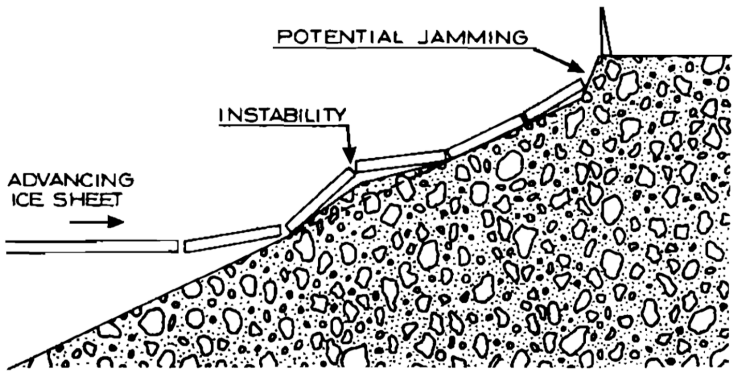

Figure 2-8 Simple schematic showing how an instability is formed due to irregularities in the slope or surface [10].

When talking about pile-up, a few characteristics are often discussed. The keel is the part of the pile below waterline, and the sail is the part of the pile above the waterline. A well-developed keel (i.e. one that has existed sufficiently long enough for thermodynamic effects to be observed) has two different layers: a consolidated layer and an unconsolidated layer. The

consolidated layer consists of ice rubble that has partially solidified as the rubble is frozen together. In the unconsolidated layer, these fusion bonds are weak and easily broken. Lastly, a rubble pile has a porosity; similar to the porosity used in geotechnical engineering, it is the volume of voids (i.e. water or air) over a representative control volume for the pile. A typical way to determine the volume of voids is to find the volume of ice within the control volume and subtract it from the total volume [11] [16].

2.4.2 Effect on structures

While ride-up has a force associated with it (H_R, above), this force is rarely discussed by itself, as it is a contributing part of a whole. The maximum ride-up height, however, is often discussed and is needed in designs in order to ensure encroachment does not occur. Encroachment can cause significant damage to the infrastructure the slope is protecting (e.g. topsides, buildings, cables). Therefore, it is strongly recommended to either design the structure to impede ice ride-up or ensure that the minimum crest height is sufficient to prevent encroachment [10] [11] [16] [19].

Pile-up can have both a negative and positive affect on sloping structures. At first, as the pile thickness increases, the ice loads increase both globally and locally. Once a pile becomes grounded, the grounded rubble can protect the structure from ice and absorb some of the incoming ice loads – actually decreasing the loads experienced by the structure [5] [16]. However, laboratory tests have shown grounded rubble can create a smooth ramp with a shallower slope over the structure, thus increasing ride-up or causing encroachment (Figure 2-9) [16]. Finally, rubble width and thickness can grow to the point where support vessels can no longer safely operate near the ice rubble; if this is at the entrance to a port, this could cause the port to close until the rubble is cleared [16].

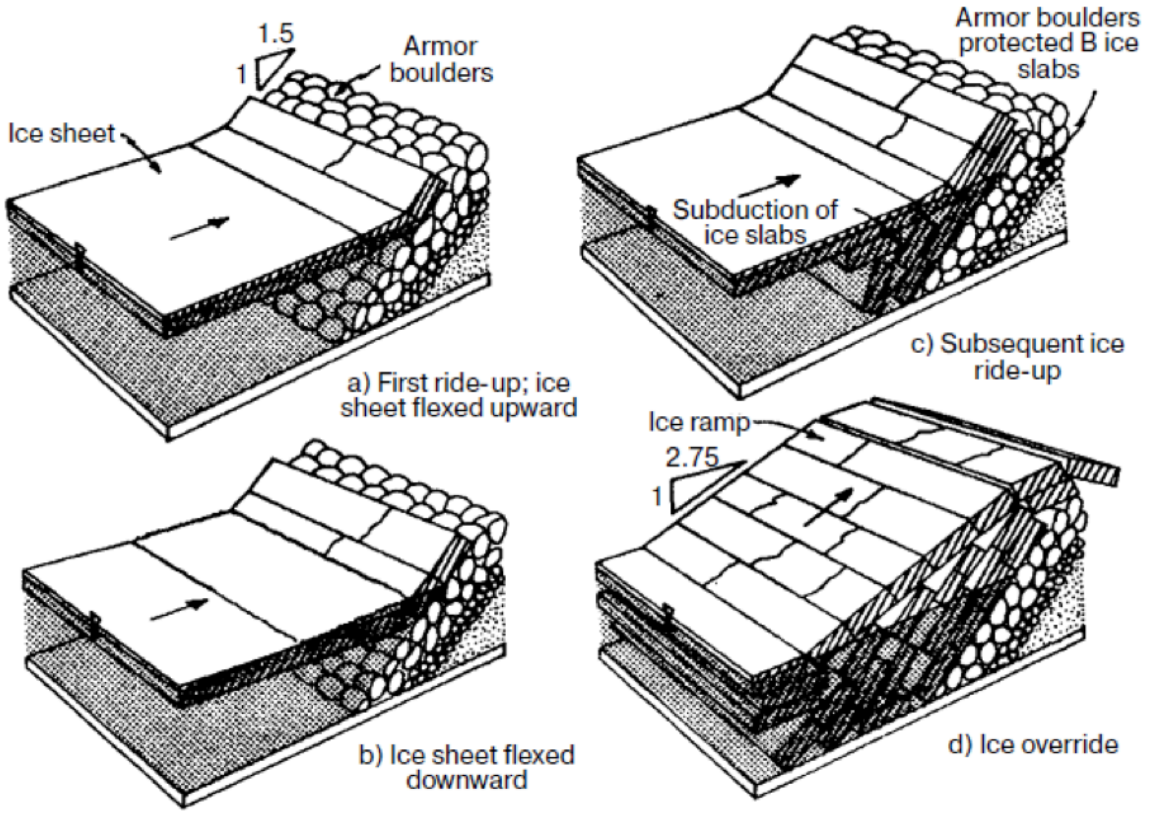

Figure 2-9 Grounded ice creating an ice ramp leading towards increased encroachment [23].

2.4.2.1 Grounded vs non-grounded pile-up

Floating rubble piles increase the global load on a sloping structure in two ways: (1) increased environmental forces due to the greater projected area and added mass, and (2) changing the ice failure mode from bending to crushing. While the increased load due to environmental forces should be accounted for, it is not as detrimental as the change in failure modes. As aforementioned, by changing the failure mode to crushing, the force on the structure increases significantly. Some of the largest forces a sloped structure experiences occur after the formation of a floating rubble pile [1] [11].

While floating rubble piles increase the load experienced by the structure, grounded rubble piles tend to decrease the load on the structure. Grounded piles are those that have significant interaction with the sea bed. Rather than just ice-structure interactions, the problem now becomes ice-structure-bed interactions, as a significant portion of the force from the advancing ice sheet is now transferred to the bed. It is commonly believed that grounded piles – once large enough – provide sufficient sliding resistance to act as a protecting barrier to the structure from later-season, thicker ice, with some studies claiming late-season ice loads were

negligible in the presence of a grounded pile. Because the pile thickness must grow large enough to interact with the bed, grounded rubble piles occur in shallow waters [1] [24] [25].

2.4.3 Ride-up: Analytical solution [10]

In 1994, F. Christensen proposed an analytical model for determining the maximum ride-up a structure will experience for a given ice condition. In his method, he suggests checking two different scenarios analogous to the limit force and limit energy mechanisms.

In the limit force scenario, he balances the driving forces (i.e. current and wind, Eq5) to the restoring forces (i.e. gravity and friction, Eq6). As long as the driving force is greater than the restoring force, ride-up will occur. After rearranging and basic trigonometry, the ride-up height (h_{ru}) is found in Eq7.

$$F_e = F_w + F_c = 0.003A_{sfc}(\rho_a V_{10}^2 + \rho_w u_c^2) \quad \text{Eq5}$$

$$R = L_{beach}\gamma_i b h_i(sin\alpha + \mu_{is}cos\alpha) \quad \text{Eq6}$$

$$h_{ru} = \frac{F_e}{\gamma_i b h_i(\mu_{is}+tan\alpha)} sin\alpha \quad \text{Eq7}$$

F_e is the environmental load. F_w and F_c are the wind and current components of the environmental load, respectively. A_{sfc} is the surface area of the floe for skin drag. ρ_a is the air density. V_{10} is the mean air velocity measured at 10 m above the surface, and u_c is the mean water velocity (current) at the surface. R is the total resistance force acting against F_e. L_{beach} is the length of beach along the slope that is experiencing ride-up. γ_i is the specific weight of ice. b is the width of the ice floe or slope. α is the angle of the slope. μ_{is} is the ice-structure friction. h_{ru} is the maximum ride-up height.

In the limit energy scenario, he balances the initial kinetic energy of the advancing ice sheet (Eq8) to the work during ride-up (Eq9). After rearranging, simplifying, and basic trigonometry, h_{ru} is found by Eq10.

$$E_K = \frac{(1+C_m)}{2} L_{sheet} b h_i \rho_i v_i^2 \quad \text{Eq8}$$

$$W = 0.5L_{beach}^2 \gamma_i b h_i(sin\alpha + \mu_{is}cos\alpha) \quad \text{Eq9}$$

$$h_{ru} = \sqrt{\frac{(1+C_m)L_i v_i^2}{g(sin\alpha+\mu_{is}cos\alpha)}} sin\alpha \quad \text{Eq10}$$

E_K is the kinetic energy of the floe, C_m is the added mass coefficient for the floe based on the shape of the floe. L_{sheet} is the length of ice sheet, ρ_i is the density of the ice (floe), and v_i is the floe's initial velocity. W is the work performed by moving ice up the slope.

During his derivation, Christensen acknowledges that energy losses due to breaking the ice, deforming the ice due to crushing, and heat are not accounted for and can be significant with steeper slopes, thus this estimation is conservative and is typically seen as a good approximation of an upper bound. One limitation of this approach comes in the assumption that ice ride-up is uniform as it covers a structure. As irregularities in the surface and differences in the size of rubble can cause instabilities along the slope, this assumption is not always the case – leading to irregular pressure distributions along the structure.

2.4.4 Pile-up: Analytical solutions

Where ride-up can easily be characterized by ride-up height, there is not one simple metric that can describe rubble piles. Rubble piles – and the force they are capable of applying to a structure – depend on several properties of the pile: the height of the sail, the depth of the keel, the height of the entire pile (if dry), and the porosity of the pile are the four main characteristics of the pile for load estimations [11] [24].

2.4.4.1 Sail height, keel depth, and pile height

For floating piles, the depth of the keel (h_k) and the height of the sail (h_k) are related to one another and estimated by statically balancing buoyancy with gravity. The main assumption here is that the porosity in the keel is approximately the porosity of the sail, which is a fairly safe assumption for newly-created piles where the keel has not yet frozen in a consolidated layer. Eq11 shows this relationship [24].

$$\frac{h_s}{h_k} = \frac{\rho_w - \rho_i}{\rho_i} \qquad \text{Eq11}$$

h_s is the height of the sail, and h_k is the depth of the keel.

Please note that Eq11 does not provide a way to predict either keel depth or sail height during an ice event; rather, it provides a way to estimate one if the other is known. To this author's knowledge, there is no accepted way to predict the keel depth or sail height for grounded rubble piles.

However, if pile-up is occurring on the slope above the waterline, there are methods used to predict the total rubble-pile height. Two methods commonly used represent the minimum

and maximum extremes in prediction: Allen's formula and Kovacs and Sodhi's formula, respectively. The key difference between the two methods is whether the advancing ice sheet lifts the ice pile-up (Allen's formula) or if it rides up the pile slope (Kovacs and Sodhi's formula) [10].

Allen's formula (Eq12) assumes the advancing ice sheet must overcome the gravity of the entire rubble pile as the sheet pushes the pile-up. When comparing it to field observations, Allen's formula provides reasonable results when the driving force (F) is limited to the horizontal failure load of the advancing ice sheet [10].

$$h_p = \left(\frac{2F}{\gamma_p b \left(1 + {}^{\varphi_p}/_{tan\theta}\right)} \right)^{0.5} \quad \text{Eq12}$$

h_p is the height of the pile, γ_{pile} is the specific weight of the pile including ice and air, φ_p is the coefficient of internal friction within a rubble pile, and θ is the angle of the slope of the pile with respect to horizontal.

Kovacs and Sodhi's formula (Eq13) assume the advancing ice sheet must overcome only the gravity of the advancing ice itself as the sheet rides up the pile. When comparing it to field observations, Kovacs and Sodhi's formula provides reasonable results when the driving force (F) is limited to the environmental loads on the ice at rest [10] [24].

$$h_p = \frac{F}{\gamma_i b h_i (\mu_{ii} cot\theta + 0.5\Omega)}, \{1 \leq \Omega \leq 2 \quad \text{Eq13}$$

Where Ω is a factor based on pile and slope geometry; please see [10] for more details on determining Ω.

2.4.4.2 Porosity

To the knowledge of this author, there are no formulas to predict or estimate the porosity of a rubble pile. Rather, field observations are used to find ranges. According to ISO19906, keel porosities typically range from 0.1 to 0.5 depending on the age of the keel and its depth [11]. However, no information is available for the porosity of newly created rubble piles, and values above 0.5 could be possible.

3 Numerical Models for Arctic Coastal Structures

3.1 Current and historical models

Researchers have been using numerical models for Arctic, coastal engineering since the 1990s. Mark Hopkins developed a two-dimensional (2D), discrete element method (DEM) numerical simulator to determine pile-up height and force on a sloped structure. The model uses a Mohr-Coulomb plastic yield criterion in order to predict the fracture of ice and the subsequent rubble generation. Using this model, he compared the results to both analytical solutions and small-scale physical tests. While the results were promising, both the above-water pile height and force on the structure were underestimated by his simulations [26] [27].

In the 2000's, A. Barker used a Particle-in-cell (PIC) model for ice-structure interaction issues. Combining discrete elements with a continuum rheology following a Mohr-Coulomb plastic yield criterion similar to Hopkins, force equations are solved over a fixed grid to predict rubble generation (bending failure), pile-up, and global loads on a structure. Unlike most other models to date, Barker's model is 3D. It was used to simulate conditions in the North Caspian Sea and test the efficacy of an ice protection barrier for a barge-like structure. This model is able to fairly accurately represent pile-up height and global loads for both floating and grounded piles. However, this model does not analyze local loads or damage to the breakwater itself [6].

In 2011, Jani Paavilainen published the results of a 2D finite-discrete element method (FEM-DEM) for ice on wide, sloping structures with a focus on offshore structures. In his approach, the ice sheet fracture was modelled using the FEM with the rubble pile response and ice loads on the structure using a DEM method – setting it apart from Hopkins's or Barker's DEM fracture analysis. In addition to bending failure, Paavilainen also models crushing force and energy loss but not further ice deformations. Over a series of tests, peak ice forces and structural responses were well represented at both model and prototype scales. However, global loads on the structure were highly variable with major force drops present; they concluded these force drops were due to the lack of rubble deformation caused by crushing as the ice sheet moved into the simulated pile. Most importantly for coastal engineering applications, unlike the previous methods, the model assumes water sufficiently deep enough that grounding is not present [24] [28] [29].

Instead of focusing on pile-up height and global force, some researchers decided to focus on other aspects of ice-breakwater interactions. Lengkeek et al. used 2D Plaxis geotechnical

software to model and evaluate the risk of rubble-mound breakwater failure modes like decapitation and edge failure. This was tuned for a specific site, but it showed that readily available simulators can be used for some of the global failure modes associated with riprap and ice. Plaxis was not used to estimate local loads on the armor unit or aid in armor unit design [5].

Rather than analyzing riprap failure, McKenna et al. implemented an empirical, probabilistic model for functional failures associated with ice pile-up. Their model estimated downtime and escape, evacuation and rescue impairment due to extreme pile-up for a specific location in the North Caspian Sea. This was used to help optimize breakwater design and orientation to minimize functional failure, but it did not analyze global or local loading on the breakwater itself [4].

While the method used by McKenna was able to analyze damage to a breakwater, none of the aforementioned models can be used to help determine the size of stone needed in the armor layer. As previously discussed in 2.3.3, the range of armor stone sizes suggested is wide, and this is a subject that needs to be better understood in order to properly design Arctic coastal protection with riprap.

3.2 Simulator for Arctic Marine Structures (SAMS)

3.2.1 Background

First released in 2017, the Simulator for Arctic Marine Structures (SAMS) is a software package primarily designed to estimate ice loads on Arctic structures. SAMS was created by combining several independent projects developed at the Norwegian University of Science and Technology (NTNU) hosting the Centre for Research-based Innovation – Sustainable Arctic Marine and Coastal Technology (SAMCoT). In general, the independently developed projects covered simulating multi-body dynamics, fracture, and hydrodynamics as they relate to ice. Since their initial development, all of the projects have been standardized and refactored to form modules within SAMS for a seamless integration in one software suite. Today, SAMS is developed and maintained through Arctic Integrated Solutions AS (ArcISo) in partnership with NTNU [30].

Because the problem of multi-body contact analysis associated with broken ice fields is highly nonlinear, SAMS is modelled in the time domain (similar to the aforementioned models above). Bodies in SAMS can be rigid (e.g. structures) or visco-elastic (e.g. ice). As a full 3D simulator, bodies have 6 Degrees of Freedom (6DoF) by default. Fluid dynamics are also

present in the form of buoyancy and drag forces from wind, current, and propeller flow – including both skin and form drag. Friction is present, but SAMS does not differentiate between static and dynamic friction [30] [31]. Crushing, radial cracking, and circumferential cracking failure modes are implemented, but the bending failure associated with wide sloping structures is not [30].

3.2.2 Technical information

Simulating ice-structure interactions is a nonlinear process whose complexity is increased by factors such as: many simultaneously contacting bodies, complicated body geometries, non-uniform and highly variable material properties, multiple fluid dynamic effects, and multiple forms of fracture utilizing different material strengths. Advances in numerical methods have made these types of simulations possible [30] [32].

SAMS uses non-smooth discrete element modelling (NDEM) – a subset of DEM – to calculate the reactions between ice floes, structures, and domain boundaries. NDEM allows larger time steps compared to smooth discrete element modelling (SDEM) while remaining numerically stable but at the sacrifice of processing time during each time step [30] [32]. SAMS couples NDEM with an implicit time integration scheme based on the Newmark-Beta method with constant acceleration assumed throughout a time step. The combination of implicit integration with NDEM has led to the coining of the term "implicit discrete element modelling", and, to this author's knowledge, SAMS is the first and only ice simulator utilizing implicit discrete element modelling. This method of modelling allows SAMS to retain a high level of accuracy for both visco-elastic and rigid contacts without numerical dampening for continuous contacts [32].

SAMS is built upon a physics engine for contact detection and force aggregation. A limitation of the contact detection scheme used is that it is difficult and computationally expensive to detect contacts with concave bodies [31]. Simplifying the geometries created during floe generation and fracture can reduce or even eliminate concave bodies from the system, but this limitation needs to be known when generating ice floes and fields to use with SAMS. In general, at the start of a time step: (1) the new positions and contacts for each body are determined, (2) contact types, energy losses due to fracture, hydrodynamics, friction, et cetera are calculated, and (3) positions are corrected to account for the energy losses during the time step [31].

The type of ice failure is not determined at the start of the time step but rather is an output during the second phase described above. Ice failure modes accounted for are narrow-body bending failure (i.e. radial and circumferential cracking), crushing, and splitting. Analytical solutions are used when possible to decrease computation time – as opposed to methods like those utilized by Paavilainen et al. Contacts are first checked if bending is possible based on parameters such as floe mass, velocity, and contact type (i.e. ice-structure contacts). Analytical solutions have been developed and validated over a series of publications by Lu et al. [30]. These narrow bending failures alter the floe definitions and can generate new floes during the simulation. If narrow bending is not possible for the contact, crushing is then analyzed. Unlike narrow bending, crushing does not deform the ice floe definition, but it does apply an energy loss proportional to the contact volume affected by crushing failure [31] [32]. Therefore, crushing within SAMS is valid for local, discontinuous crushing only, and continuous brittle crushing or creep are not valid [32]. How much energy is lost during crushing is configurable through a crushing energy absorption parameter.

3.2.3 Accuracy and validation

The time integration method used in SAMS is the Newmark-Beta method – a second-order accurate method for continuous contacts. However, numerical accuracy describes deviations from the actual solution due to the numerical method and does not describe the accuracy of the solution itself. Each of the analytical solutions have been validated in a series of papers [33] [34] [35] [36] [37]. As a whole simulator combining the numerical methods with the analytical solutions, SAMS has been validated for certain applications using full-scale data.

The Oden Arctic Technology Research Cruise of 2015 provided data from both cameras and sensors used to validate each module independently and collectively. Ice fields were digitally created based on high-resolution, aerial photography during the research cruise, and the mechanical properties of the ice were documented during the trip. Sensors on the icebreaker Oden recorded thruster information, acceleration information from Inertia Motion Units (IMU), position-related information such as speed, heading, and pitch, and weather information such as wind speed. The geometry of Oden was recreated digitally in the form of a Wavefront Object file (*.OBJ) utilizing over 4000 faces. As with ice, the simulated Oden has 6DoF in the validation study [30].

The results between the data collected during the voyage and those simulated through SAMS are statistically satisfactory. The ice load was calculated from a combination of the IMU

and propulsion sensor data due to the difficulty of directly measuring ice loads on ice breakers, thus some error exists in the calculated values and the instantaneous magnitudes of peak forces might not be well represented. That said, the average load between the real-life and simulated data was -13.1%, and peaks were typically on the same order of magnitude. Additionally, the complex interaction of the ice bodies – 6DoF movement, splitting, bending – was observed in both footage from the voyage and within the simulator [30]. This validation study shows that SAMS as a whole is validated for ship-shape structures in floe ice, while previous studies have shown parts of SAMS validated in other areas range. That said, wide, upward-sloping structures like breakwaters have not yet been validated in SAMS.

4 Experiment Design

4.1 Modifications to SAMS

As typical with any model that is used in a way that it was not designed for, modifications to the source code are needed in order to use SAMS with coastal structures. The following changes to the source code were identified and proposed: the body types need to be expanded, the available contact types need to be expanded, compound structures with concave surfaces are needed to simulate riprap on a rubble-mound breakwater, adjustments need to be made for the starting and ending conditions for a non-moving, non-floating structure, and adjustments need to be made to the starting conditions of ice. Additionally, during development, it was determined that some additional minor modifications were needed in order to utilize batch loading for large quantities of simulations.

SAMS uses three types of bodies for its simulation: structure, ice, and tank. The tank bodies produce walls and a floor for confining pressure. There is little configuration available for the tank floor, and any geometry other than horizontal and flat is not available. Therefore, adding a bed body type that can handle more complex bathymetries (e.g. slopes) is required. The bed also needs to be able to interact with the ice in the case of grounded piles, and if global breakwater failures such as sliding are to be simulated, the bed needs to interact with the structure.

In the version of SAMS used in this thesis, contacts always involve ice. As SAMS was originally designed to tow a structure through an ice sheet or field of ice floes, non-ice contacts mean that the structure crashed into the tank wall, tank floor, or another structure. As this situation is outside the scope of the intended use, non-ice contacts were not implemented. However, this is not the case with rubble-mound structures. Rocks in the structure interact with other rocks, and the structure interacts with the bed.

While SAMS accepts compound structures in the form of multiple objects defined through a Wavefront Object file (*.OBJ), these are fixed in relation to each other at the program's initial configuration and cannot interact with each other. This modification is related to the previous two conceptually, but the implementation within the code is different and unrelated.

As SAMS is intended to simulate a floating structure moving through an ice field, the starting and ending conditions respectively require that the structure has a velocity and reaches

the end of the simulated area. For stationary structures with moving ice, different end conditions based on either a maximum simulation time or a minimum velocity threshold across all dynamic bodies. Additionally, in order to better represent the 6-DoF body dynamics for the structure, buoyancy (and the center of buoyancy) are calculated on program initialization, and structures that are negatively buoyant are not allowed. This requirement needs to be removed, and buoyancy initializations need to be updated.

While current and air forces are capable of driving ice in SAMS, an initial velocity is needed to reduce the spin-up time of the simulation.

Finally, as SAMS is under active development, documenting and fixing bugs is within the scope of the project. Other changes, such as changes to fracture mechanics or non-ice body deformations, are outside the scope of this thesis. Please see Appendix B for a changelog of modifications to SAMS made during this project.

4.2 Preliminary tests and their conclusions

4.2.1 Description

An initial testing phase was carried out to both learn the software and to verify basic behavior for wide, upward bending structures. Two categories of initial tests were carried out: sheet ice with fracture mechanics enabled and rigid ice with fracture mechanics disabled. As SAMS is under active development, some conclusions drawn from these tests are applicable to more current versions.

4.2.2 Sheet ice with fracture mechanics

In the initial tests with fracture mechanics, it was discovered that upward bending with wide, sloping structures was not well represented by the version of SAMS used in this thesis, for SAMS was originally developed for shipshape (i.e. narrow) structures, and downward bending has been the focus. At first, upward bending was not possible Figure 4-1. After this was fixed, it was discovered that bending failure only occurred for ice-structure contacts, and a similar situation to Figure 4-1 occurred because the initial ride-up caused all subsequent contacts to be ice-ice.

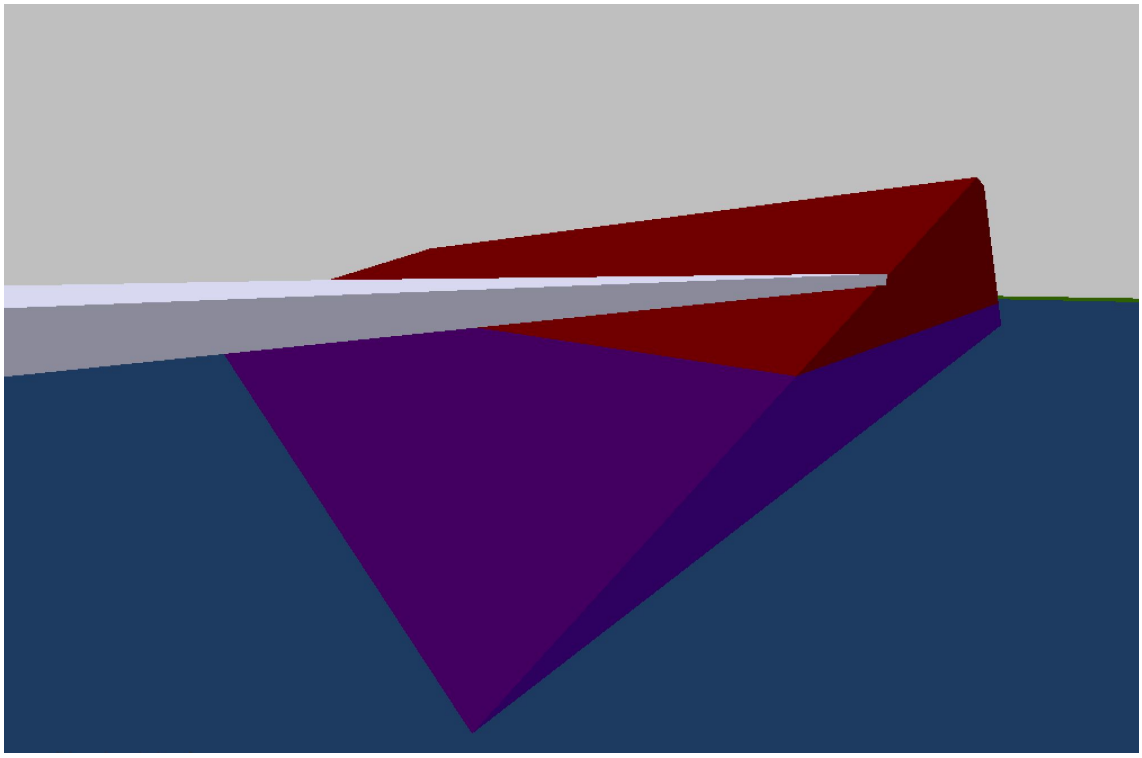

Figure 4-1 Example simulation with upward bending not working. Notice how the ice is out of the water as it rides up the slope without breaking.

Shipshape structures are typically narrow and move through ice – as opposed to coastal structures which are wide and ice moves to the structure. Narrow structures are more likely to cause radial and circumferential cracking originating from the center of mass of the contact area, and wide structures cause bending failure along the width of the structure. Ships typically travel at faster speeds than environmentally-driven ice sheets and floes. Circumferential and radial cracking lengths are related to the speed, and the breaking length for wide bending failure is independent of speed at the velocities associated with ice drift (*see section 2.2.2*). Because the breaking length implemented was modeled for speed-dependent circumferential and radial cracking, it does not represent the size or shape of ice rubble one would expect for wide, upward sloping structures.

Shipshape structures also are downward bending rather than upward bending. With downward bending, ice rubble is more likely to clear a structure, thus ice-ice reactions are limited. While SAMS calculates the nonlinear forces involved with multi-body floes, ice in this version of SAMS only deforms with ice-structure or ice-bed contacts and not ice-ice contacts (*this has since been updated, and ice-ice contacts can cause deformations*).

Because of this, initial tests were performed to check the behavior of SAMS with wide, upward-sloping structures. Unfortunately, the ice behavior modeled by SAMS did not

represent the expected behavior, and it was decided to limit the analysis to rigid body simulations. Therefore, all tests utilizing fracture mechanics could not be performed. The consequence of this limitation is:

1) Local loads and damage to the armor layer cannot accurately be represented, as failure modes other than bending failure are needed for the higher loads found in non-bending failure;
2) Global loads in a pile-up situation might not be well approximated, for deformations caused by the ice sheet advancing through the rubble pile cannot occur; and
3) Grounded rubble might not transfer force to the bed appropriately, as the contact area is limited due to the rigidity of the bodies.

Consequence 1 immediately changes the scope and direction of the source code modifications and experiments, while consequences 2 and 3 means special attention needs to be paid to pile-up to properly validate the results.

4.2.3 Rigid body preliminary tests

After it was determined that fracture mechanics could not be used, pre-broken ice sheets were tested. Originally, the tests described in this section were not intended to be preliminary but rather final tests. When reviewing the results, it was noticed that many simulations experienced extremely low ride-up, as detailed in Table 4-1 Initial ride-up tests with unreasonably low ride-up. Crushing energy absorption was the likely cause and was therefore analyzed in a series of tests. Those results are presented in Table 4-2.

Table 4-1 Initial ride-up tests with unreasonably low ride-up

Slope	**1:3**	**1:4**	**1:5**
Number of Tests	40	40	40
Number with low ride-up	11	7	8
% with low ride-up	28%	18%	20%

Table 4-2 Crushing energy absorption investigative tests.

Crushing Energy Absorption	**1E+05**	**5E+05**	**1E+06**	**2E+06**	**3E+06**
Number of Tests	120	120	120	120	120
Number with low ride-up	5	3	8	13	23
% with low ride-up	4%	3%	7%	11%	19%

It is clear from Table 4-2 that low values of crushing energy absorption were less likely to cause extremely low ride-up. As fracture mechanics were already disabled, tests were carried out to see how low crushing energy absorption could be set. It discovered that this version of SAMS uses the energy loss calculated with crushing energy absorption for ice rotation. In other words, if the crushing energy absorption is too low compared to the ice's mass, ice would not rotate and ride-up the slope. A lower limit was visually determined by watching simulations, and that value is reflected in the configuration parameters described in 4.4.1.

However, as Table 4-2 indicates, reducing crushing energy absorption only reduced the number of simulations that experienced extremely low ride-up. After more tests and observations, it was determined that this only occurred when domain boundaries were used for confining pressure. This happened because, during some simulations, the unbroken ice sheet rotated slightly into the boundary causing extreme energy loss, and the velocity of the sheet dropped to 0 m/s Figure 4-2.

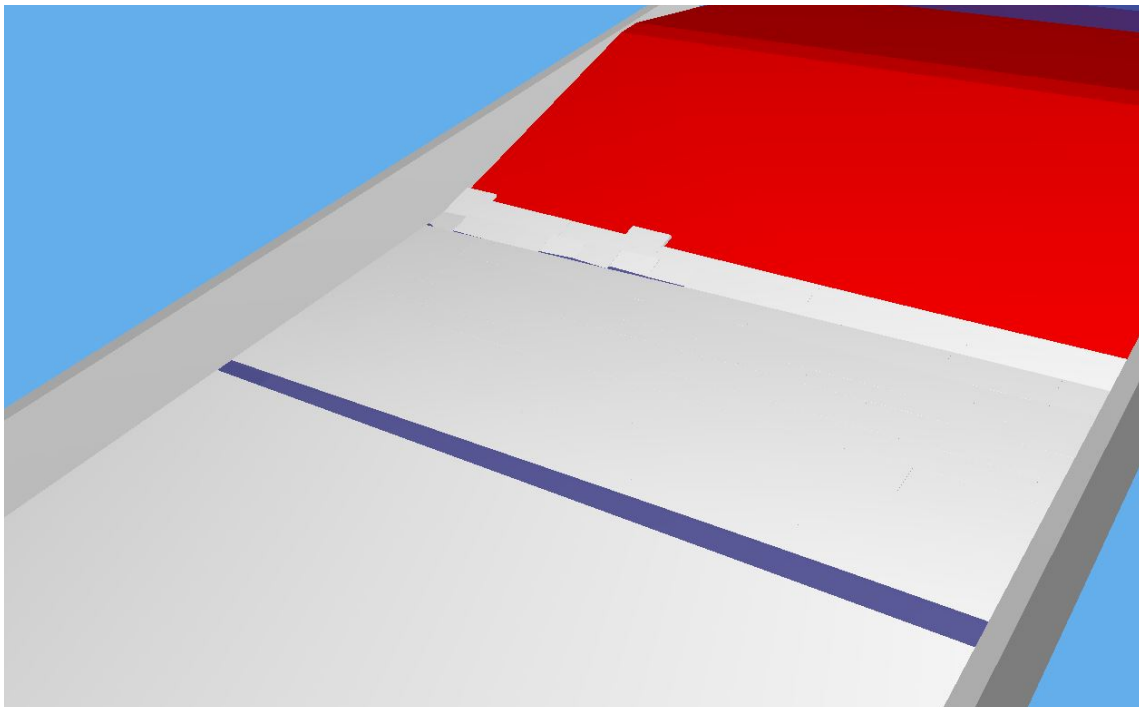

Figure 4-2 An example of ice-sheet separation leading to extremely low ride-up. The separation can be seen in the blue band (water) going across the domain.

The root cause of this is that the boundaries are considered to be a static object – that is, a rigid body with a fixed location – and bodies in SAMS do not bounce (i.e. change direction after a collision) *during* a timestep. Rather, their direction can change *after* their velocity reaches 0 m/s. Because the location of the boundary object is fixed, the only option SAMS has to prevent the ice sheet and the boundary from overlapping is to completely remove the velocity

of the ice sheet. To fix this issue for this thesis, a configuration solution was implemented. The domain boundaries were removed, and confining pressure was introduced by creating massively large ice sheets on either side of the testing area to supply the confining pressure. To this author's best knowledge, this issue has since been fixed within SAMS.

4.3 Configuration scripts

All scripts described in this section were created by the author of this thesis. The source code for these scripts is public domain and available upon request without accreditation or restriction on use.

4.3.1 Breakwater generation

The breakwater needs to be defined in a Wavefront Object file (*.OBJ). In their most basic form, OBJs are a collection of objects composed of vertices and faces created by vertex indices. More complex properties exist – such as face normal vectors and edges – but SAMS disregards these additional properties when loading the OBJ. All objects defined in an OBJ are treated as a single, compound body within SAMS. However, even though its treated as a single body, collisions will still be detected if faces of a body overlap. Therefore, care should be taken when creating complex breakwaters.

Using Matlab, simple and complex breakwaters were generated and saved to an OBJ. The breakwater consists of a core (i.e. trapezoid) and armor. Each armor unit is specified as a new object in the OBJ. Configurable parameters of the breakwater include: height, slope angle, crest width, and armor type. In its current form, the only armor types supported are smooth and cube-type. Each Cube packing densities and orientations can be specified with default values representing those found by randomly placed cubes according to [38]. An example of a cube-type breakwater is shown in Figure 4-3.

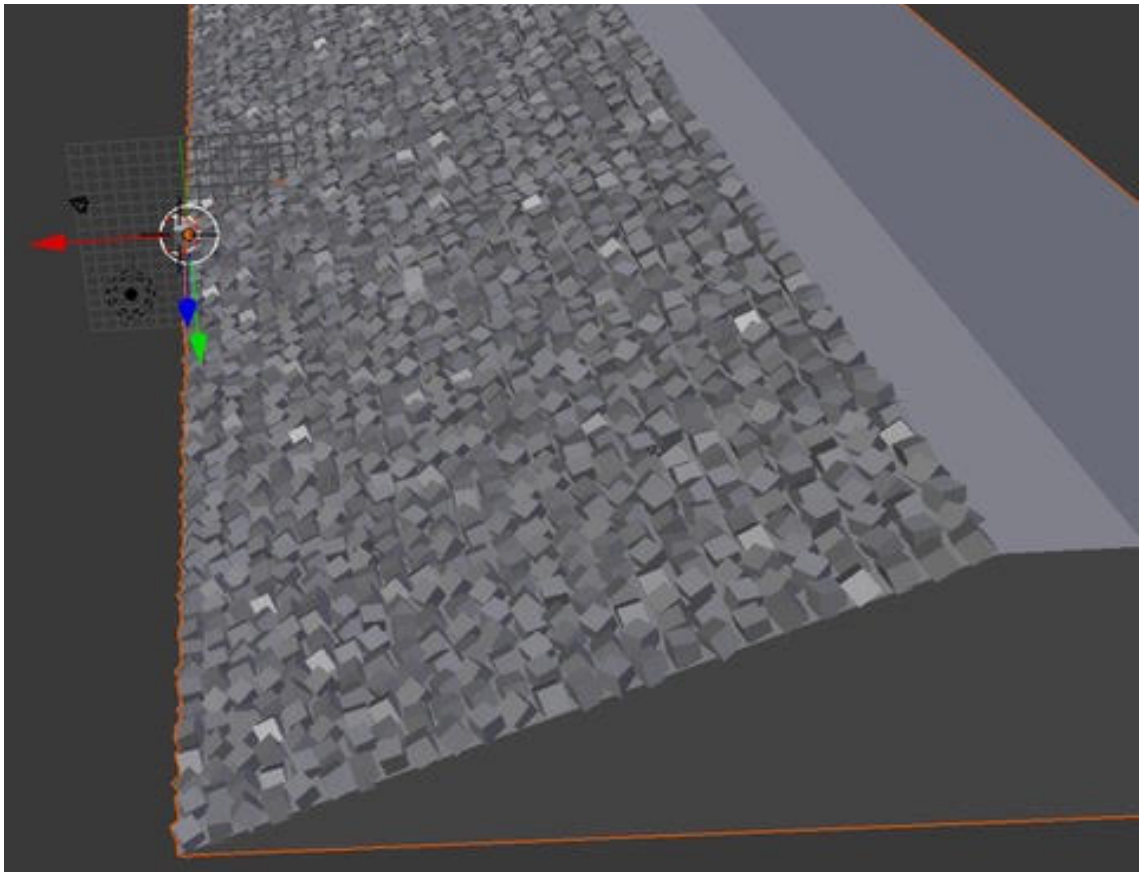

Figure 4-3 Example of a cube-type breakwater generated for use with SAMS

As observed in Figure 4-3, the cubes can overlap with the core or each other, and in this event, collisions will be detected by SAMS. Initially, intra-structure collisions were disabled to avoid contact detection. After preliminary testing proved the rigid-body limitation, it was decided to restrict breakwaters to smooth surfaces, and issues like initially-overlapping within the structure were not addressed. However, the script still proved to be useful for generating the various breakwater widths and slopes used in the tests.

4.3.2 Ice-sheet generation

As discussed above, the experiments are limited to rigid bodies, therefore a way to create a realistically pre-broken ice sheet is needed. Each sheet can contain hundreds of floes, so creating a way to systematically generate ice sheets was needed for the rigid body experiments. SAMS uses JSON to format a proprietary file extension (*.ICE) to configure ice sheets. How to properly define the sheet and floes, their required mass properties, their geometric boundaries, and their locations had to be reverse engineered to eliminate configuration errors. Using Matlab, an ice generation script was developed to generate an ice sheet with realistically-sized ice rubble and a variety of floe geometries.

Elastic plate theory is used to determine the characteristic length (L_c) and the breaking length (L_b) of ice. Eq14 gives estimates on the average and maximum breaking length [1]. Once the average breaking and maximum breaking length was determined, a lognormal distribution was used to randomize the breaking length; lognormal was chosen in order to reduce the left tail while still allowing values up to the maximum predicted size.

$$L_b = l * L_c = l * \sqrt[4]{\frac{Eh_i^3}{12\rho_i g(1-\nu)}}, \begin{cases} l = 0.5\ (avg) \\ l = 0.78\ (\max) \end{cases} \quad \text{Eq14}$$

L_b is the breaking length, l is the ratio between the breaking length (L_b) and the characteristic length (L_c), E is modulus of elasticity for ice, and ν is Poisson's ratio for ice.

To help determine the sensitivity of SAMS to different rubble geometries, three types of geometries can be created: rectangular, trapezoidal, and triangular. The only geometry combination that is mutually exclusive is both rectangular and trapezoidal ice in the same sheet; this was done to ensure all floes are generated without overlap. Triangular geometry was achieved by simply splitting a floe along a diagonal. These basic shapes where chosen as a way to increase or decrease the nonlinear complexity of floe interactions as needed. The geometry type and percent of triangles is specified in configuration. An example output is graphically shown in Figure 4-4 detailing trapezoidal and triangular rubble.

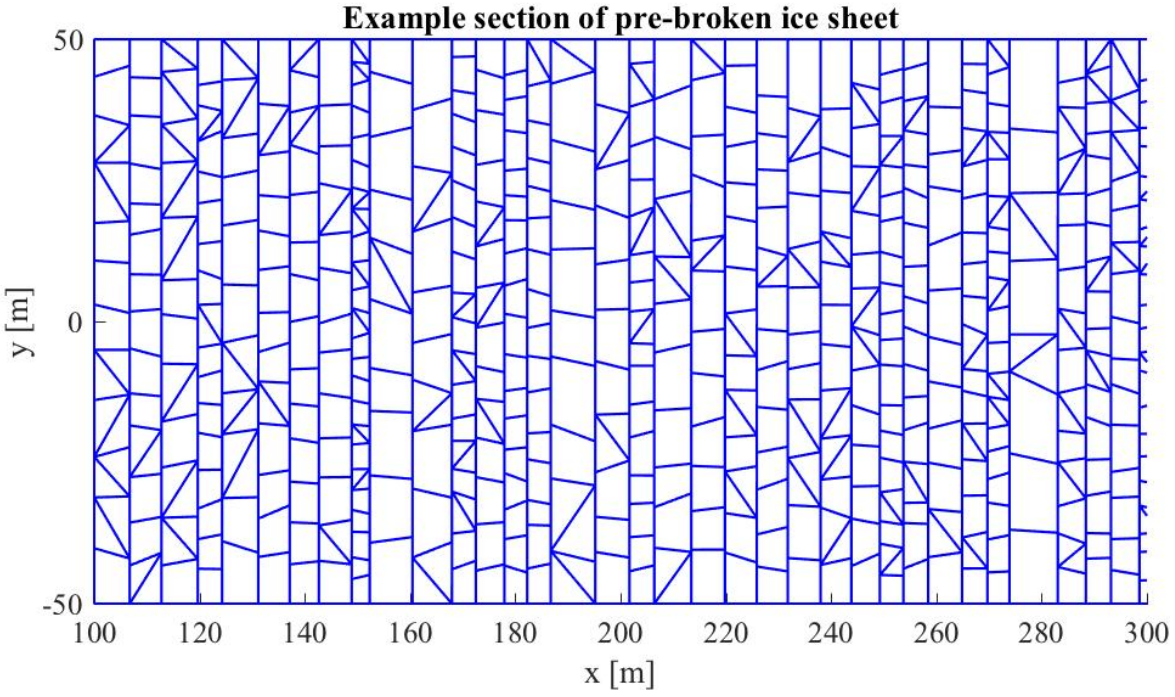

Figure 4-4 Example pre-broken ice sheet generated by a Matlab script.

4.4 Configuration and testing matrix

The experimental design revolved around validating SAMS for wide, upward sloping structures. Due to limitations in the ice failure modes (described in 4.2 above), the final experiments focus on validating base the phenomena of ride-up and pile-up.

While pre-broken ice was used, ice concentrations in the field were set to 100% to approximate a sheet of ice interacting with a breakwater rather than floe ice interacting with a breakwater. Therefore, confining pressure was needed to keep the sheet intact and reduce 3D effects introduced by broken ice.

In keeping with the coordinate convention used in Coastal Engineering, x is the cross-shore direction and y is the longshore direction – that is, x goes away from the breakwater and y along the breakwater. Due to how the pre-broken ice was calculated, the initial ice movement and the current flow is purely in the x direction; oblique tests were not performed Figure 4-5.

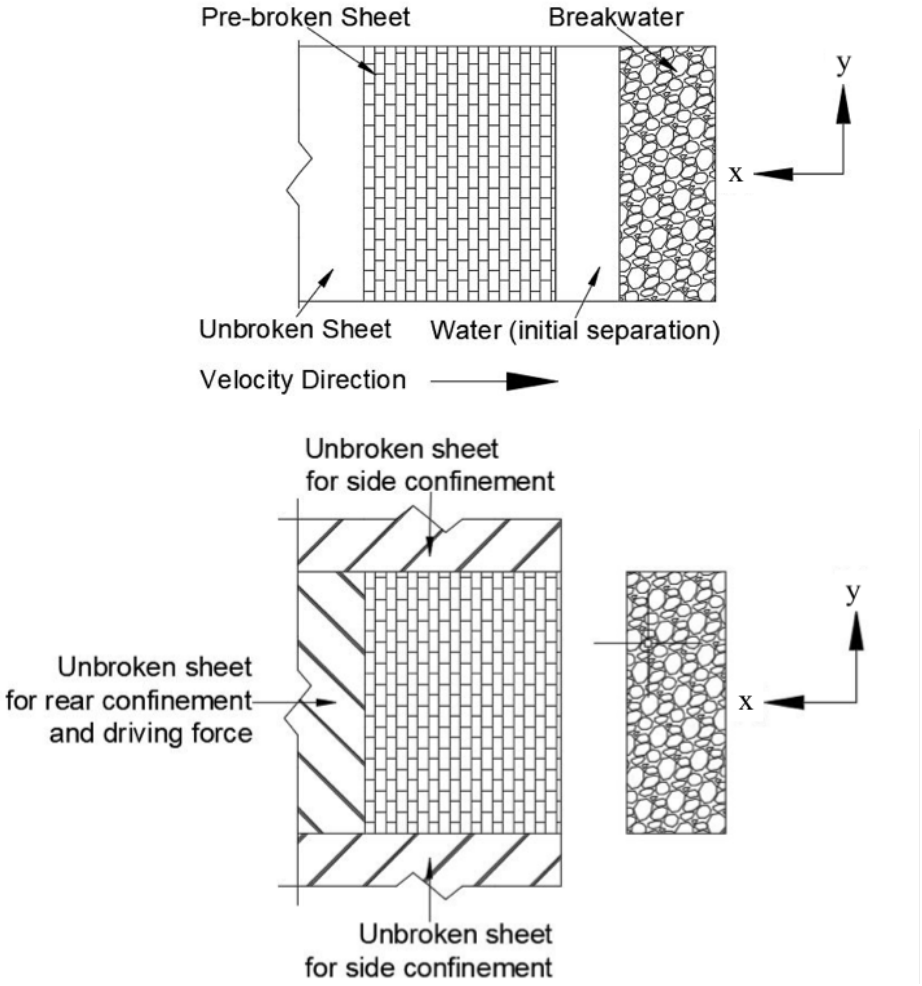

Figure 4-5 Schematic of test setup: Top) Main elements and direction of movement; Bottom) Large ice sheets used for confining pressure

4.4.1 General configuration

General configuration for the tests is summarized in Table 4-3. The values chosen represent values typically found for Arctic engineering with exception to explicitly mentioned below. The timestep used was 0.01 for both ride-up and pile-up. The water depth (4 m) was chosen to represent typical values for the North Caspian Sea.

Table 4-3 General configuration for SAMS used during the experiments.

Parameter	**Value**
Δt	0.01 s
Fracture	FALSE
Confining Pressure	TRUE
ρ_i	900 kg/m^3
h_i	0.15 to 1.0 m
Crushing Energy Absorption	2e6 Pa
E	5e9 Pa
υ	0.3
μ_{ii}	0.15
μ_{is}	0.15
μ_{ib}	0.15
α	1:3 to 1:6
Water Depth	4 m
v_i (x-only)	0.1 to 2.0 m/s
ρ_w	1020 kg/m^3
ρ_a	1.04 kg/m^3
Air-skin Friction	0.003
Water-skin Friction	0.003

A large ice sheet was generated at the end of the broken field to provide a more-constant driving force and confinement on the back side of the ice field. Side confining pressure was generated by creating massively large ice sheets on either side of the testing area rather than by using the domain boundaries.

Crushing energy absorption was kept due to how it influences body rotation within SAMS. The value used for crushing energy absorption was determined during the initial test phase; it represents the lowest value where the ice consistently moves and interacts realistically.

This means that energy losses due to crushing needs to be accounted for when comparing with analytical formulas.

4.4.2 Ride-up

Ride-up tests were decided on to validate ride-up across a range of slopes, ice thicknesses, and velocities as compared to Christensen's analytical model for ride-up. Three slopes, four ice thicknesses, and three velocities were tested for a total of 36 testing conditions. Each breakwater was 100 m wide, and each ice sheet was 500 m long to provide enough driving force to generate statistically-different results across the different conditions. Rectangular ice rubble was simulated in the ice sheets to represent the geometry assumptions of Christensen's model. A summary of testing conditions is in Table 4-4.

Table 4-4 Parameter ranges tested for ride-up validation.

h_i	**[m]**	0.25	0.5	0.75	1
α	**[H:W]**	1:4	1:5	1:6	
v_i	**[m/s]**	1	1.5	2	

Each ice thickness was used to make 40 different ice sheets, and each testing condition was simulated 40 times corresponding to 40 the different ice sheets for that ice thickness. This was done for two reasons. First, the sample size allows statistically-relevant comparisons and conclusions for each testing conditions. Secondly, as each ice sheet is pre-broken, and the generation algorithm uses randomness to vary the rubble size, using many different ice sheets helps identify whether the results were common to the test condition or to the ice sheet itself. The latter was possible because each ice sheet was tested 9 different times – that is, once for each combination of slope and ice velocity.

4.4.3 Pile-up

Originally, the pile-up tests were designed to represent conditions found in the North Caspian Sea, as pile parameters like the sail height and keel depth in addition to the magnitude of force expected is better known. Keeping it to values more similar to the North Caspian Sea lead to a reduction in ice thickness, and 0.15 m was chosen to best represent those conditions [6]. A current velocity of 0.5 m/s was used, as this is representative of current velocities during the primary time ice piles are formed in the North Caspian Sea [6]. A slope angle of 1:3 along with a depth of 4 m was chosen to help induce pile-up at the waterline and form a grounded rubble pile. As testing proceeded, the matrix was modified in order to find a range of parameters that

best approximates rigid-body rubble. Namely, ice sheets with different rubble geometries were used to test SAMS's sensitivity to geometry type, and ice-ice and ice-structure friction were varied.

During the initial pile-up tests and observations made during the ride-up simulations, rectangular rubble tended to stack in a way similar to Figure 2-9 – that is, rubble tended to lie flat against a slope and other pieces of rubble when forming a pile. This resulted in wide and short piles with a porosity approaching 1. Therefore, it was decided that rubble with more complex geometries was needed when simulating pile-up. Two ice sheets were made: one with purely trapezoidal rubble and the other with a combination of trapezoidal and triangular rubble.

Friction in SAMS is limited to contact friction, and no difference is made between static and dynamic friction. Other frictions, such as the internal friction in a rubble pile utilized by Allen's formula, are not present. Therefore, to increase the internal friction, ice-ice friction was incremented in a series of tests.

A series of tests designed to analyze the results of increasing ice-structure friction were also carried out. While these tests increase ice-structure friction beyond the typically accepted values for ice-stone friction, SAMS's sensitivity to ice-structure friction needed to be investigated due to the highly non-linear nature of the dynamics in these problems. Additionally, one idea to approximate irregularly-surfaced breakwaters was to increase the ice-structure friction. Knowing the general trend for increasing ice-structure friction is needed to see if this approximation is feasible.

As an additional difference to the pile-up tests, ice sheet size was increased to 15,000 m to provide a larger volume of rubble and enough driving energy with which to create a rubble pile. The significantly larger ice sheets greatly increased the computation time. To help reduce the number of bodies during the simulation, the breakwater width was reduced to 50 m. Even with reducing the breakwater width, each test took approximately 1 day to complete. This increase in computation time limited the number of tests that could be performed, and a total of 18 test were performed as detailed in Table 4-5.

Table 4-5 Test specifications for pile-up validation

Test Code	μ_{ii}	μ_{is}	ν_i	Geometry
WoT_base	0.15	0.15	0.5	Trapezoidal
WoT_fi0.30	0.30	0.15	0.5	Trapezoidal
WoT_fi0.45	0.45	0.15	0.5	Trapezoidal
WoT_fi0.60	0.60	0.15	0.5	Trapezoidal
WoT_fi0.75	0.75	0.15	0.5	Trapezoidal
WoT_fs0.30	0.15	0.3	0.5	Trapezoidal
WoT_fs0.45	0.15	0.45	0.5	Trapezoidal
WoT_fs0.60	0.15	0.6	0.5	Trapezoidal
WoT_fs0.75	0.15	0.75	0.5	Trapezoidal
WT_fi0.15	0.15	0.15	0.5	Trapezoidal and Triangular
WT_fi0.30	0.30	0.15	0.5	Trapezoidal and Triangular
WT_fi0.45	0.45	0.15	0.5	Trapezoidal and Triangular
WT_fi0.60	0.60	0.15	0.5	Trapezoidal and Triangular
WT_fi0.75	0.75	0.15	0.5	Trapezoidal and Triangular
WT_fs0.30	0.15	0.3	0.5	Trapezoidal and Triangular
WT_fs0.45	0.15	0.45	0.5	Trapezoidal and Triangular
WT_fs0.60	0.15	0.6	0.5	Trapezoidal and Triangular
WT_fs0.75	0.15	0.75	0.5	Trapezoidal and Triangular

As indicated by Table 4-5, pile-up tests were conducted by changing a single variable from the base case with a trapezoidal-only rubble geometry. These simulations were then repeated for the more complex trapezoidal and triangular rubble geometry. Therefore, multi-variable changes (e.g. increasing both ice-ice and ice-structure friction) were not performed.

5 Results and Discussion

5.1 Ride-up

When processing results from each test, the maximum ride-up (h_{ru}) was determined and then aggregated by test situation. Summary statistics for the maximum ride-up across the 36 test situations is presented in Table 5-1 through Table 5-4 – each table representing one ice thickness. The statistics presented are for the maximum ride-up (h_{ru}) calculated in the 40 simulations for each test condition. They include the mean (μ), standard deviation (σ), maximum (max), and minimum (min) in addition to the mean over the expected ride-up (μ/E) and the percent difference ($\%_{Diff}$) from the expected value. Expected values can be calculated from either Eq7 or Eq10, however the limit energy scenario (Eq10) controlled in each situation. Full results for ride-up including the relative $\%_{Diff}$ for each test can be found in Appendix C.

Table 5-1 Ride-up results for 0.25 m thick ice. All applicable units are in meters.

h_i	0.25								
α	1:4			1:5			1:6		
v_i	1.00	1.50	2.00	1.00	1.50	2.00	1.00	1.50	2.00
μ	2.76	4.05	5.10	2.40	3.49	4.72	2.05	3.12	4.22
σ	0.40	0.30	0.72	0.17	0.15	0.19	0.01	0.02	0.01
Max	4.03	4.69	7.10	3.08	3.76	4.87	2.09	3.21	4.24
Min	1.93	2.83	3.66	2.18	3.16	4.08	2.03	3.09	4.19
μ/E	0.91	0.89	0.84	0.92	0.89	0.90	0.89	0.91	0.92
$\%_{Diff}$	9.9%	12.1%	17.6%	8.8%	11.8%	10.5%	11.3%	10.0%	8.7%

Table 5-2 Ride-up results for 0.5 m thick ice. All applicable units are in meters.

h_i	0.5								
α	1:4			1:5			1:6		
v_i	1.00	1.50	2.00	1.00	1.50	2.00	1.00	1.50	2.00
μ	2.56	3.88	5.21	2.15	3.35	4.56	1.89	2.93	3.99
σ	0.28	0.39	0.39	0.10	0.11	0.10	0.07	0.06	0.01
Max	3.17	5.03	6.07	2.47	3.90	4.91	2.30	3.25	4.01
Min	1.94	2.78	4.11	1.71	2.97	4.24	1.86	2.9	3.97
μ/E	0.84	0.85	0.86	0.82	0.85	0.87	0.82	0.85	0.87
$\%_{Diff}$	17.2%	16.3%	15.6%	19.4%	15.9%	13.9%	19.4%	16.2%	14.3%

Table 5-3 Ride-up results for 0.75 m thick ice. All applicable units are in meters.

h_i	0.75								
α	1:4			1:5			1:6		
v_i	1.00	1.50	2.00	1.00	1.50	2.00	1.00	1.50	2.00
μ	2.42	3.83	5.06	2.05	3.17	4.38	1.76	2.80	3.85
σ	0.37	0.65	0.52	0.16	0.23	0.26	0.02	0.02	0.02
Max	3.45	5.44	6.31	2.43	3.32	4.82	1.80	2.84	3.89
Min	1.63	2.25	3.82	1.21	1.94	3.08	1.72	2.75	3.81
μ/E	0.80	0.84	0.83	0.78	0.81	0.84	0.77	0.81	0.84
$\%_{Diff}$	22.7%	17.5%	18.5%	24.4%	21.3%	17.7%	26.5%	20.7%	17.7%

Table 5-4 Ride-up results for 1.0 m thick ice. All applicable units are in meters.

h_i	1								
α	1:4			1:5			1:6		
v_i	1.00	1.50	2.00	1.00	1.50	2.00	1.00	1.50	2.00
μ	2.22	3.31	4.73	1.93	3.05	4.26	1.62	2.67	3.71
σ	0.26	0.84	0.81	0.14	0.21	0.12	0.01	0.01	0.02
Max	3.06	5.66	6.58	2.55	3.69	4.91	1.68	2.72	3.75
Min	1.56	2.11	3.48	1.88	1.88	3.97	1.61	2.65	3.69
μ/E	0.73	0.72	0.78	0.74	0.78	0.81	0.71	0.77	0.81
$\%_{Diff}$	31.4%	32.0%	25.1%	30.0%	25.1%	20.7%	34.5%	25.7%	21.5%

In general, the ride-up results match well to Christensen's model for ride-up height with an overall percent difference of 18.9% across all tests. When looking at Table 5-1 through Table 5-4, it is evident that thicker ice or steeper slopes deviate more from the expected value than thinner ice or gentler slopes, and that faster velocities tend to have greater ride-up than slower velocities.

To help visualize the data, each unique slope and velocity was plotted in a series of violin plots alongside the predicted value from Eq10. Distributions shown in the violin plots are empirically determined and include all ice thicknesses for each slope and velocity combination. Combining all of the ice thicknesses for the distribution information was done to help clearly convey as much information as possible. Because the mean for each ice thickness is still displayed, trends in ice thickness can still be seen. These violin plots are found in Figure

5-1 through Figure 5-3 for ride-up vs slope and Figure 5-4 through Figure 5-6 for ride-up vs velocity.

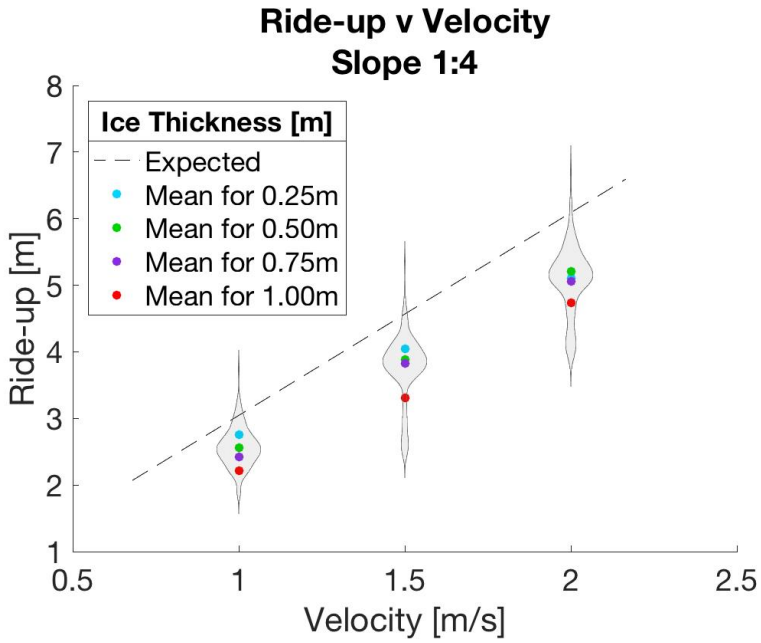

Figure 5-1 Ride-up v Velocity violin plot for 1:4 slope

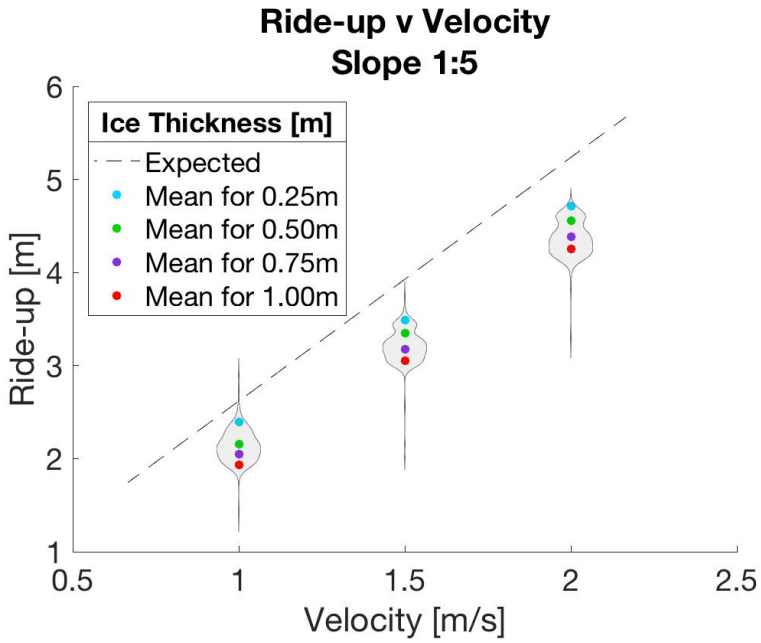

Figure 5-2 Ride-up v Velocity violin plot for 1:5 slope

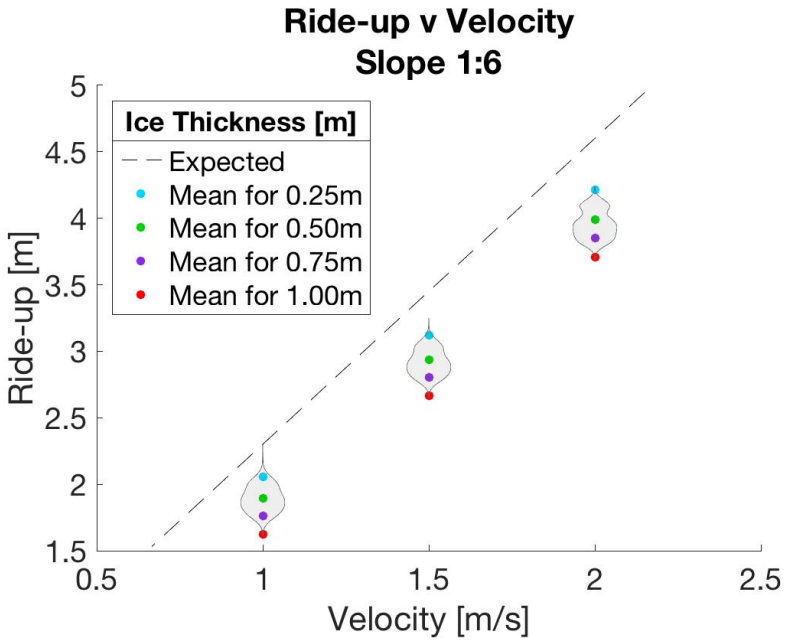

Figure 5-3 Ride-up v Velocity violin plot for 1:6 slope

As evident in Figure 5-1 through Figure 5-3, the range of each distribution is wider for steeper slopes, but the range of means for the different ice thicknesses is approximately equal across a particular slope. Additionally, the distribution density is highest around the means for each ice thickness. This means that, within SAMS, steeper slopes can cause more extreme ride-ups, but over a large number of tests the mean value for ride-up converges to a narrower range.

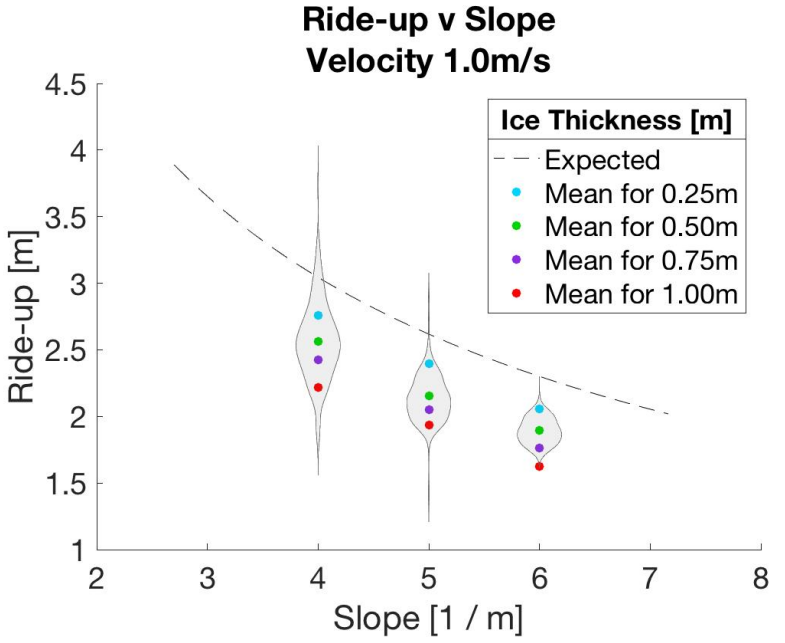

Figure 5-4 Ride-up v Slope violin plot for 1.0m/s velocity

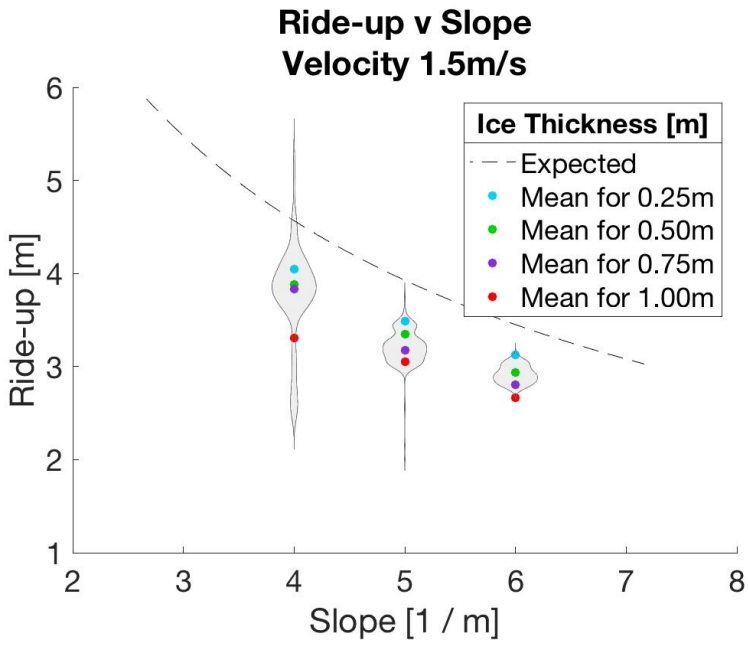

Figure 5-5 Ride-up v Slope violin plot for 1.5m/s velocity

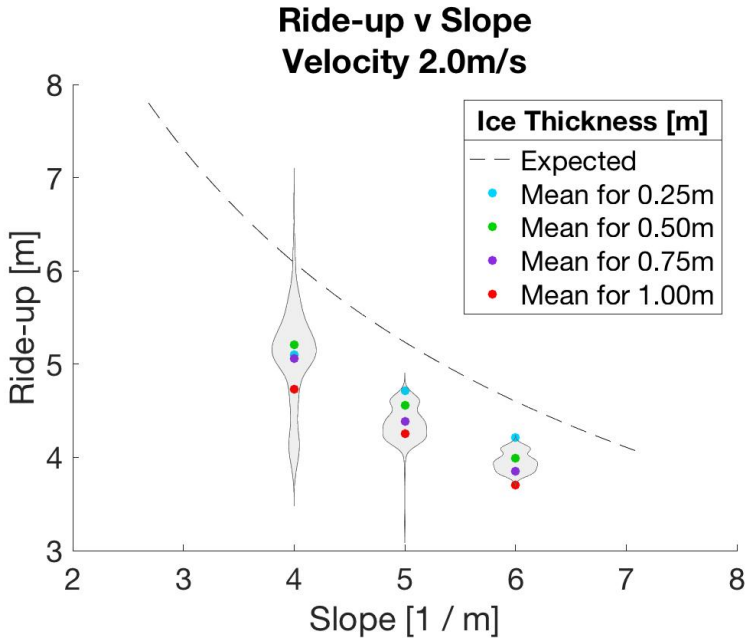

Figure 5-6 Ride-up v Slope violin plot for 2.0m/s velocity

The above conclusion is also evident in Figure 5-4 through Figure 5-6, however one can now see that the range of means for ice thicknesses appears to decrease with a decreasing slope in addition to the range of data in general. This suggests that at a shallow enough slope, ice thickness will have little effect on the simulated ride-up. This behavior can be explained by crushing energy losses and overlapping volumes.

As aforementioned, SAMS uses crushing forces to aid in floe movement and orientation, and Christensen's method ignores the effects of energy losses due to ice failure. SAMS calculates crushing energy loss through the overlapping volume of two bodies. With both steeper slopes and thicker ice, there is a larger overlapping volume as the ice rotates and begins to move up the slope (*see Figure 5-7*). Hence, SAMS typically simulates higher energy losses due to crushing for thicker ice or steeper slopes. This energy loss is real, and Christensen himself acknowledges that it can be significant in steeper slopes. Therefore, while this means SAMS simulates values further from the expected, its application of crushing energy losses is closer to reality than Christensen's model with regards to slope steepness. However, full-scale data is difficult to obtain, and this increased crushing might nor might not be the case with regards to ice thickness.

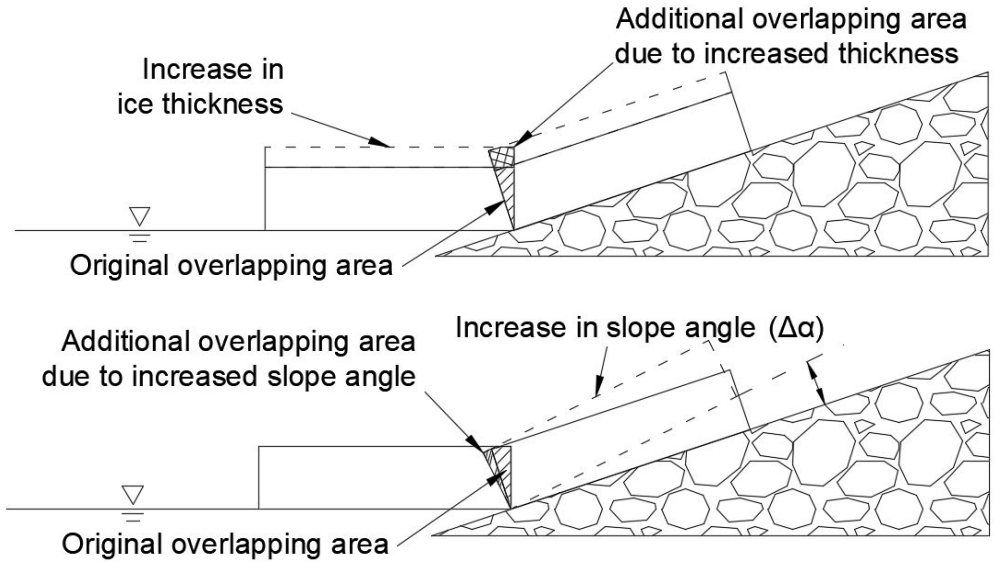

Figure 5-7 Schematic showing how increased ice thickness (top) and or increased slope angle (bottom) increases the contact volume as ice starts to move up a slope.

In addition to crushing energy losses, further slope-dependent ride-up differences can be explained by assumptions in the analytical model. Christensen's model is simplified to a 2D scheme. One of the assumptions caused by this is that the pressure distribution across the breakwater is constant, and that ice coverage along the slope is constant. Back pressure causing instabilities leading to localized pile-up are more common with steeper slopes. In other words, the steeper the slope, the greater the back pressure, the more likely an instability will cause rubble to slide down and start to generate pile-up. Additionally, because higher velocities will have greater driving energies, larger back pressures are expected, which makes instabilities and pile-up more likely to occur. Figure 5-8 shows an example simulation with localized pile-up and an uneven pressure distribution at the waterline.

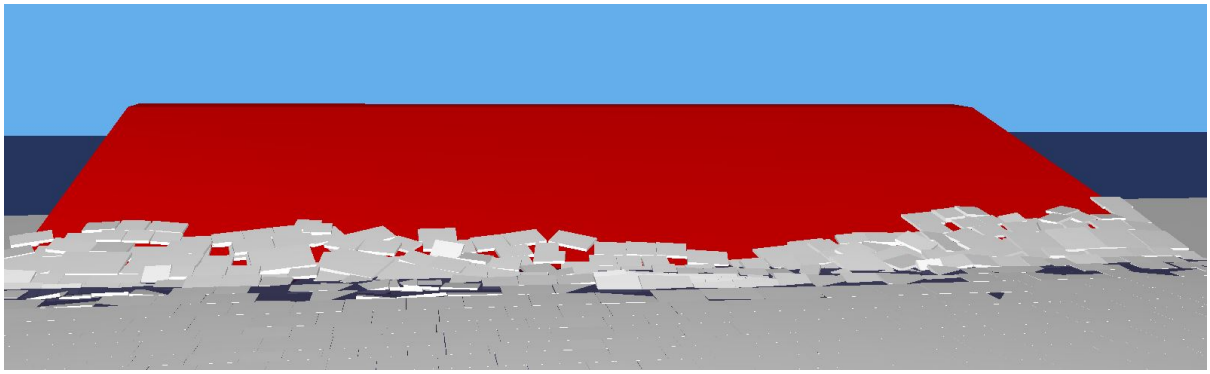

Figure 5-8 Example SAMS ride-up output showing localized pile-up leading to a non-uniform pressure distribution at the waterline.

In either case, localized pile-up leads to an uneven pressure distribution at the waterline. Areas that are not yet experiencing pile-up will have higher pressures, as some ice along the slope will be in contact with the driving energy while other areas lose their connection. Thus, these areas with higher-than-predicted pressure will have higher ride-up heights. This helps explain the greater variability and higher maximums observed with steeper slopes. Again, SAMS seems to better represent real-world situations than Christensen's model.

5.2 Pile-up

As aforementioned in 4.4.3, in all of the following tests, the structure used had a 1:3 slope, the ice thickness was 0.15 m, and the depth is at 4 m. The velocity was 0. 5 m/s. For a full list of the configuration parameters, please refer to 4.4.1. Force and sail height plots include average values found for similar conditions in the North Caspian Sea as reported in [6]. Porosity plots include the ISO19906 suggested range for porosity in rubble piles [11].

Directly comparing the simulated force to any analytical formula (such as Eq1) or even to observed values is extremely difficult and should be done with caution. This is largely due to the differences in the experimental design and reality – namely the rigid body limitation. This limitation essentially makes the ice floe ice at 100% concentration rather than sheet ice. Analytical formulas assume – and observations are made with respect to – sheet ice rather than floe ice. Aside from using bending strength in its primary term (H_B), Eq1 assumes sheet failure occurs at the ice-structure interface; this assumption means the other terms are not represented when ice always stacks up against the pile's edge. That said, the average observed value for similar conditions is included as a reference and order of magnitude check.

The average porosity was determined by calculating the volume of submerged ice in a control volume. A minimum ice volume and keel depth were put in place to make sure the

rubble pile was developed enough to calculate porosity. The control volume went up to but not beyond the waterline, thus only the keel porosity was determined. Finally, the control volume was limited to no more than 50 m from the toe of the breakwater; this helped reduce the 3D effects of the current clearing the rubble from the edges. The limits are graphically shown in Figure 5-9 along with a potential source of error due to using a rectangular control volume.

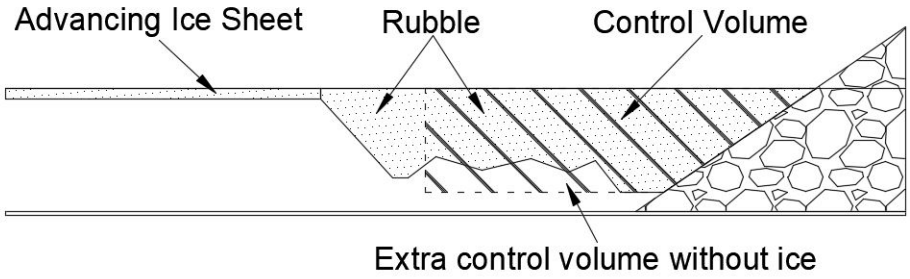

Figure 5-9 Schematic showing the limits of the control volume for porosity calculations

Whether or not ice was inside the control volume was based on the ice rubble's center of mass. While using the center of mass is not the most accurate method, it was found as a good balance between accuracy and computation time. If the center of mass is just outside the control volume, the none of the rubble's volume inside the control volume counted towards porosity; likewise, if the center of mass was just inside the control volume, all of the rubble's volume counted towards the porosity. When testing this algorithm, this more or less averaged out, and there were no noticeable differences between this method and the more accurate method of "trimming" the rubble to the control volume.

5.2.1 Base Test

Pile-up processing was first performed on the base test case with a combination of visual observations during the simulation and simulation output files for ice loads on the structure and spatial ice information. From the visual observations, 5 distinct stages of simulation were identified:

1. Initial ice ride-up with some localized pile-up,
2. Initial ice pile-up due to instabilities in ride-up across the entire breakwater,
3. Rubble pile formation at pile edge rather than due to ride-up and instabilities,
4. Ice-sheet failures occurring both at and significantly away from the rubble pile, and
5. The unbroken ice sheet significantly influences the rubble pile.

Stages 1 and 2 are representative behavior for ride-up and pile-up in SAMS, but stages 3 through 5 are a direct result of using pre-broken ice driven by a large driving sheet/force. Figure 5-10 to Figure 5-14 show examples of these 5 stages, respectively.

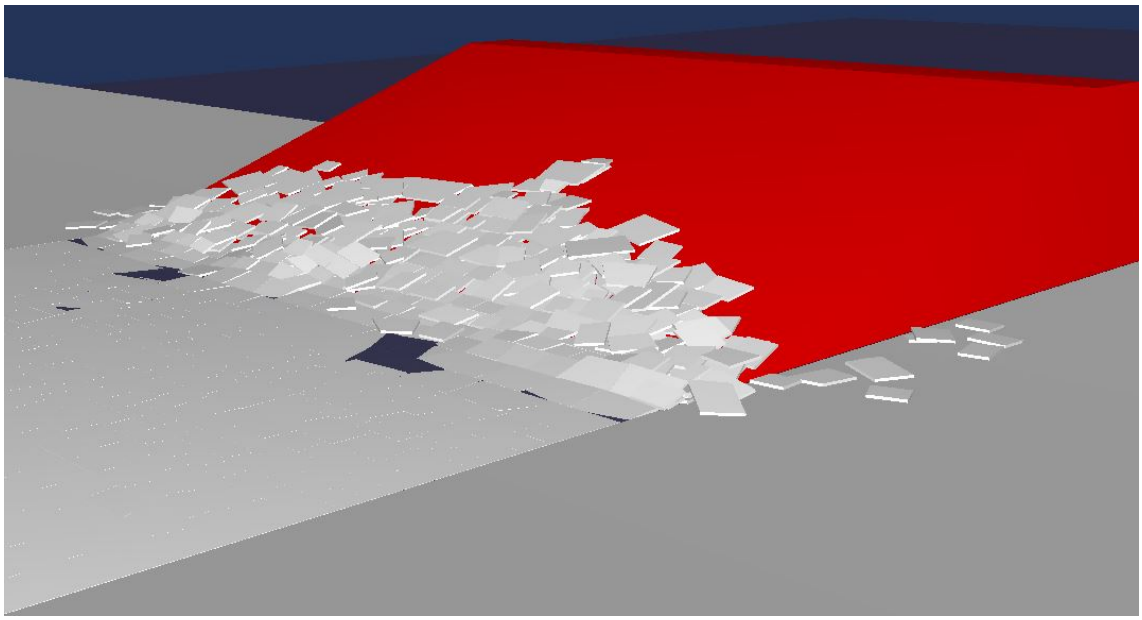

Figure 5-10 Pile-up: Stage 1 - Ride-up with minor localized pile-up

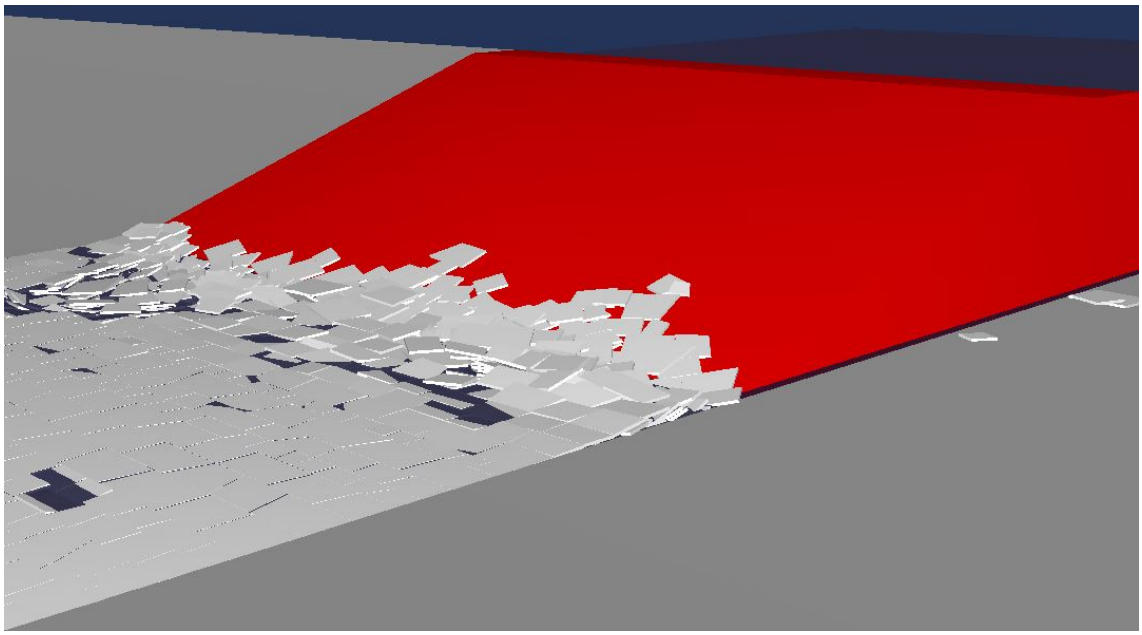

Figure 5-11 Pile-up: Stage 2 - Initial rubble pile formed after ice on slope fell down

Figure 5-12 Pile-up: Stage 3 - Rubble pile development

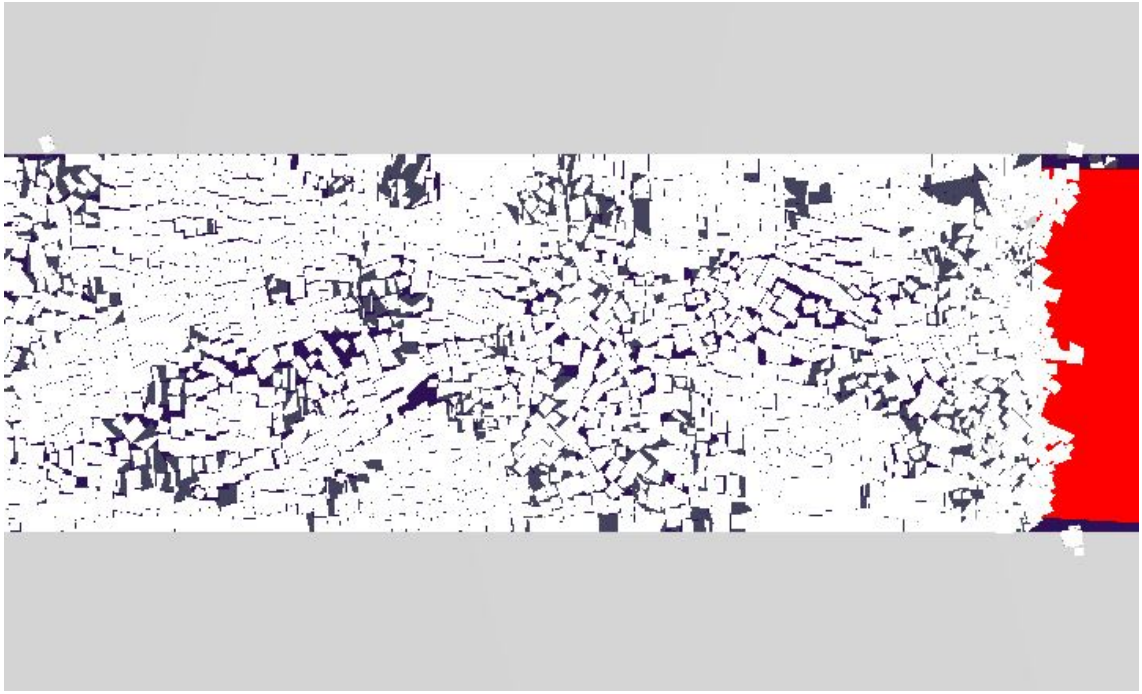

Figure 5-13 Pile-up: Stage 4 - Most of the sheet failure is not occuring at the rubble pile or near the breakwater

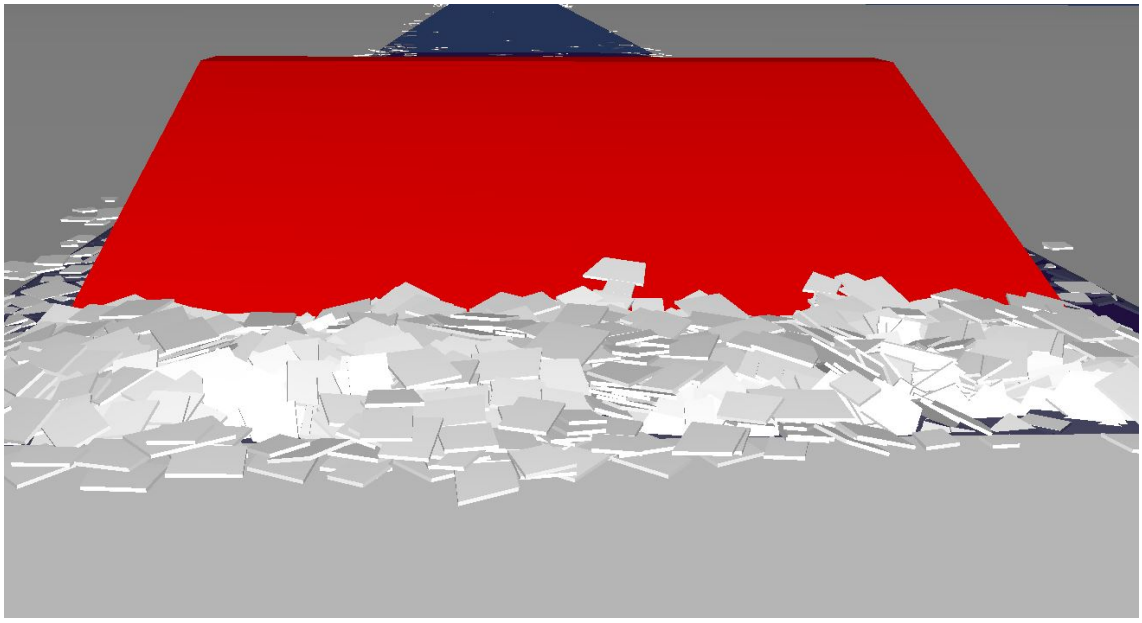

Figure 5-14 Pile-up: Stage 5 - Notice the solid sheet compressing the pile

Simulation output information was passed through a moving-point average (MPA) for 30s of data; this was done to decrease the noise in the signal so that trends and conclusions could be more easily drawn – especially when looking at multiple datasets in one figure. Figure 5-15 shows an example of a porosity signal with and without using an MPA.

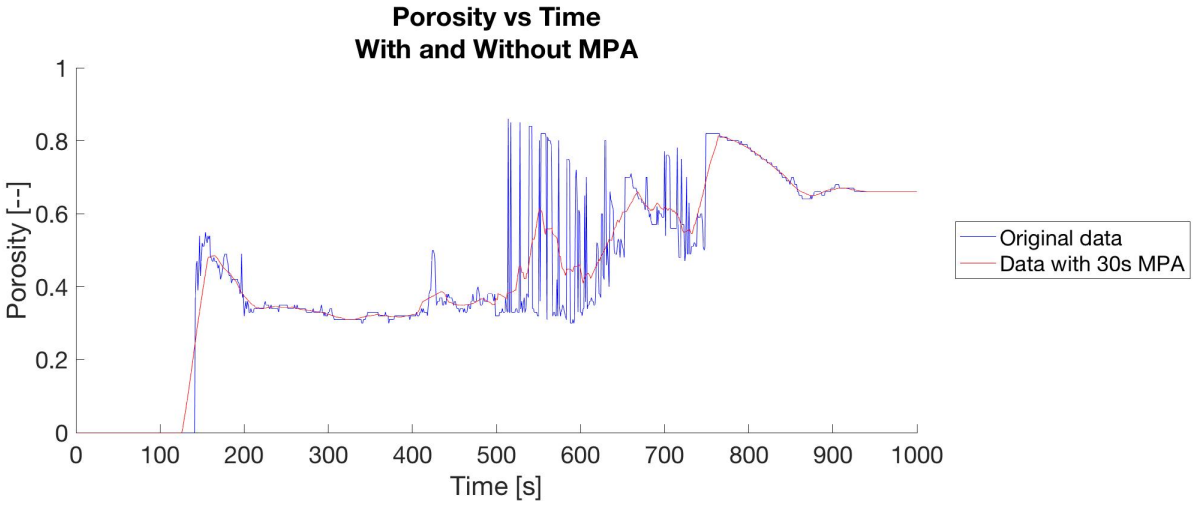

Figure 5-15 Example of porosity with and without using an MPA

All of the results below are compared to field observations for similar situations. This field data gives averages, minimums, or maximums and not time-series information. Therefore, it was decided that better clarity in the data would be more beneficial than data peaks – which are all eliminated during the moving point average. That said, peaks – including load – are all in the same order of magnitude as the results presented below.

The output results are plotted in Figure 5-16 to Figure 5-18. Figure 5-16 shows the average ice load per meter of breakwater vs simulation time. Figure 5-17 shows the average porosity of the rubble pile vs simulation time. Figure 5-18 shows the maximum sail height and keel depth over simulation time. Additionally, each figure has lines added with which one can identify the five stages.

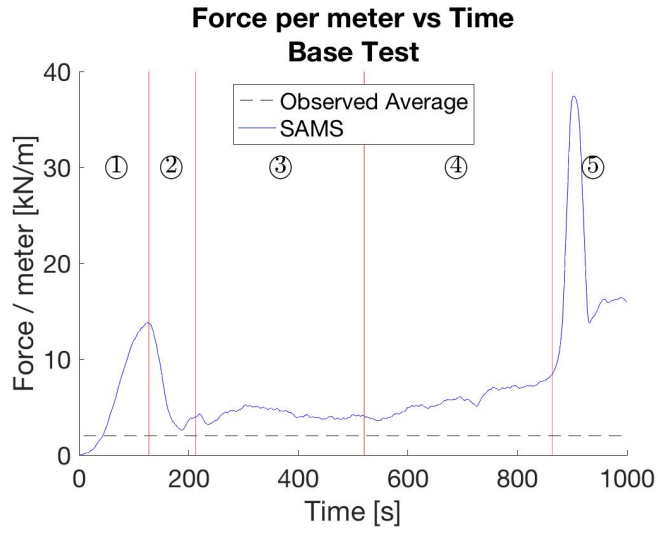

Figure 5-16 Pile-up - Base test – Average force per meter width over time

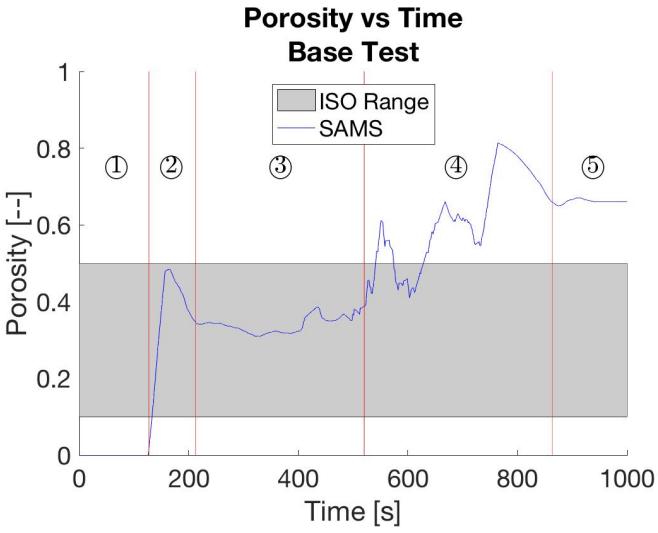

Figure 5-17 Pile-up - Base test – Average porosity over time

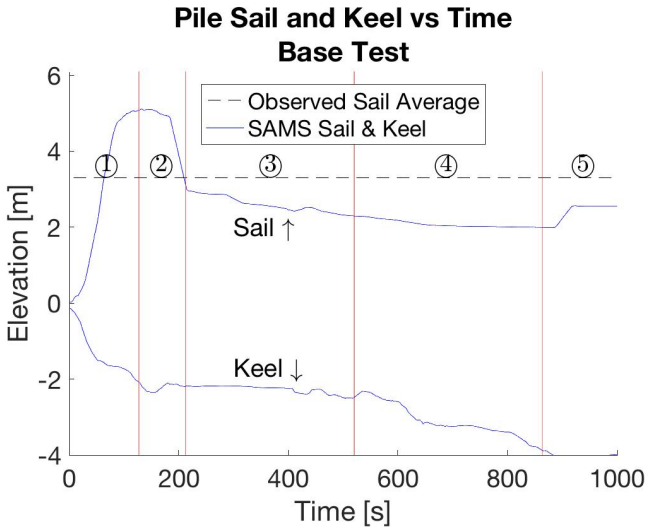

Figure 5-18 Pile-up - Base test – Maximum sail height and keel depth over time

As observed in Figure 5-16 to Figure 5-18, during stage 1, there is no porosity due to insufficient pile formation, the sail* reaches a maximum height as the maximum ride-up is achieved, some local instabilities form a pile-up keel, and the force is positively correlated to ride-up height. During stage 2, the force decreases as rubble slides down the slope and the initial pile is formed; this stage concludes with a sharp drop in the sail height*.

During stage 3, all values approximately stabilize as the pile grows in length (x-axis) rather than increasing the sail height or keel depth. The stable sail height and keel depth are likely the result of sheet failure always occurring at the rubble pile's edge rather than pushing rubble up or down as the sheet moves through the pile before failing. The constant rubble pile thickness also results in a nearly-stable load. While these results are a direct consequence of using rigid bodies and pre-broken ice, it is unknown if the failure modes implemented in this version of SAMS can model the expected behavior. Bending failure and deformation from crushing are likely needed to better model the expected behavior.

During stage 4, pre-broken ice starts to fail away from the rubble pile. As this rubble is introduced to the pile, the keel depth and, consequently, the sail height, increases. As the keel depth increases, the force increases due to a larger projected area and form drag force. This increased force causes more frequent sheet failures away from the pile – resulting in a positive feedback cycle with keel depth and force increasing more rapidly as well. These failures also appear to cause increased and erratic behavior in the porosity (also seen in the raw data in Figure 5-15); the saw-toothed behavior is most likely due to an error in the porosity algorithm as rubble generated away from the pile moves within the algorithm's length buffer and increases the control volume.

During stage 5, the unbroken ice sheet begins to directly influence the rubble pile. This is seen in a sharp increase in force. The increased confining pressure causes the keel depth and sail height to increase, and a grounded rubble pile forms. Unfortunately, with rigid bodies the effects of a grounded rubble pile cannot be seen, for the increased strength from grounding the rubble is overshadowed by the greatly increased load from an ice sheet that cannot break and a breakwater that cannot move.

5.2.2 Sensitivity Tests: Ice-ice friction

The results for ice-ice friction sensitivities are presented in Figure 5-19 through Figure 5-21. As aforementioned in 4.4.3, these tests are used to test the sensitivity to ice-ice friction and the feasibility of using increased friction to better represent the internal friction of a rubble pile. Please note the change in test duration as presented, for some of these tests reached an equilibrium state and the simulation ended before 1000s.

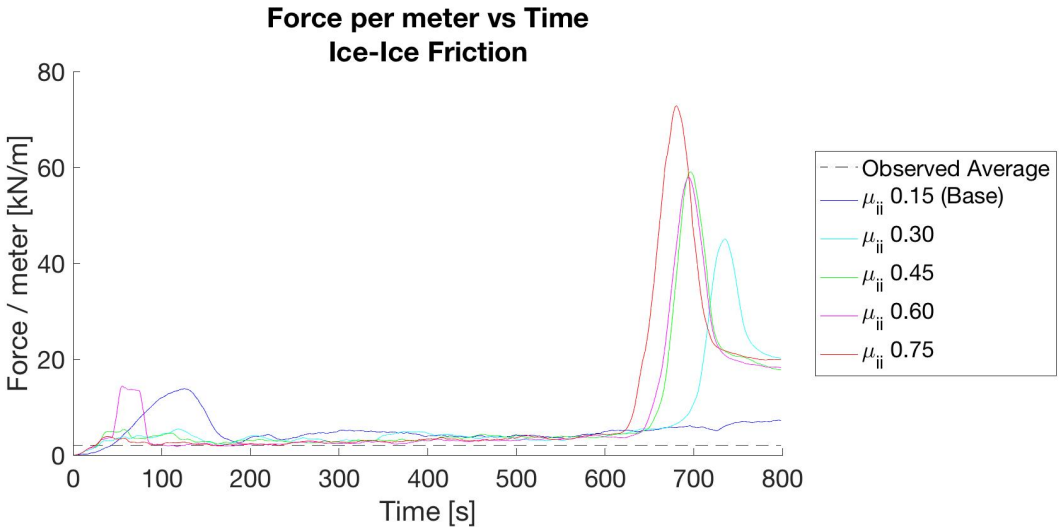

Figure 5-19 Pile-up - μ_{ii} Sensitivity – Average force per meter width over time

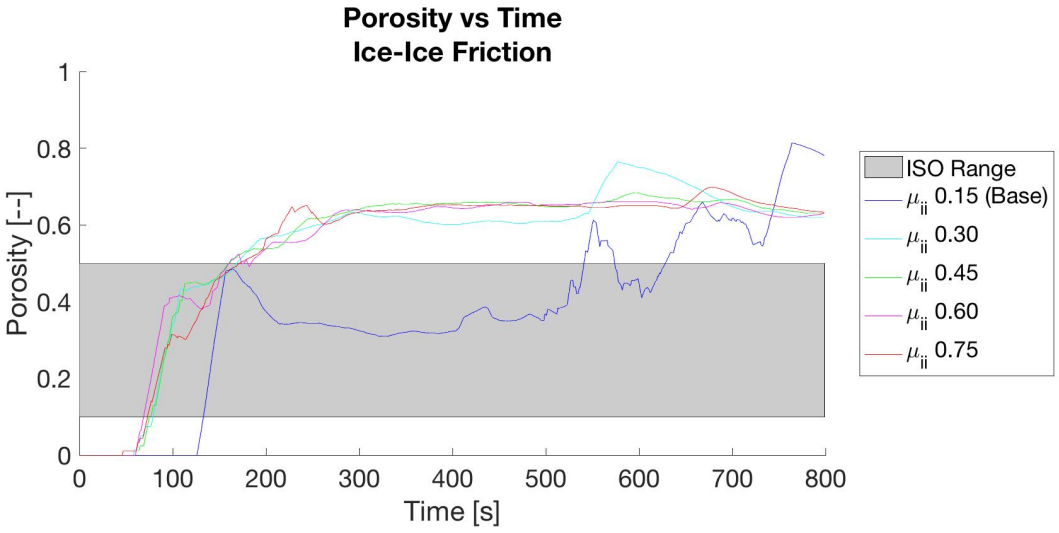

Figure 5-20 Pile-up - μ_{ii} Sensitivity – Average porosity over time

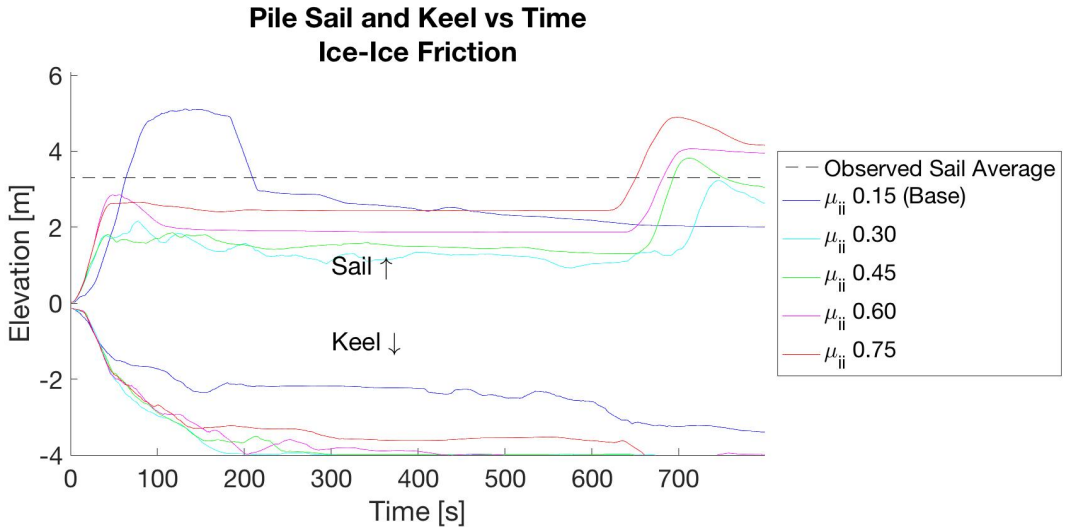

Figure 5-21 Pile-up - μ_{ii} Sensitivity – Maximum sail height and keel depth over time

As observed in Figure 5-19 through Figure 5-21, when comparing any of the simulations with the base test, ride-up is decreased and pile-up starts almost immediately after initial contact with the breakwater. Additionally, the sail height and keel depth increase earlier, and the pile typically becomes grounded before stage 5 is reached. The average porosity is nearly identical across the non-base simulations (~0.65) – albeit it is larger than the suggested range. Porosity is also not erratic throughout most of the simulations, thus it appears that stage 4 is either delayed or eliminated. The increased porosity, sail height, and keel depth are most likely a result of the rubble pile having more internal friction. The delay or elimination of stage 4 is most likely the result of increased friction inter-rubble friction keeping the sheet together and preventing sheet failure away from the rubble pile.

When compared to each other, increasing the ice-ice friction increases the sail height and decreases the force to the breakwater. In fact, for the two largest ice-ice friction tests, the average force is approximately the average observed force. This decrease to force is likely due to more force being transferred from the x-axis to the z-axis – resulting in the increased sail height and decreased keel depth. However, increasing the ice-ice friction also results the rubble pile length increasing quicker. Therefore, stage 5 occurs earlier. Also notable is that the peak force observed during stage 5 is noticeably larger as ice-ice friction increases.

Concerning sensitivity, past the initial increase from 0.15 to 0.30, SAMS is relatively insensitive to changes in ice-ice friction for the keel depth and porosity. The sensitivity to sail height and force is relatively low.

5.2.3 Sensitivity Tests: Ice-structure friction

The results for ice-structure friction sensitivities are presented in Figure 5-22 through Figure 5-24. As aforementioned in 4.4.3, these tests are used to test the sensitivity to ice-structure friction and the feasibility of using increased friction to approximate non-smooth surfaces.

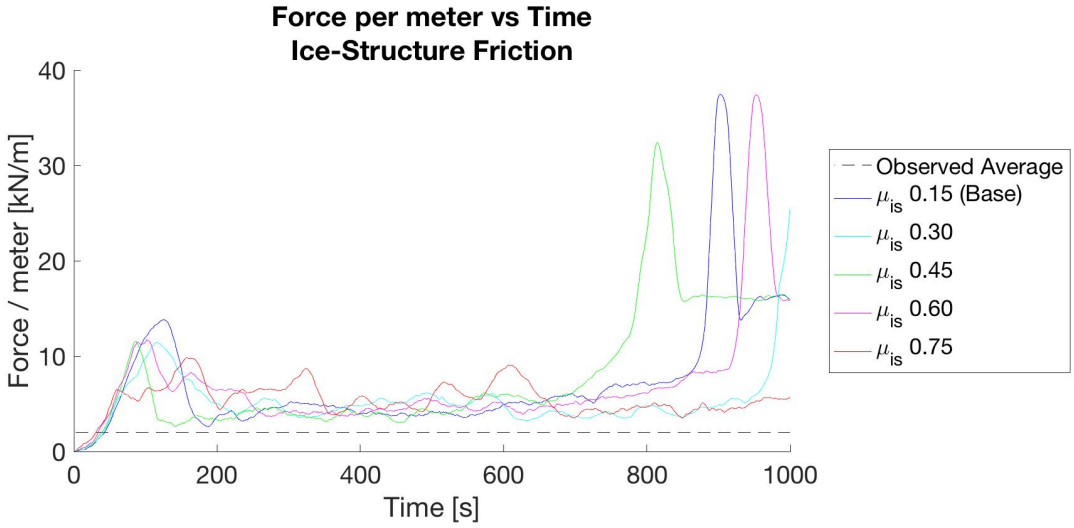

Figure 5-22 Pile-up - μ_{is} Sensitivity – Average force per meter width over time

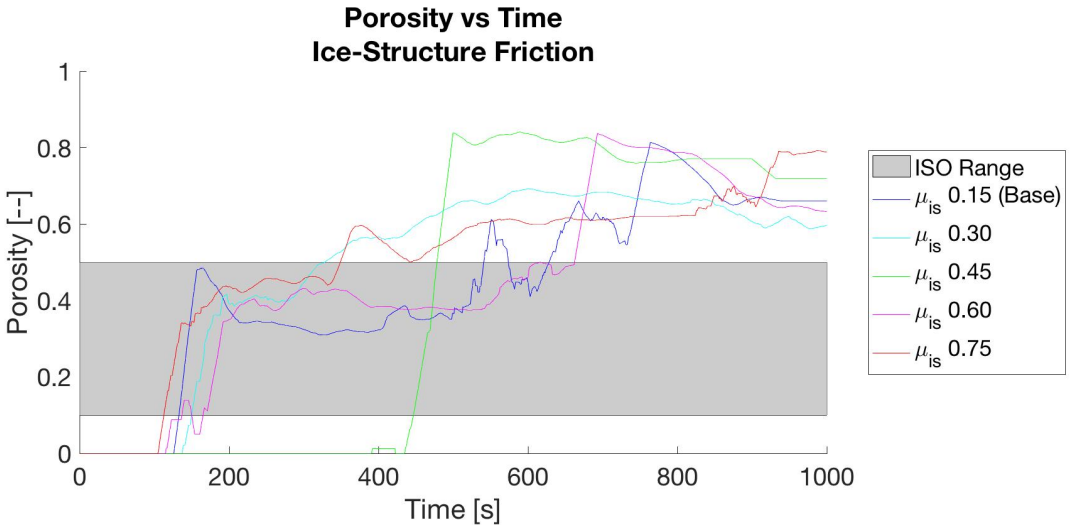

Figure 5-23 Pile-up - μ_{is} Sensitivity – Average porosity over time

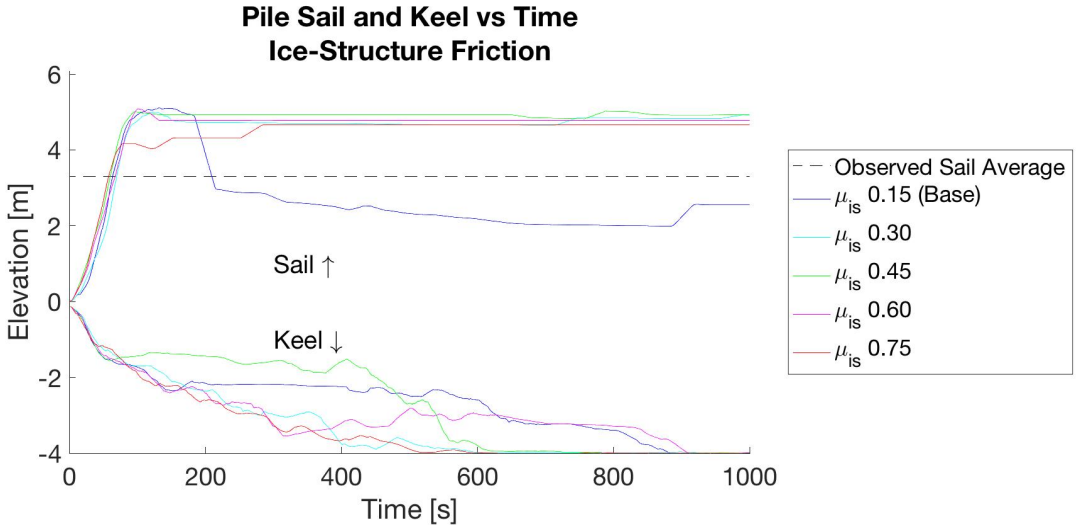

Figure 5-24 Pile-up - μ_{is} Sensitivity – Maximum sail height and keel depth over time

As observed in Figure 5-22 through Figure 5-24, in all of the tests with increased ice-structure friction, the initial ride-up instabilities causing pile-up are reduced or even eliminated. While some local pile-up did occur in the simulations, most areas never became unstable, and the maximum ride-up height was kept throughout the entire simulation. However, this does not affect the control volume for porosity, for porosity was only calculated for keel. Also observed in Figure 5-24, the general trend in most of the tests is that increasing the ice-structure friction increases the keel depth. As aforementioned, this increased keel depth increases the force on the structure resulting in stage 4 occurring earlier. Stage 4 occurring earlier explains the trend of higher porosities and forces, though a clear correlation between ice-structure friction and porosity or force cannot be determined.

The exception to this trend is the simulation when μ_{is} was 0.45 (colored green in the figures). Most likely due to the highly non-linear nature of these simulation, this simulation experienced significant 3D effects. As seen in Figure 5-25, the keel grew unevenly across the breakwater. This resulted in a sudden, large increase in porosity due to how the algorithm calculates porosity. The control volume used is rectangular, and the lower limit corresponds to the maximum keel depth. The uneven keel depth set the limit for the control volume across the entire width of the breakwater. Thus, once the keel threshold was reached, there existed a large void of water counted in the control volume with very little ice and a large calculated porosity.

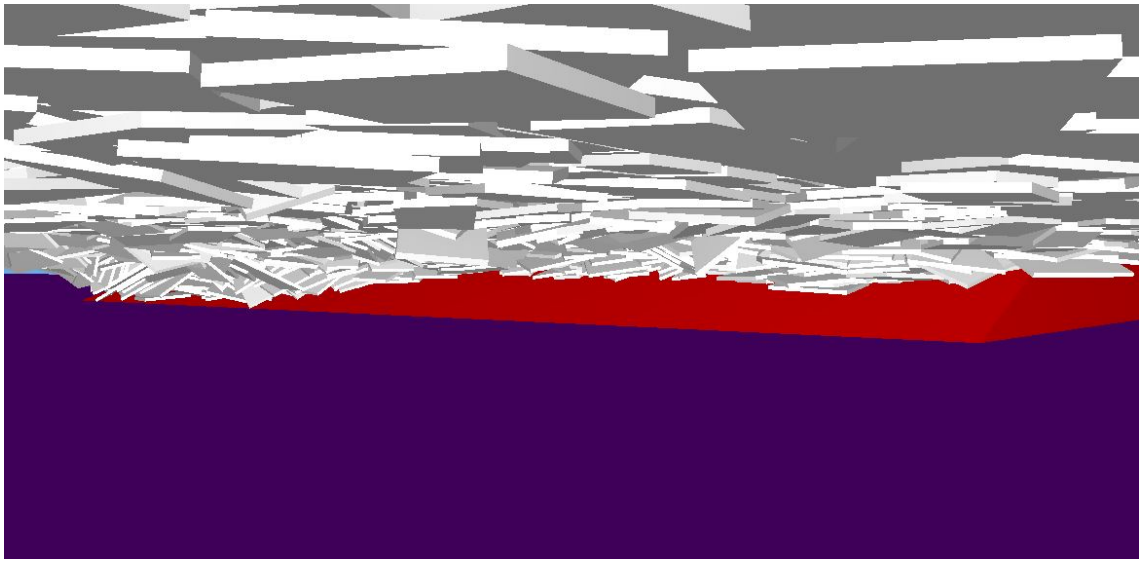

Figure 5-25 Pile-up: Control volume with significant extra voids leading to increased porosity

Concerning sensitivity, past the initial increase of ice-structure friction, SAMS is relatively insensitive to changes in ice-structure friction for the keel depth. It is difficult to comment on the sensitivity with respect to force, porosity, or sail height, for these metrics not well correlated. This lack of correlation is most likely due to the erratic behavior of stage 4.

5.2.4 Geometry Comparison

While all of the above sensitivity tests were run with both trapezoidal-only and trapezoidal and triangular geometries, only the base test case is presented here, for general results from this case can be seen across all of the simulations with the more complex geometry. For plots of all of the simulations – including those with trapezoidal and triangular geometries not presented in this section – please refer to Appendix D.

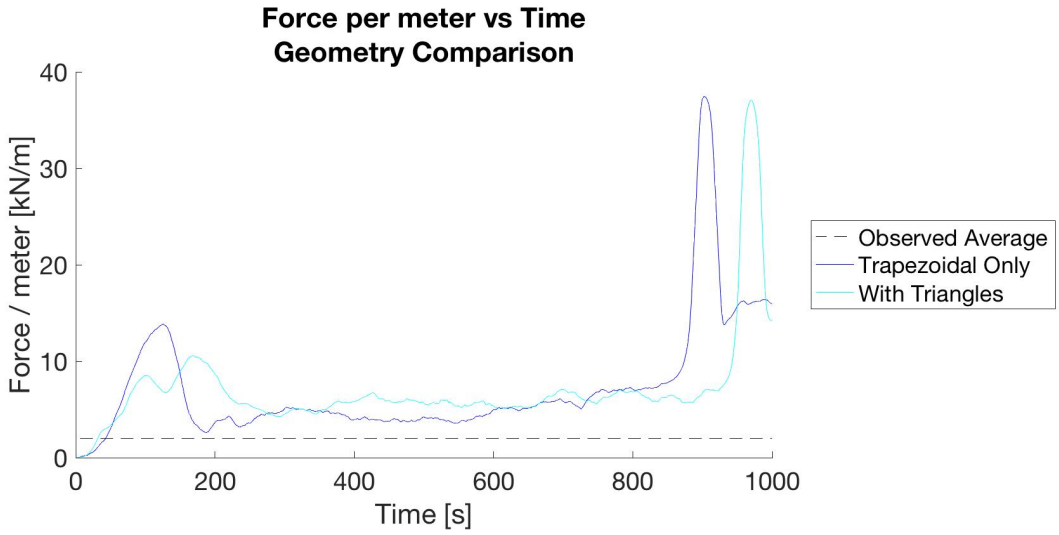

Figure 5-26 Pile-up - Geometry comparison – Average force per meter width over time

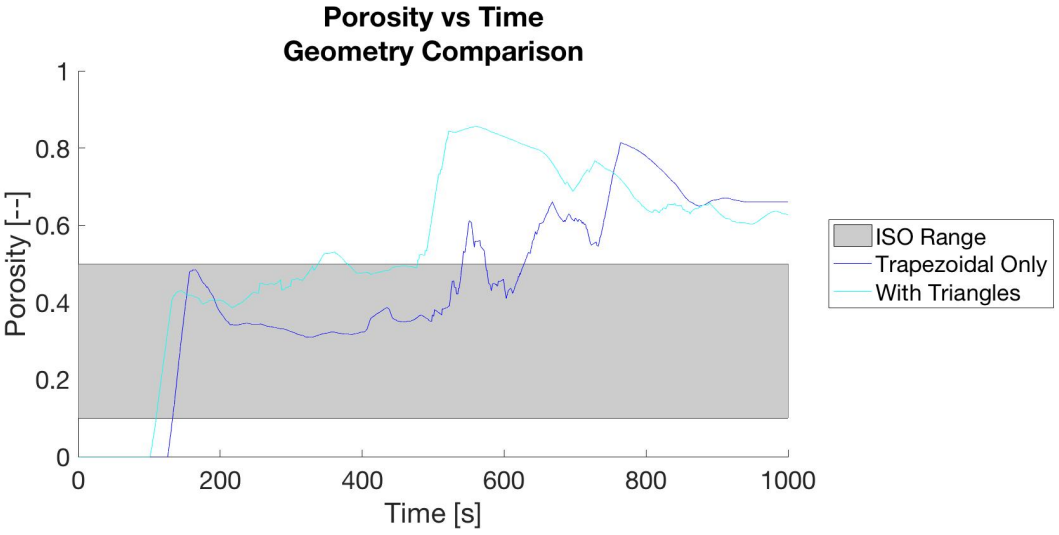

Figure 5-27 Pile-up - Geometry comparison – Average porosity over time

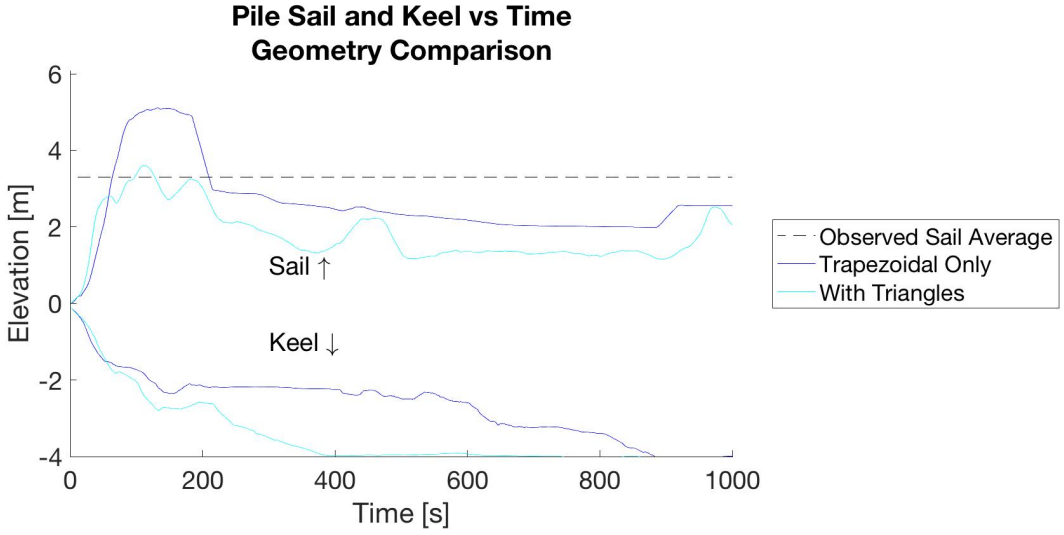

Figure 5-28 Pile-up - Geometry comparison – Maximum sail height and keel depth over time

As observed in Figure 5-26 through Figure 5-28, with more the more complex, trapezoidal and triangular geometry, the keel depth increases and grounds more rapidly than the trapezoidal-only geometry. Based on visual observations made during the simulation, this appears to happen because stage 3 is nearly non-existent and stage 4 is reached earlier. The increased load is due to the keel depth increase. Curiously, the sail height decreases rather than increases with the increasing keel depth.

As indicated in Figure 5-27 and Figure 5-28, maximum ride-up is not reached and pile-up starts earlier. This is most likely responsible for the overall decreased sail height, for the maximum sail typically occurred at the ice-breakwater interface Figure 5-12.

6 Conclusions and Future Work

6.1 Conclusions

This thesis studied numerically modelling the interaction between pre-broken, rigid ice sheets and wide, sloping structures. This thesis focused on adapting a numerical model (SAMS) and validating the base phenomena of the simulated ride-up and pile-up. The most important conclusions drawn are as follows:

- The simulated ride-up had a percent difference of 18.9% from Christensen's model;
- The simulated pile-up had 5 distinct stages – the first 3 are in accordance with the expected behavior, but the last 2 are aberrant consequences of using rigid ice;
- The simulated pile-up load to the structure ranged between 2 and 9 kN/m, which is on the same order of magnitude as field observations (2 kN/m average);
- The simulated pile-up porosity ranged between 0.35 and 0.65 during pile creation (stage 3) depending on the model's configuration parameters, while the range suggested by ISO19906 is 0.2 to 0.5 (0.5 corresponding to young piles);
- The simulated pile-up keel depth did not ground in every simulation, yet grounding was expected for the water depth (3 m);
- The simulated pile-up sail ranged between 1 and 2.5 m, which is lower than the 3 m average from field observations;
- Ice-ice friction sensitivity tests demonstrated that increasing μ_{ii} qualitatively improved the simulations by some aberrant behavior (stage 4) and typically resulted in grounded piles;
- Ice-structure friction sensitivity tests demonstrated that increasing μ_{is} qualitatively worsened the simulations by exaggerating aberrant behavior (stage 4) and reducing expected behavior (stages 2 and 3); and
- Rubble geometry tests demonstrated that the simulated pile-up behavior is sensitive to the shape of rubble. More complex geometries (i.e. trapezoidal and triangular) qualitatively worsened the simulations by exaggerating aberrant behavior (stage 4) and reducing expected behavior (stage 3).

As the above list suggests, most of the deviations from the observed or expected behavior are due to simulating rigid ice bodies rather than a visco-elastic ice sheet. This decision was made because of what ice failure modes and fracture mechanics were implemented in this

version of SAMS. That said, this study has shown SAMS has a good potential to simulate ice interactions with coastal structures in future versions. In the current version, ride-up results compare favorably with analytical models, and certain aspects of pile-up are represented reasonably well.

Where differences exist between the ride-up analytical model and SAMS, the differences can be explained both physically and within the rules of the simulator. Christensen specifically mentioned that energy losses from crushing can be significant with steeper slopes, and SAMS simulations show that behavior. In SAMS, increasing the ice thickness also causes increased energy losses from crushing, and this might or might not be the case in real-world, full-scale events.

Pile-up simulations tend to exhibit 5 stages of development: (1) initial ride-up, (2) initial pile-up, (3) rubble-pile development, (4) ice-sheet failure away from the pile, and (5) the unbroken ice sheet directly influencing the pile. The accuracy of stages 1-3 depend on the configuration parameters, and stages 4 and 5 represent unrealistic, aberrant behavior caused by rigid-body simulations.

While stage 3 in pile-up was not as well-matched as ride-up, many of the inconsistencies are explained by the rigid-body tests performed in this thesis. For typical values for ice-ice and ice-structure friction, the sail height never reached the average observed average value. However, the advancing ice sheet was incapable moving into the pile to lifting up and pushing down the rubble. Likewise, with typical values for ice-ice friction, keel depths never increased beyond 2 m until confining pressure was increased due to the unbroken ice sheet directly influencing the rubble. If the sheet were deformable rather than rigid, pressure would larger from the beginning, and the keel is expected to more closely resemble real life. Porosity tends to be on the high end or even above the range found in ISO19906. This, too, is likely influenced by the rigid-body limitation of these tests.

That said, it appears that increasing the ice-ice friction appears to yield more realistic results when using a rigid-body approximation and pre-broken sheet ice. Increasing the ice-ice friction led to a better-developed sail and keel during stage 3, and – probably most importantly – it eliminated the erratic behavior during the simulations caused by stage 4. Further tests should be carried out to verify these findings but using a high ice-ice friction appears promising for rigid bodies.

6.2 Future Work

The following section proposes future work both to validate SAMS and for the development of the simulator. The list is in order of how this author proposes the work should be carried out.

6.2.1 Pile-up: Velocity sensitivity

Velocity sensitivity tests were carried out to a limited extent, but, due to a configuration error, the simulation did not run long enough to draw observe trends and draw conclusions. Because pile-up simulations took approximately one day for each simulation, there was not enough time to rerun the simulations after this error was discovered.

6.2.2 Pile-up: Multi-parameter sensitivities

Especially in the case of pile-up, one parameter was changed while holding others constant. This led to the conclusion that increasing the ice-ice friction better approximated rubble piles and pile-up behavior. However, systems of multi-body dynamics like those tested in this thesis are highly non-linear, and small changes can alter system behavior. Therefore, to better test how SAMS simulates pile-up, more tests need to be conducted and analyzed across a broader range of parameters, and a testing matrix like that used for ride-up should be generated and analyzed. Rigid bodies can still be used if enhanced fracture mechanics have not been implemented in SAMS.

6.2.3 Pile-up: Multiple ice sheets per thickness, and multiple thicknesses

It is possible that some of the results and thus conclusions are because only 2 ice sheets were used. Especially with steeper slopes – like the one tested in pile-up – there was a large range for maximum ride-up. This range is assumed to be limited due to the greater size of the sheet and longer test duration, but testing more ice sheets of the same thickness will verify this.

6.2.4 SAMS Development: Fracture mechanics for bending failure

A lot of limitations existed due to the rigid body limitation. Pile-up simulations and processing took hours for each test due to the large number of bodies from start to finish. When bending failure is introduced into SAMS, this should greatly decrease the simulation time and data generated – thus allowing more tests to better determine trends in aberrant behavior.

When simulation time is a priority, deriving and implementing analytical solutions should be used. However, implementing a 3-D lattice model as discussed by van den Berg in

[39] can be used when high-accuracy results are needed and simultaneous crushing and bending failure could occur – such as on the highly irregular surface of rubble-mound breakwaters. Lattice models have been used in other engineering areas to represent inhomogeneous materials like sea ice [39]. Implementing and using a lattice model would most likely help when researching armor unit movement and damage.

6.2.5 Pile-up: Model- and full-scale data comparison

Comparing the data to both laboratory data and full-scale data will help validate SAMS for wide, sloping structures. Laboratory data is more controlled, the material properties and conditions are better recorded, and the forces are more accurately measured, thus they serve as a good starting place for comparisons. The Shoulder Ice Barrier discussed in [1] would serve as a good, initial testing subject, for it is smooth-sloped breakwater that can be used to compare ride-up, pile-up, and loads.

6.2.6 Pile-up: Oblique driving force

One of the benefits of SAMS over other numerical models is the ability to run 3D simulations. While the tests described in this thesis were limited to ice being driven in the x-direction only, testing oblique ice movements could help us better understand how rubble piles form around actual breakwaters and to identify problem areas in ride-up and pile-up with breakwater designs.

6.2.7 Ride-up and pile-up: Irregular surfaces

While many Arctic breakwaters have a smooth surface to better handle ice loads, this practice contradicts breakwaters designed for wave loads (*see section 2.3.1*). As polar lows become more common, Arctic breakwaters might need to utilize irregular, non-smooth slopes to better dissipate wave energy from summer storms. Additionally, Icelandic-style berm breakwaters and other dynamically stable breakwaters do not rely on large armor units to protect against external loads. These surfaces are more akin to rock beaches and are not smooth.

6.2.8 Ride-up and pile-up: Armor unit movement

Originally, one of the main goals of this thesis was to analyze armor stone movement on a breakwater due to ice loads. However, due to limitations with the current version of SAMS, the aims were scaled down, but the original goal and motivation for research is still there. From a research point of view, better understanding armor unit movement and breakwater damage is an interesting topic typically limited to laboratory studies. As mentioned in SEC, these suffer

scale effects and are cautioned against in ISO literature for Arctic engineering [11]. Using SAMS to simulate full-scale experiments could provide valuable insights into armor unit designs and guidelines. Once validated, armor stone movement can then be used to help engineers more effectively design Arctic breakwaters.

References

[1] A. Gürtner, "Experimental and Numerical Investigations of Ice-Structure Interaction (PhD Thesis)," Norwegian University of Science and Technology, Trondheim, 2009.

[2] R. Lubbad and S. Løset, "A Numerical Model for Real-time Simulation of Ship-ice Interaction," *Cold Regions Science and Technology,* vol. 65, pp. 111-127, 2011.

[3] J. Pahl and B. Kaiser, "Arctic Port Development," in *Arctic Marine Resource Governance and Development*, Cham, Switzerland, Springer Polar Sciences, 2018, pp. 139-184.

[4] R. McKenna, D. McGonigal, P. Stuckey, G. Crocker, B. Marcellus, K. Croasdale, P. Verlaan and A. Abuova, "Modelling of Ice Rubble Accumulations in the North Caspian Sea," in *Proceedings of the 21st International Conference on Port and Ocean Engineering under Arctic Conditions*, Montréal, Canada, 2011.

[5] H. J. Lengkeek, K. R. Croasdale and M. Metge, "Design of Ice Protection Barrier in Caspian Sea," in *Proceedings of OMAE03: 22nd International Conference on Offshore Mechanics and Arctic Engineering*, Cancun, Mexico, 2003.

[6] A. Barker and K. Croasdale, "Numerical Modelling of Ice Interaction with Rubble Mound Berms in the Caspian Sea," in *17th International Symposium on Ice*, Saint Petersburg, Russia, 2004.

[7] W. Østreng, K. M. Eger, B. Fløistad, A. Jørgensen-Dahl, L. Lothe, M. Mejlænder-Larsen and T. Wergeland, Shipping in Arctic Waters: A comparison of the Northeast, Northwest, and Trans Polar Passages, Heidelberg: Springer-Verlag, 2013.

[8] E. Struzik, "Shipping Plans Grow as Arctic Ice Fades," Yale School of Forestry & Environmental Studies, 17 November 2016. [Online]. Available: https://e360.yale.edu/features/cargo_shipping_in_the_arctic_declining_sea_ice. [Accessed 2018].

[9] K. M. Eger, "Marine Insurance Aspects of the NSR/NEP," CHNL, 2010.

[10] F. T. Christensen, "Ice Ride-Up and Pile-Up on Shores and Coastal Structures," *Journal of Coastal Research,* vol. 10, no. 3, pp. 681-701, 1994.

[11] ISO 19906, "Petroleum and natural gas industries - Arctic offshore structures," Geneva, 2010.

[12] S. Løset, *AT327 - Lecture Slides on Ice-Structure Interactions,* Svalbard: NTNU / UNIS, 2017.

[13] K. V. Høyland, *TBA4265 - Ice and Arctic (Lecture Notes),* Trondheim: NTNU, 2016.

[14] S. Løset, K. N. Shkhinek, O. T. Gudmestad and K. V. Høyland, Actions from Ice on Arctic Offshore and Coastal Structures, St. Petersburg: "LAN", 2006.

[15] A. H. V. Repetto-Llamazares, "Experimental basin- and laboratory-scale studies related to ice ridges, rubble, accumulations and freeze-bonds (PhD Thesis)," Norwegian University of Science and Technology, Trondheim, 2011.

[16] A. Tørum, Coastal Structures (Lecture Notes), NTNU, 2010.

[17] K. R. Croasdale and A. B. Cammaert, "An improved method for the calculation of ice loads on sloping structures in first-year ice," *Hydrotechnical Construction,* vol. 28, no. 3, pp. 174-179, 1994.

[18] CIRIA, CUR, CETMEF, The Rock Manual. The use of rock in hydraulic engineering, 2nd Edition ed., London: C683, CIRIA, 2007.

[19] K. J. MacIntosh, G. W. Timco and D. H. Willis, "Canadian experience with ice and armor stone," in *Proceedings of the 1995 Canadian Coastal Conference*, Dartmouth, Nova Scotia, CA, 1995.

[20] D. S. Sodhi and C. J. Donnelly, "Ice Effects on Riprap: Model Tests," in *Proceedings 10th International Conference on Cold Regions Engineering*, Lincoln, NH, USA, 1999.

[21] D. S. Sodhi, S. L. Borland and J. M. Stanley, "Ice Action on Riprap: Small-scale tests," CRREL, Springfield, VA, USA, 1996.

[22] S. F. Daly, J. Zufelt, L. Zabilansky, D. Sodhi and K. Bjella, "Estimation of Ice Impacts on Armor Stone Revetments at Barrow, Alaska," in *19th IAHR International Symposium on Ice*, Vancouver, BC, CA, 2008.

[23] R. Ettema, J. F. Kennedy and M. G. Horton, "Ice study for the port development at Nome, Alaska," in *7th International Conference on Port and Ocean Engineering under Arctic Conditions*, Helsinki, Finland, 1983.

[24] D. S. Sodhi, *Land-ice interaction: Ice pile up and ride up on land (Keynote Slides),* 2014.

[25] G. W. Timco and M. Johnston, "Ice loads on the caisson structures in the Canadian Beaufort Sea," *Cold Regions Science and Technology,* vol. 38, pp. 185-209, 2004.

[26] M. A. Hopkins, "The ice pile-up problem: A comparison between experiments and simulations," *AMD - Ice Mechanics,* vol. 207, pp. 211-218, 1995.

[27] M. A. Hopkins, "Onshore ice pile-up: A comparison between experiments and simulations," *Cold Regions Science and Technology,* vol. 26, pp. 201-214, 1997.

[28] J. Paavilainen, J. Tuhkuri and A. Polojärvi, "2D numerical simulations of ice rubble formation process against an inclined structure," *Cold Regions Science and Technology,* vol. 68, pp. 20-34, 2011.

[29] J. Paavilainen and J. Tuhkuri, "Parameter effects on simulated ice rubbling forces on a wide sloping structure," *Cold Regions Science and Technology,* vol. 81, pp. 1-10, 2012.

[30] R. Lubbad, S. Løset, W. Lu, A. Tsarau and M. van den Berg, "An overview of the Oden Arctic Technology Research Cruise 2015 (OATRC2015) and numerical simulations performed with SAMS driven by data collected during the cruise," *Cold Regions Science and Technology,* no. https://doi.org/10.1016/j.coldregions.2018.04.006, pp. 1-22, 2018.

[31] ArcISo, *SAMS Source Code,* Private, unpublished, 2018.

[32] M. van den Berg, R. Lubbad and S. Løset, "An Implicit Time Stepping Shceme and an Improved Contact Model for Ice-Structure Interaction Simulations," Trondheim, 2018.

[33] W. Lu, R. Lubbad, K. Høyland and S. Løset, "Physical model and theoretical model study of level ice and wide sloping structure interactions," *Cold Regions Science and Technology,* vol. 101, pp. 40-72, 2014.

[34] W. Lu, R. Lubbad and S. Løset, "In-plane fracture of an ice floe: A theoretical study on the splitting failure mode," *Cold Regions Science and Technology,* vol. 110, pp. 77-101, 2015.

[35] W. Lu, R. Lubbad and S. Løset, "Out-of-plane failure of an ice floe: Radial-crack-initiation-controlled fracture," *Cold Regions Science and Technology,* vol. 119, pp. 183-203, 2015.

[36] W. Lu, R. Lubbad, S. Løset and M. Kashafutdinov, "Fracture of an ice floe: Local out-of-plane flexural failures versus global in-plane splitting failure," *Cold Regions Science and Technology,* vol. 123, pp. 1-13, 2016.

[37] W. Lu, H.-M. Heyn and S. Løset, "Large Scale Simulations of Floe-Ice Fractures and Validation against Full-scale Data," in *Proceedings of the 24th International Conference on Port and Ocean Engineering under Arctic Conditions*, Busan, Korea, 2017.

[38] H. J. Verhagen, K. d'Angremond and K. van der Vliet, "Positioning of cubes on a breakwater slope," in *Proceedings of the 28th International Conference, Coastal Engineering*, Cardiff, Wales, 2002.

[39] M. van den Berg, "A 3-D Random Lattice Model of Sea Ice," in *Arctic Technology Conference 2016*, St. John's, Newfoundland and Labrador, 2016.

A ISO19906 equations for global ice loads on wide, sloping structures

List of Symbols

b	Width of structure
c	Cohesion of the ice rubble pile
E	Modulus of elasticity
F_H	Total horizontal force
F_V	Total vertical force
H_B	Load required to break the sheet in bending failure
H_P	Load required to push the advancing sheet through the ice rubble
H_R	Load required to push the blocks up the slope
H_L	Load required to lift the ice rubble on top of the advancing ice sheet
H_T	Load required to turn the ice block at the top of the slope
h_i	Thickness of the ice sheet or floe
h_{ru}	Height of ride-up
L_c	Characteristic length (typically determined by elastic plate theory)
l_c	Estimated circumferential crack length
α	Slope of the structure (with respect to the horizontal axis)
θ	Angle of the seaward side of a rubble pile (with respect to the horizontal axis)
μ_{ii}	Ice-ice friction coefficient
μ_{is}	Ice-structure friction coefficient
ν	Poisson's ratio of ice
ξ	Vertical/horizontal force transform
ρ_i	Average density of ice
ρ_w	Density of water
σ_f	Flexural strength
φ_p	Internal friction angle of the rubble pile

Horizontal and vertical force

$$F_V = \frac{F_H}{\xi}$$

$$F_H = \frac{H_B + H_P + H_R + H_L + H_T}{1 - \frac{H_B}{\sigma_f L_c h_i}}$$

Horizontal force components

$$H_B = 0.68\xi\sigma_f \left(\frac{\rho_w g h_i^5}{E}\right)^{0.25} \left(b + \frac{\pi^2 L_c}{4}\right)$$

$$H_P = b h_{ru}^2 \mu_{ii} \rho_i (1-e) \left(1 - \frac{tan\theta}{tan\alpha}\right)^2 \frac{1}{2tan\theta}$$

$$H_R = bP \frac{1}{cos\alpha - \mu_{is} sin\alpha}$$

$$H_L = 0.5 b h_{ru}^2 \rho_i g (1-e) \xi \left(\frac{1}{tan\theta} - \frac{1}{tan\alpha}\right)\left(1 - \frac{tan\theta}{tan\alpha}\right) +$$
$$+0.5 b h_{ru}^2 \rho_i g (1-e) \xi tan\varphi_p \left(1 - \frac{tan\theta}{tan\alpha}\right)^2 +$$
$$+\xi c b h_{ru} \left(1 - \frac{tan\theta}{tan\alpha}\right)$$

$$H_T = 1.4 b h_i^2 \rho_{ice} g \frac{cos\alpha}{sin\alpha - \mu_{is}}$$

Supporting equations

$$\xi = \frac{sin\alpha + \mu_{is} cos\alpha}{cos\alpha - \mu_{is} sin\alpha}$$

$$L_c = \left(\frac{E h_i^3}{12 \rho_w g (1 - \nu^2)} \right)^{0.25}$$

$$l_c = b + \frac{\pi^2}{4} L_c$$

$$P = 0.5 \mu_{ii} (\mu_{ii} + \mu_{is}) \rho_i g (1 - e) h_{ru}^2 sin\alpha \left(\frac{1}{tan\theta} - \frac{1}{tan\alpha} \right) \left(1 - \frac{tan\theta}{tan\alpha} \right) +$$
$$+ 0.5 (\mu_{ii} + \mu_{is}) \rho_i g (1 - e) h_{ru}^2 \frac{cos\alpha}{tan\alpha} \left(1 - \frac{tan\theta}{tan\alpha} \right) +$$
$$+ h_{ru} h_i \rho_i g \frac{sin\alpha + \mu_{is} cos\alpha}{sin\alpha}$$

B Changelog for SAMS

All source code found within SAMS is property of ArcISo and cannot be released without explicit permission from ArcISo. It is not publicly available upon request. The changelog has been redacted to reflect only those changes introduced by the author of this thesis and some sensitive information has been removed in compliance to the non-disclosure agreement between ArcISo and the author of this thesis.

```
David Massey committed on May 25

Fixed: rotation bug for incorrectly generated ice; the principle transform
was not applied to the vertices of the floes -- just the basis of the
transform.

Fixed: keep tank walls. Tank walls no longer generate when set to false.

Added: minimum and maximum simulation times to configuration file.

Changed: Minor changes to end conditions for non-moving structures.


David Massey committed on May 2

Added: command line argument '-f <FILE>' to specify itconfig file

Added: command line argument '-x' to exit SAMS on successful simulation.

Added: 'enableGUI' to itconfig and associated parsing


David Massey committed on Apr 26

Changed: Tank wall heights have been increased by 10m.

Removed: The print statements during execution for iteration and such.

Changed: The values saved to the *.ice files.

Changed: End conditions for non-moving structures. Now ends when >= 90% of
the ice is stationary.


David Massey committed on Mar 21

Fixed: OpenGL performance error with compound shapes causing extreme
slowdowns when using the visualization window.
```

David Massey committed on Mar 13

Fixed: Bed origin as defined in itconfig should follow the files definition (x,y,z), however SAMS uses y-up.

David Massey committed on Mar 11

Added: and end-of-simulation condition based on the velocity of dynamic bodies. Only checked if the towing carriage velocity is (0., 0., 0.).

David Massey committed on Mar 11

Added: BODY_BED

Added: Appropriate bed initialization and configuration

Changed: where SAMSBodyFlags are located

Changed: where color information is

David Massey committed on Mar 4

Added: show or hide tank wall visualization

David Massey committed on Mar 4

Added: initial ice velocity vector to iceFieldInfo that is applied at the simulation configuration.

Removed: configuration error for towingCarriageSpeed == 0.

Added: configuration error for all velocity vectors == 0.

Changed: simulation end conditional to also check for towingCarriageVelocity.

TODO: add simulation end conditional to check for a global state delta (e.g. ice origins, carriage force) for simulations that do not move the carriage.

C Results for each ride-up test

The following four pages detail ride-up tests results for each simulation. Simulation data is simplified to a color scale: light green means the percent difference is within 17.5%, dark green is between 17.5 and 35%, and red is larger than 35%. All applicable units are in meters [m]. For details on the symbols, please refer to section 5.1.

h_i	0.25								
α	1:4			1:5			1:6		
v_i	1.00	1.50	2.00	1.00	1.50	2.00	1.00	1.50	2.00
μ	2.76	4.05	5.10	2.40	3.49	4.72	2.05	3.12	4.22
σ	0.40	0.30	0.72	0.17	0.15	0.19	0.01	0.02	0.01
Max	4.03	4.69	7.10	3.08	3.76	4.87	2.09	3.21	4.24
Min	1.93	2.83	3.66	2.18	3.16	4.08	2.03	3.09	4.19
μ/E	0.91	0.89	0.84	0.92	0.89	0.90	0.89	0.91	0.92
$\%_{Diff}$	9.9%	12.1%	17.6%	8.8%	11.8%	10.5%	11.3%	10.0%	8.7%

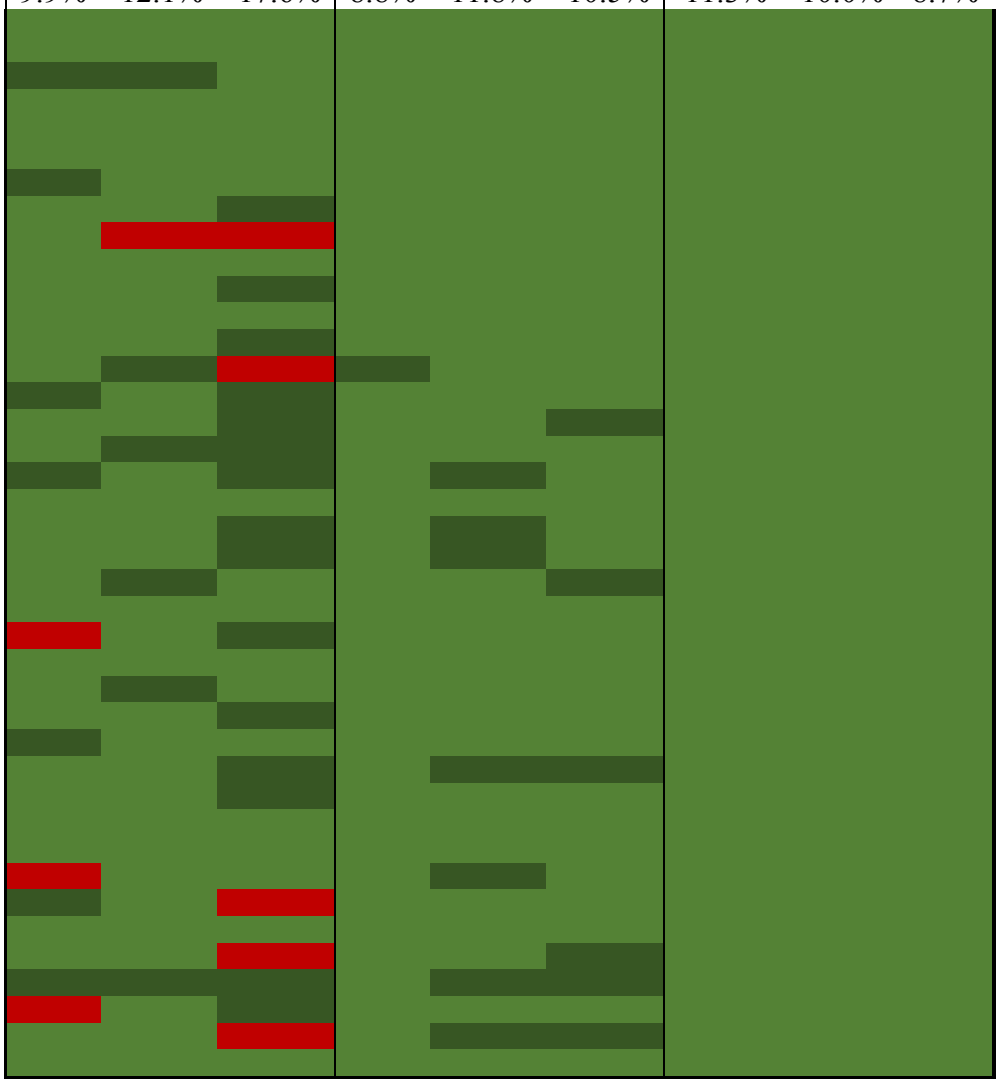

h_i	0.5								
α	1:4			1:5			1:6		
v_i	1.00	1.50	2.00	1.00	1.50	2.00	1.00	1.50	2.00
μ	2.56	3.88	5.21	2.15	3.35	4.56	1.89	2.93	3.99
σ	0.28	0.39	0.39	0.10	0.11	0.10	0.07	0.06	0.01
Max	3.17	5.03	6.07	2.47	3.90	4.91	2.30	3.25	4.01
Min	1.94	2.78	4.11	1.71	2.97	4.24	1.86	2.9	3.97
μ/E	0.84	0.85	0.86	0.82	0.85	0.87	0.82	0.85	0.87
$\%_{Diff}$	17.2%	16.3%	15.6%	19.4%	15.9%	13.9%	19.4%	16.2%	14.3%

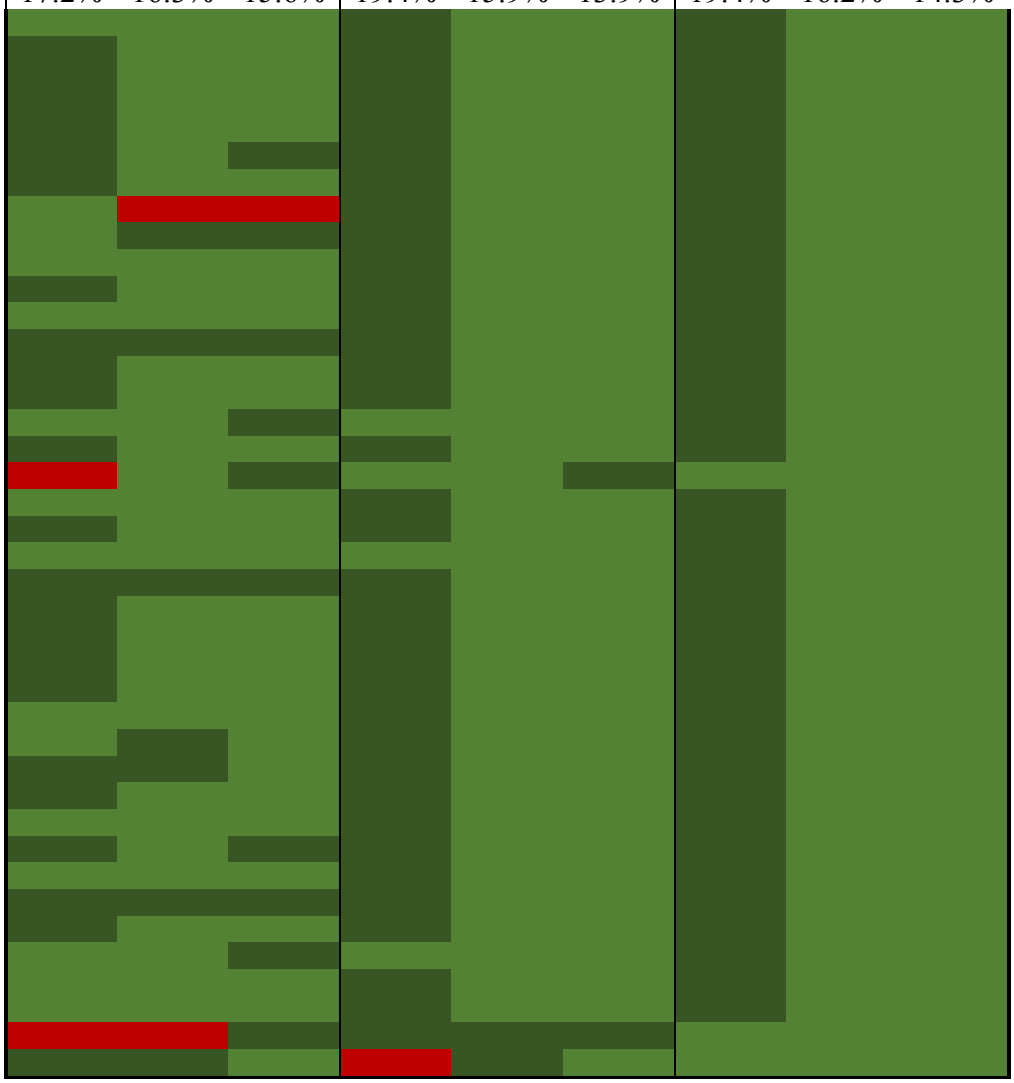

h_i	0.75								
α	1:4			1:5			1:6		
v_i	1.00	1.50	2.00	1.00	1.50	2.00	1.00	1.50	2.00
μ	2.42	3.83	5.06	2.05	3.17	4.38	1.76	2.80	3.85
σ	0.37	0.65	0.52	0.16	0.23	0.26	0.02	0.02	0.02
Max	3.45	5.44	6.31	2.43	3.32	4.82	1.80	2.84	3.89
Min	1.63	2.25	3.82	1.21	1.94	3.08	1.72	2.75	3.81
μ/E	0.80	0.84	0.83	0.78	0.81	0.84	0.77	0.81	0.84
$\%_{Diff}$	22.7%	17.5%	18.5%	24.4%	21.3%	17.7%	26.5%	20.7%	17.7%

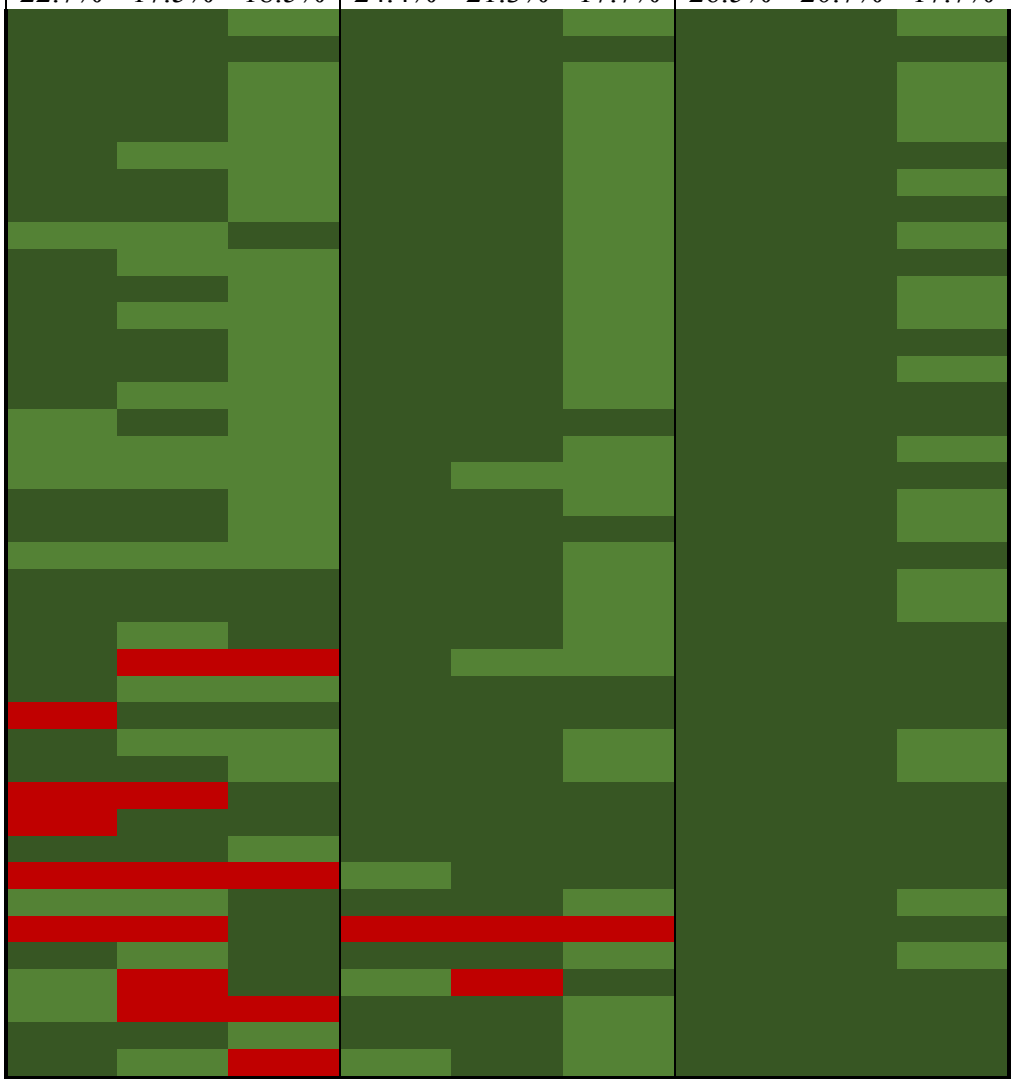

h_i	1								
α	1:4			1:5			1:6		
v_i	1.00	1.50	2.00	1.00	1.50	2.00	1.00	1.50	2.00
μ	2.22	3.31	4.73	1.93	3.05	4.26	1.62	2.67	3.71
σ	0.26	0.84	0.81	0.14	0.21	0.12	0.01	0.01	0.02
Max	3.06	5.66	6.58	2.55	3.69	4.91	1.68	2.72	3.75
Min	1.56	2.11	3.48	1.88	1.88	3.97	1.61	2.65	3.69
μ/E	0.73	0.72	0.78	0.74	0.78	0.81	0.71	0.77	0.81
$\%_{Diff}$	31.4%	32.0%	25.1%	30.0%	25.1%	20.7%	34.5%	25.7%	21.5%

D Results for all pile-up sensitivity tests

Trapezoidal Geometry

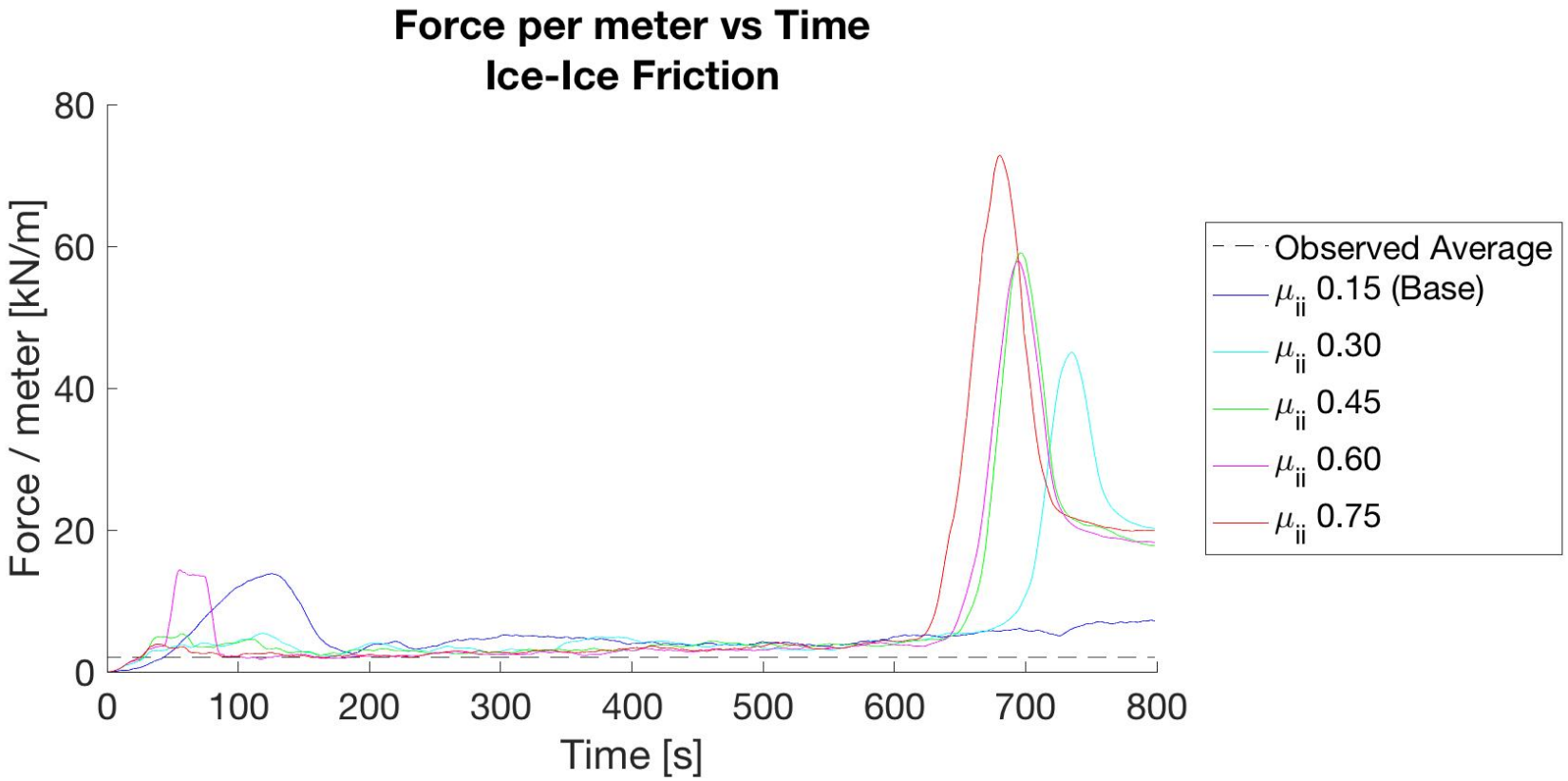

Trapezoidal Geometry

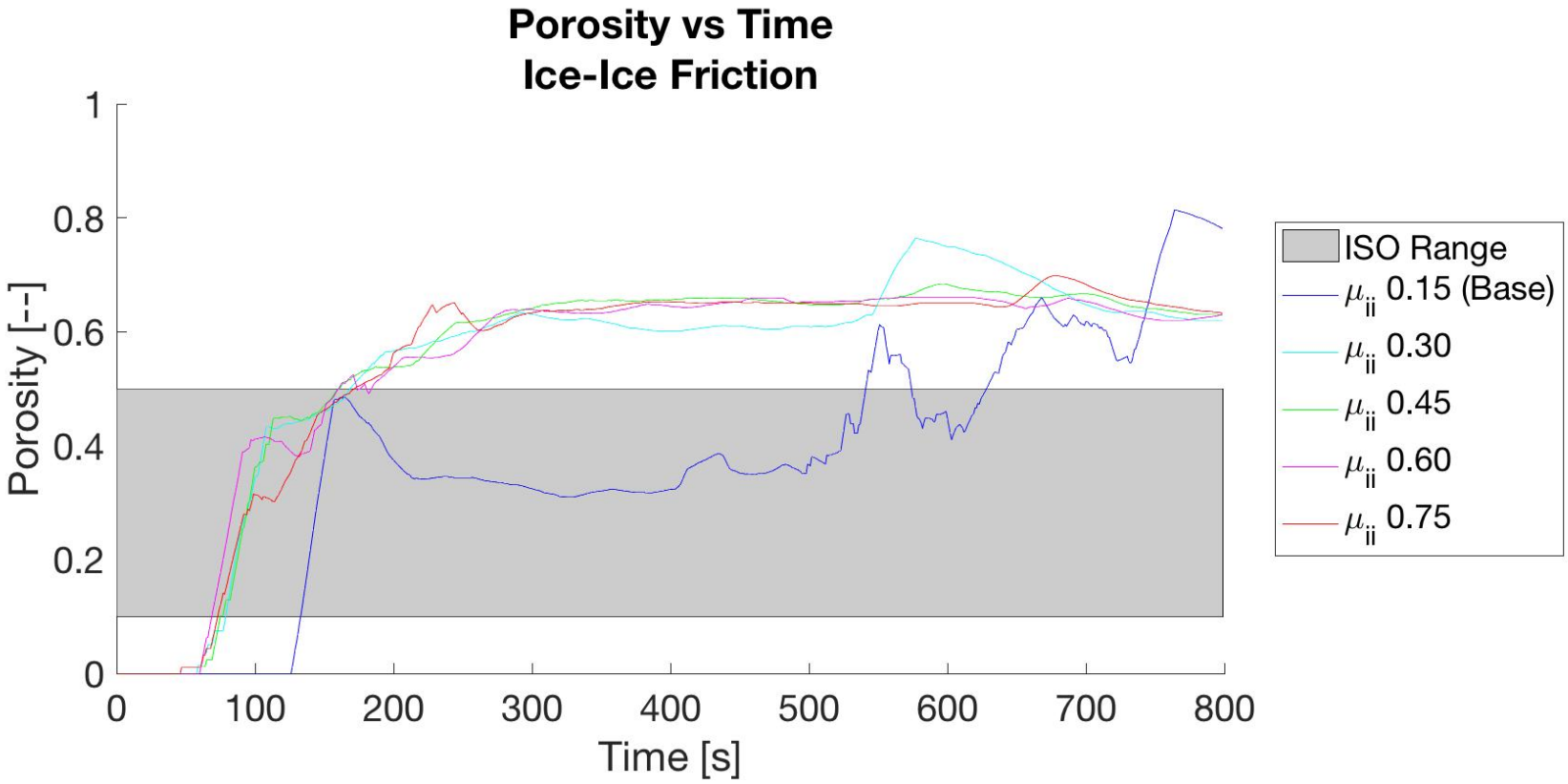

Trapezoidal Geometry

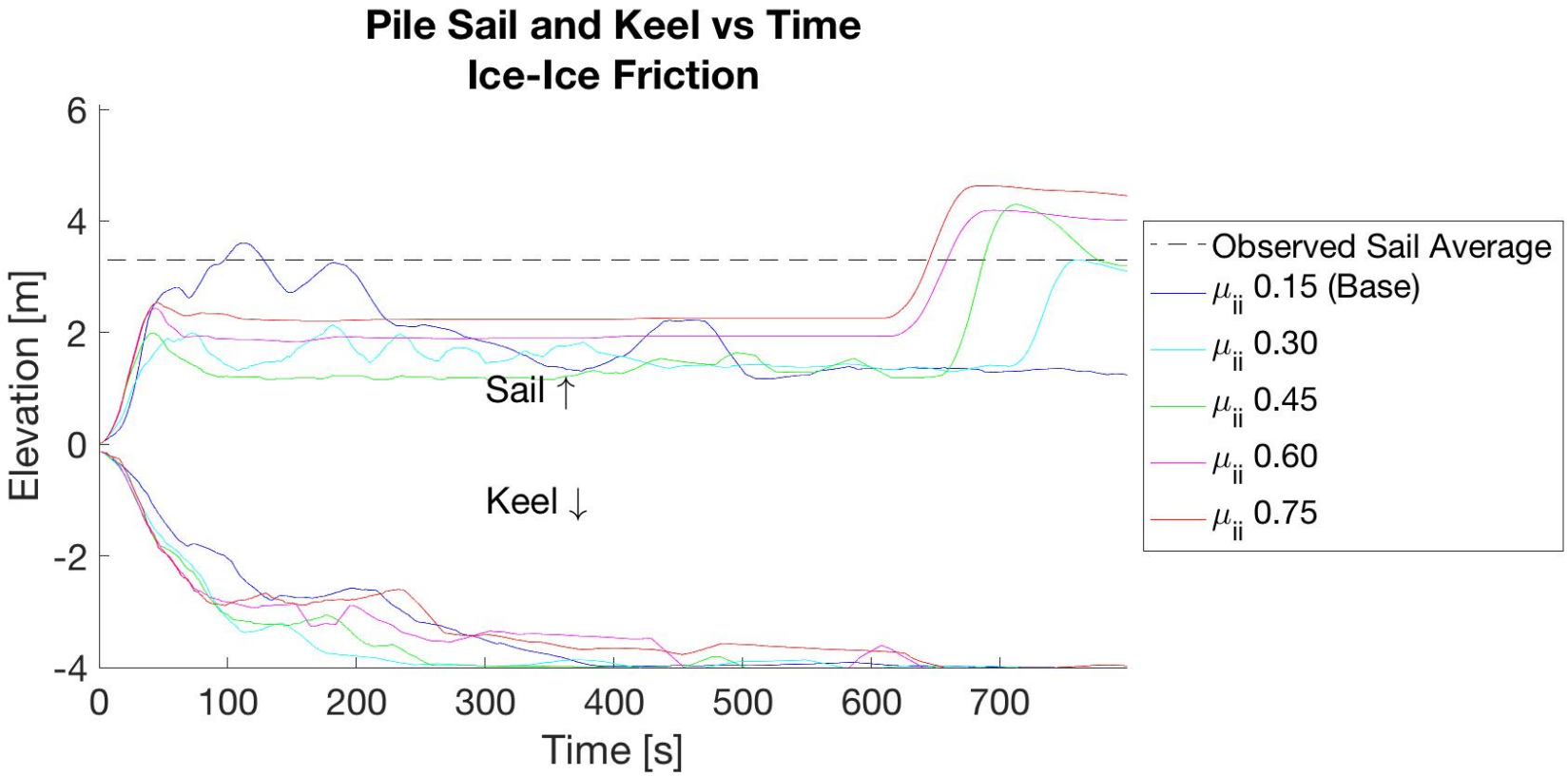

Trapezoidal Geometry

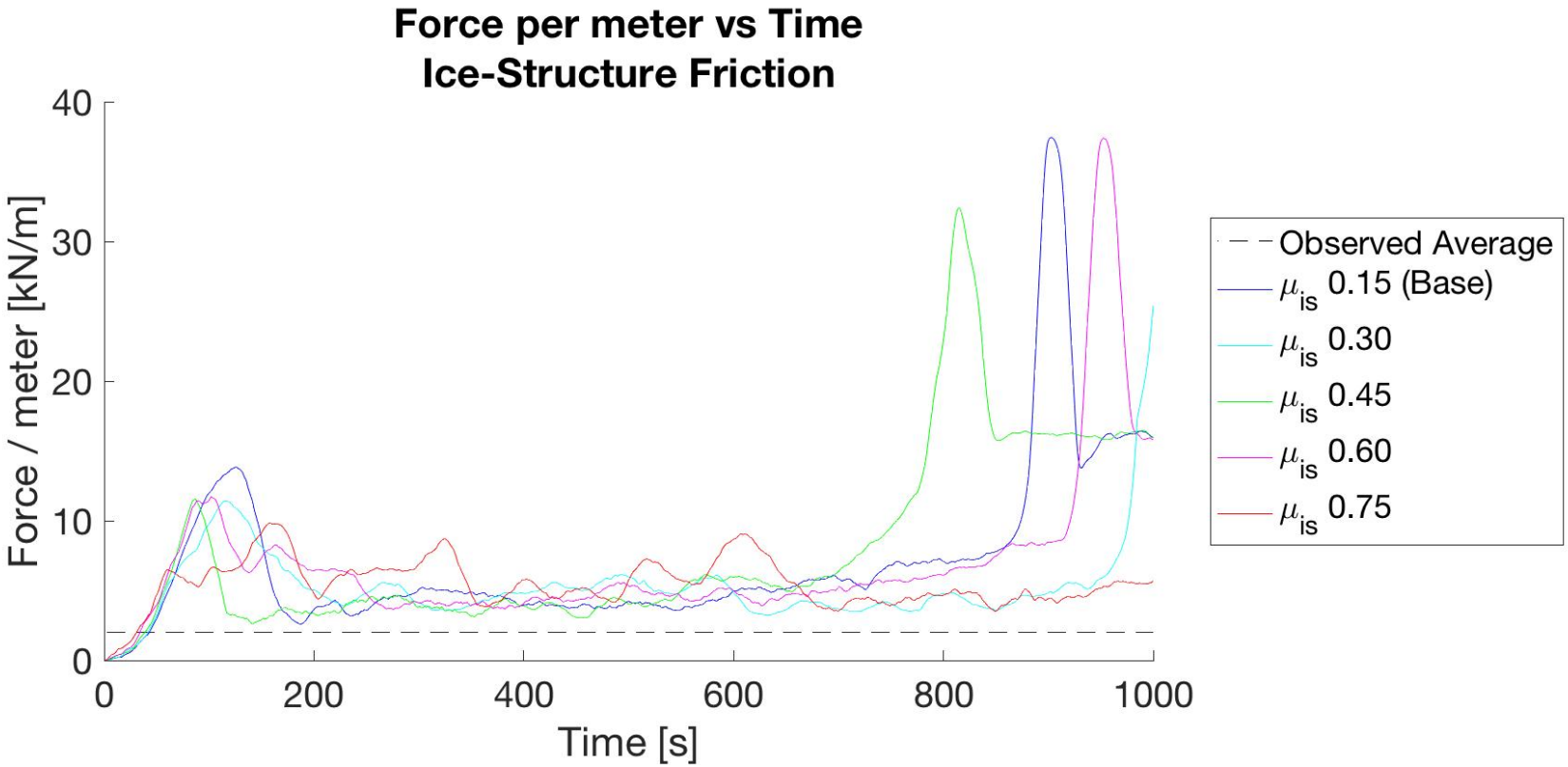

Trapezoidal Geometry

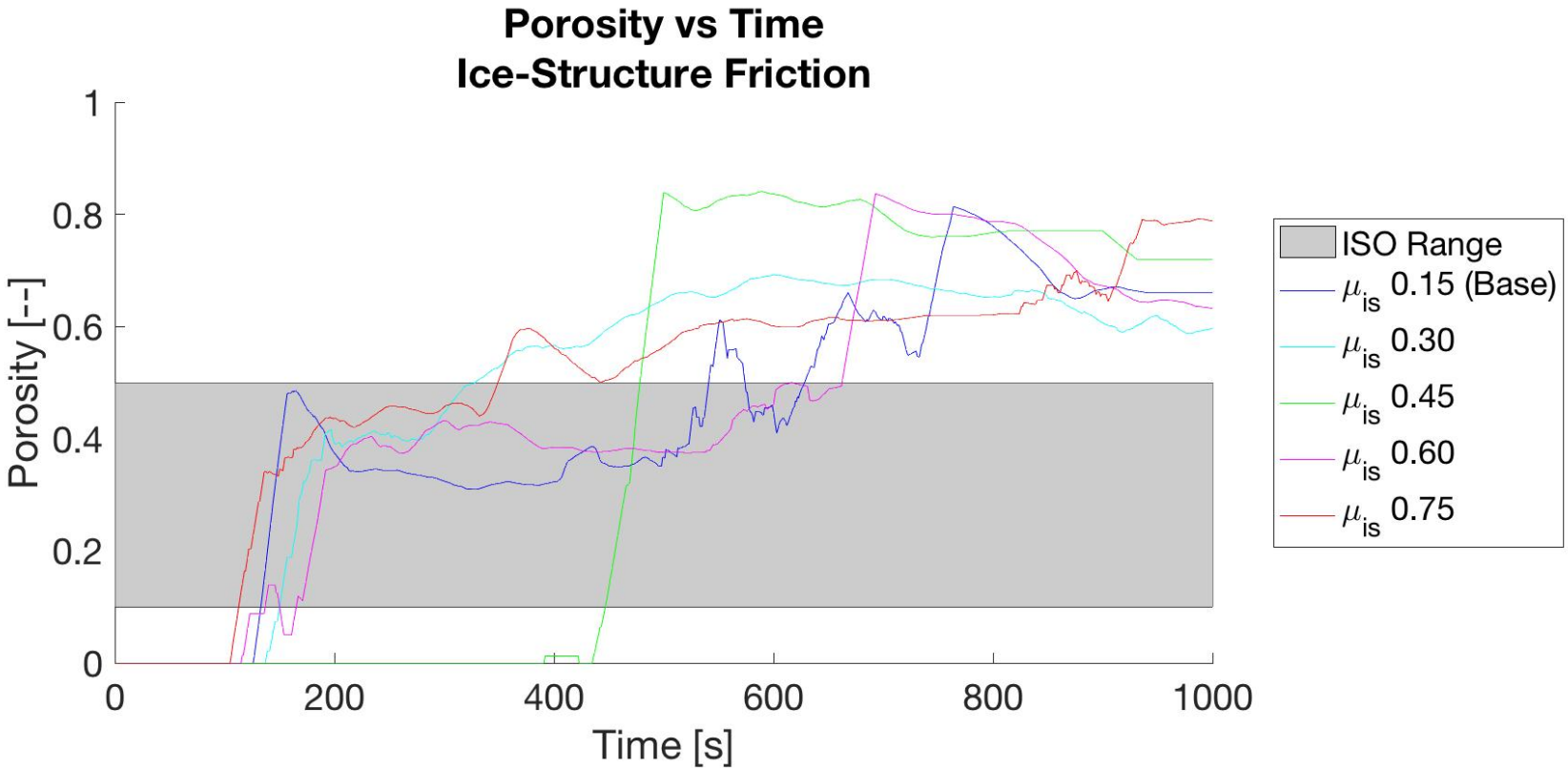

Trapezoidal Geometry

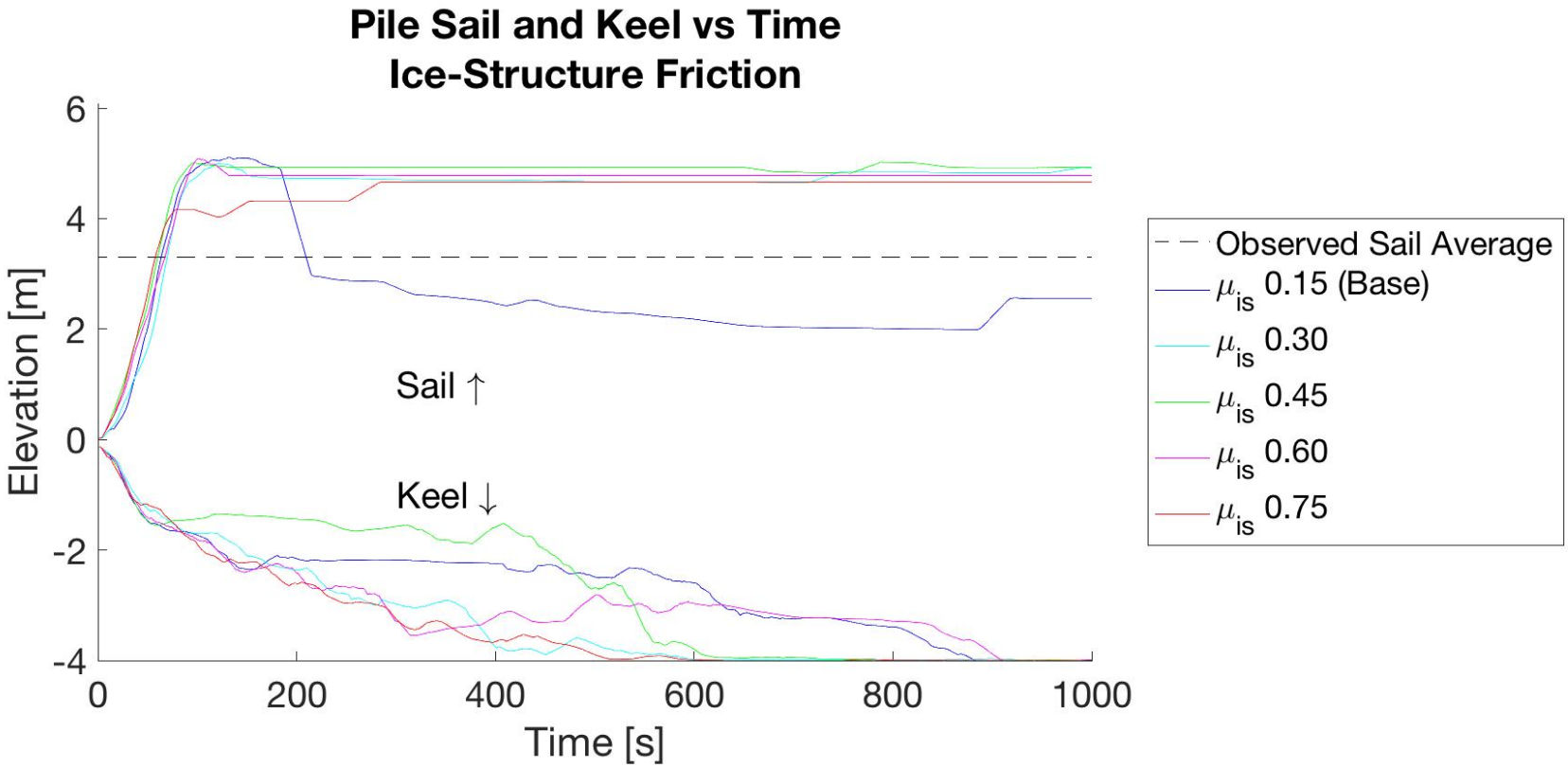

Trapezoidal Geometry

Trapezoidal and Triangular Geometry

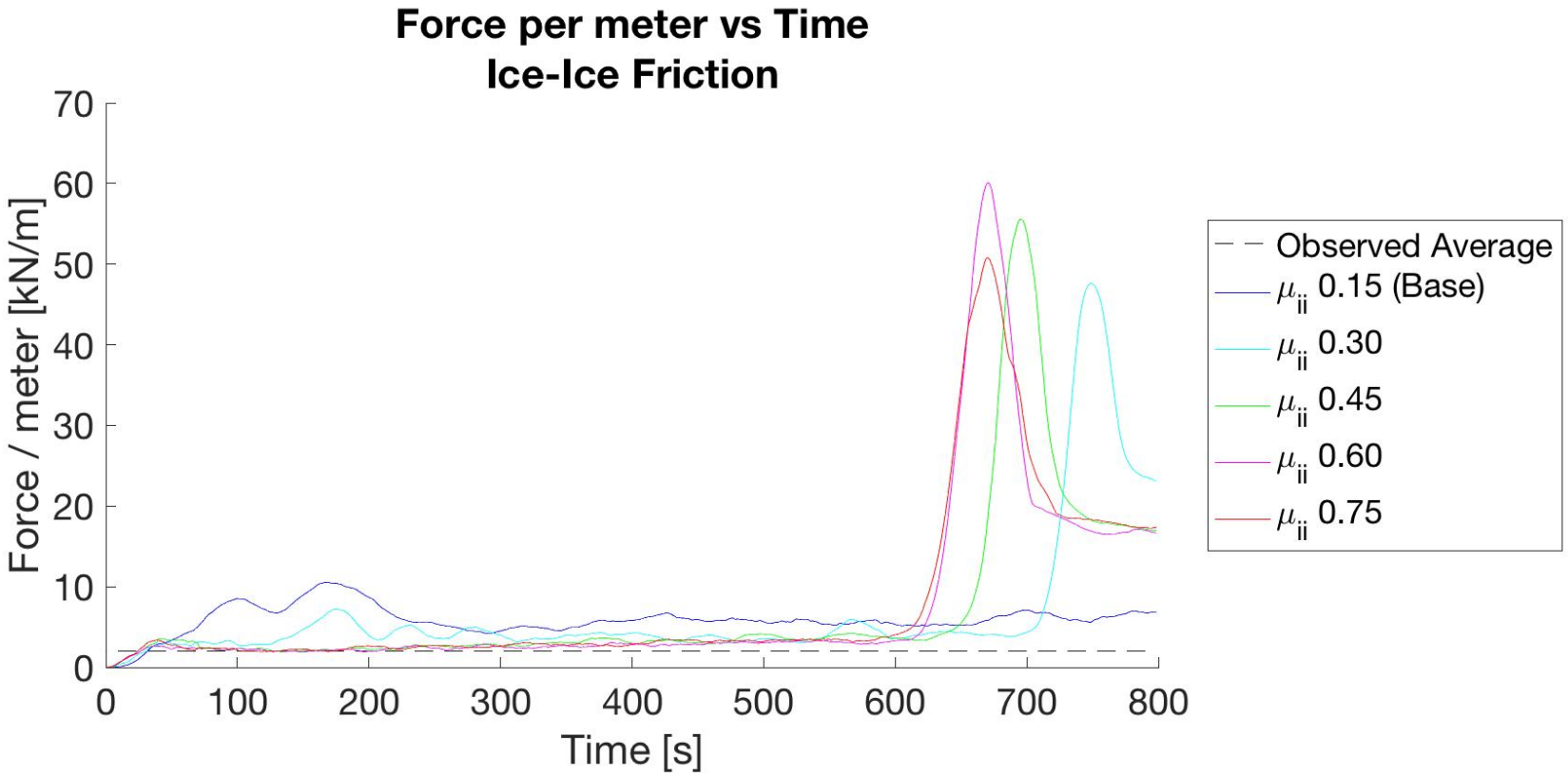

Trapezoidal and Triangular Geometry

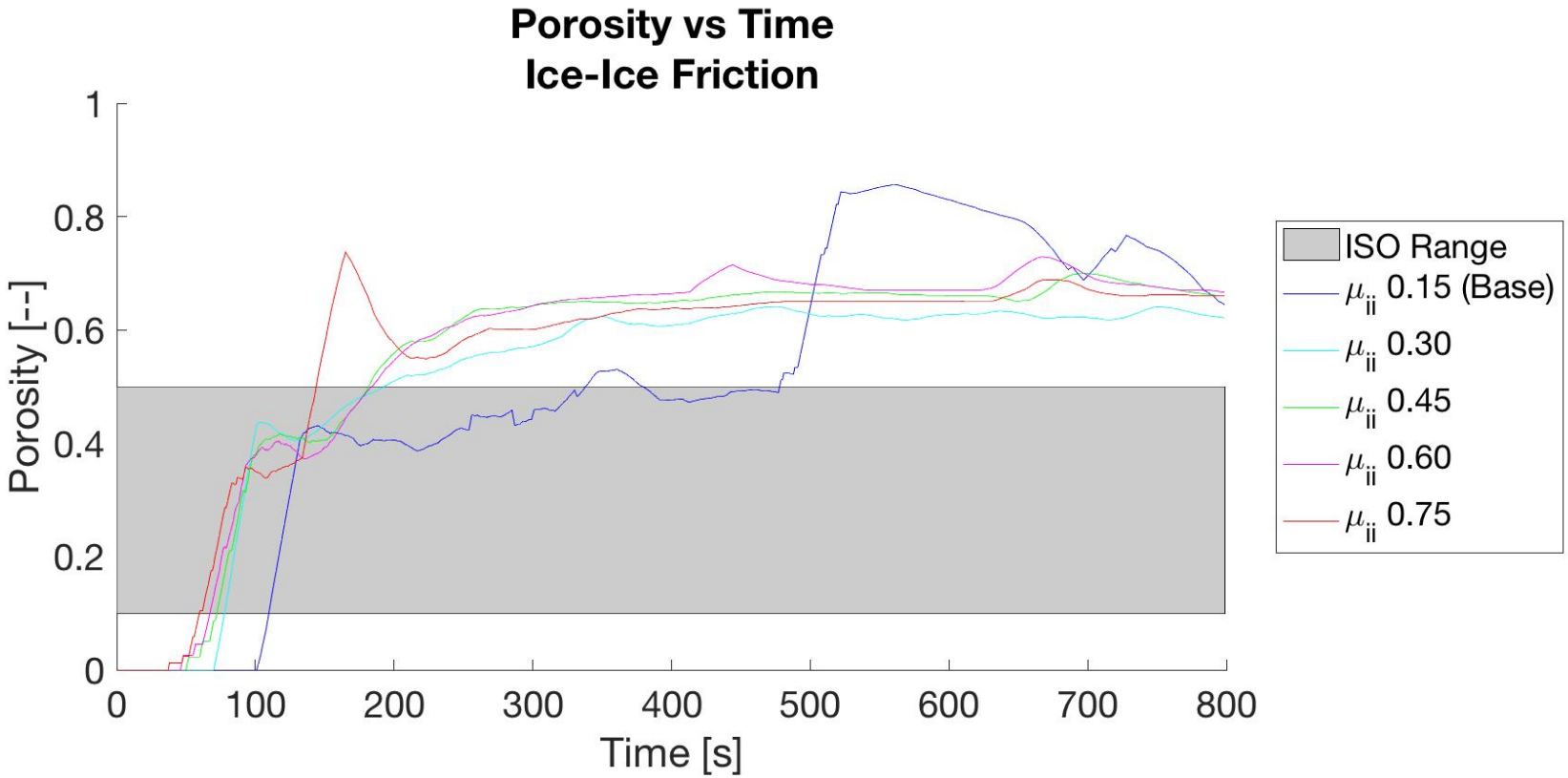

Trapezoidal and Triangular Geometry

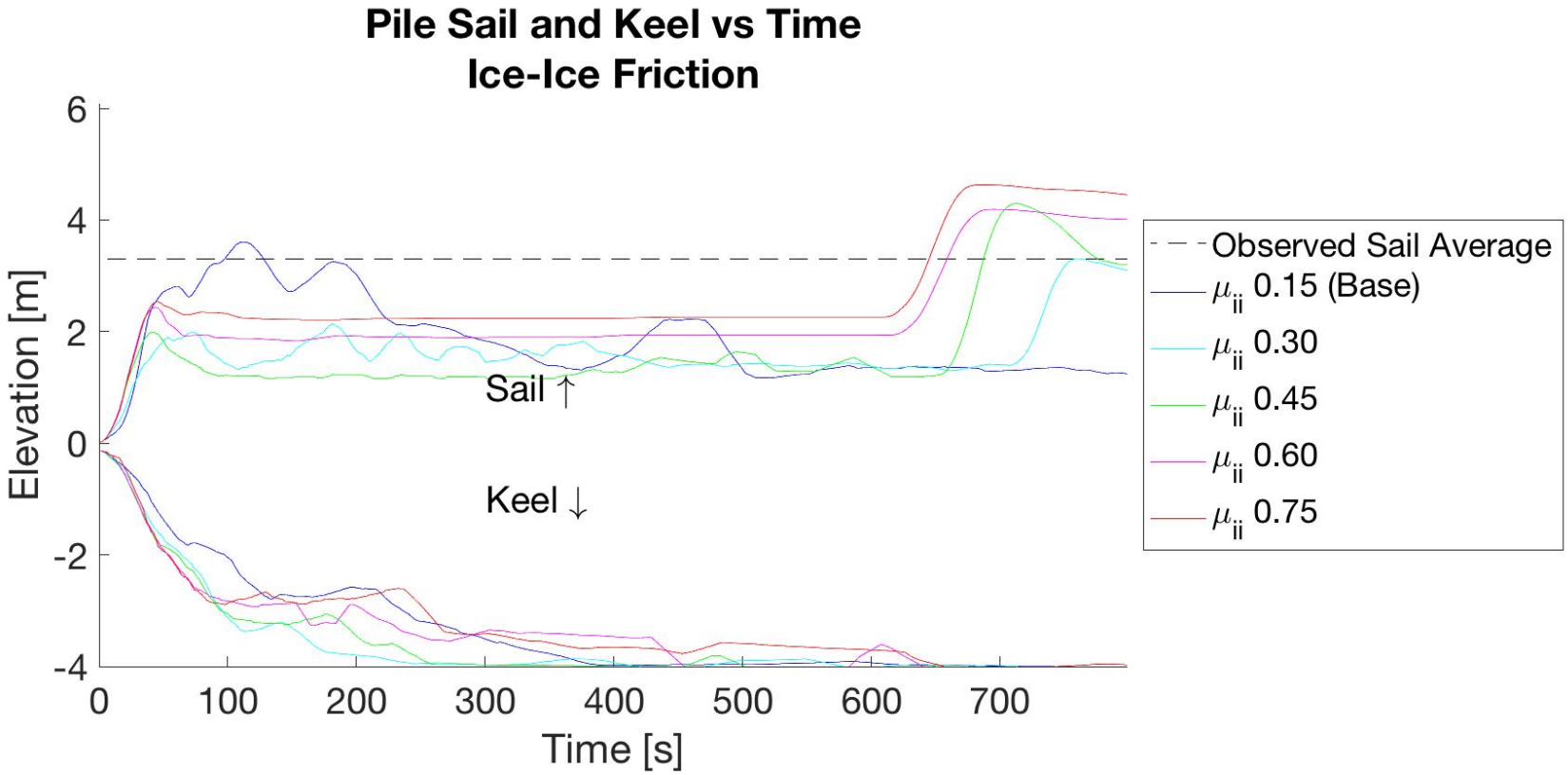

Trapezoidal and Triangular Geometry

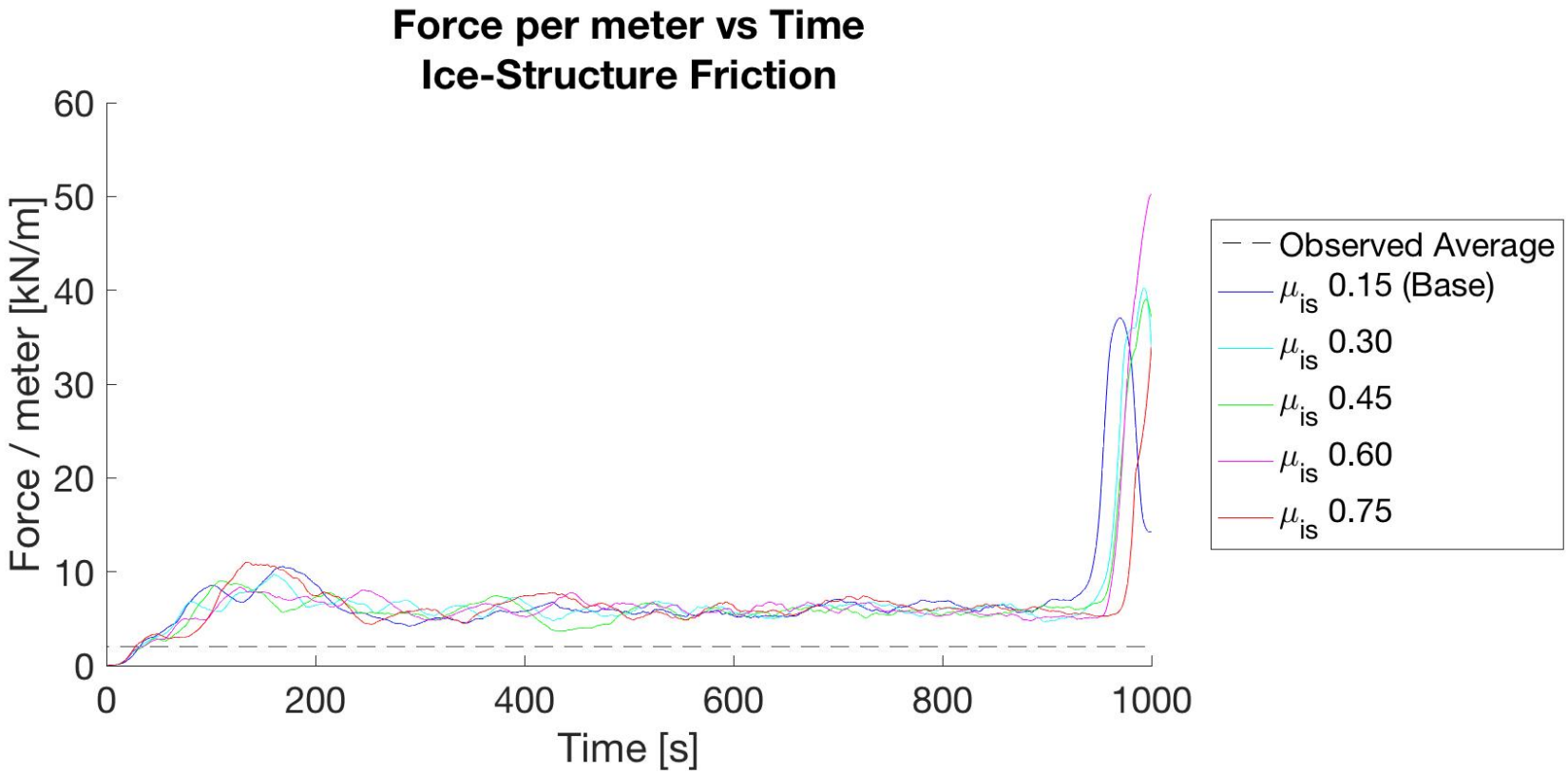

Trapezoidal and Triangular Geometry

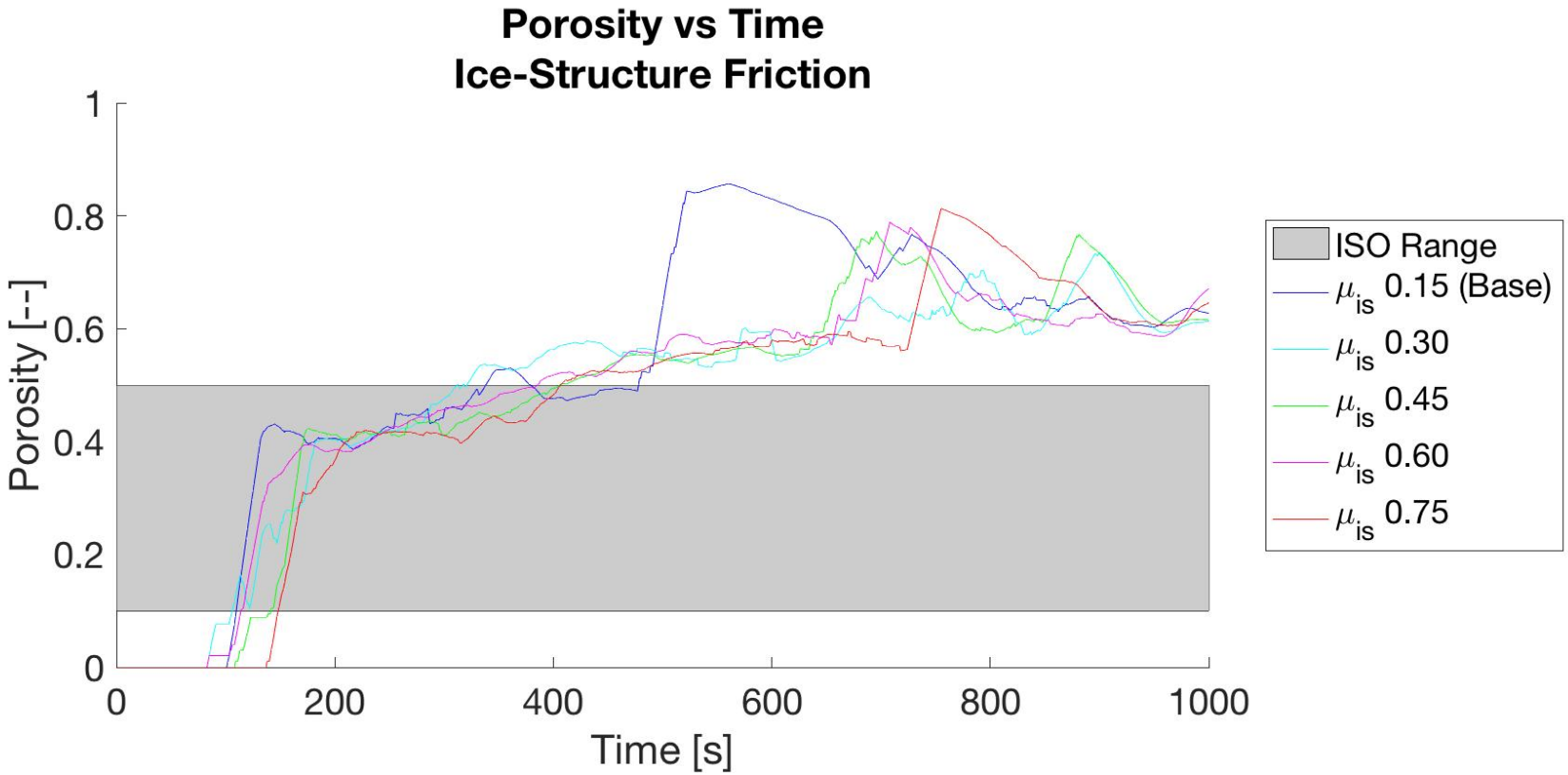

Trapezoidal and Triangular Geometry

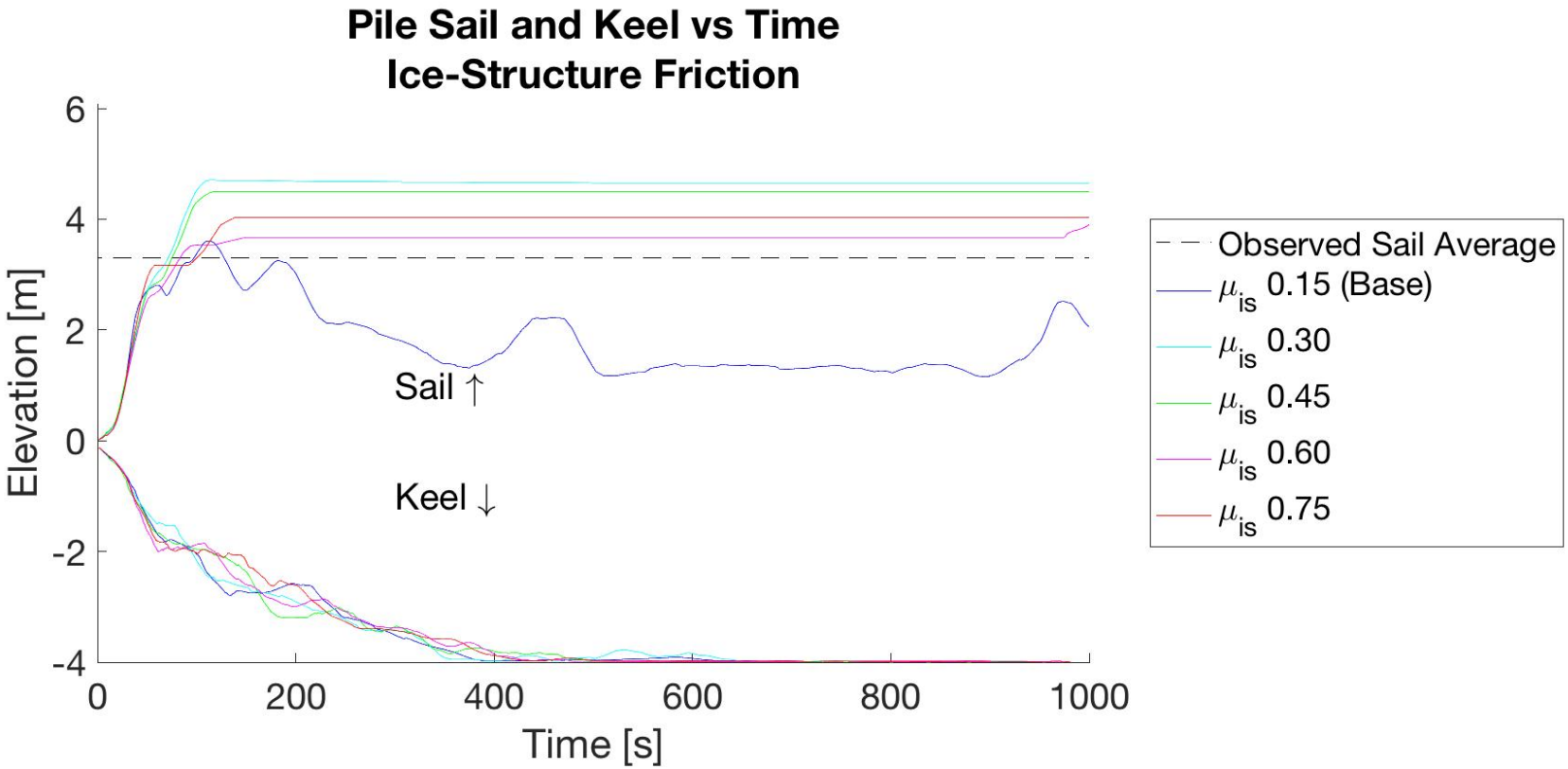

Trapezoidal and Triangular Geometry